Dissecting classical cadherins roles in motor neuron nuclear organization in the spinal cord

Inaugural-Dissertation

to obtain the academic degree

Doctor rerum naturalium (Dr. rer. nat.)

submitted to the Department of Biology, Chemistry and Pharmacy

of Freie Universität Berlin

by

CAROLA DEWITZ

2019

The following work was carried out in the research group of Niccolò Zampieri between November 2014 and January 2019 at the Max Delbrück Center for Molecular Medicine in the Helmholtz Association in Berlin.

1. Reviewer: Niccolò Zampieri, PhD
Department of Diseases of the Nervous System
Max Delbrück Center for Molecular Medicine
in the Helmholtz Association, Berlin

2. Reviewer: Prof. Dr. Peter Robin Hiesinger
Institute of Biology, Neurobiology
Freie Universität Berlin

Day of Disputation: May 15th, 2019

Acknowledgements

Foremost, I would like to thank my supervisor Niccolò Zampieri for giving me the opportunity to perform my graduate work in his laboratory. Being part of his group and having him as a mentor has taught me every single aspect of being a sophisticated scientist by planning experiments thoroughly, performing them accurately and interpreting the results critically. I highly appreciate his constant support, patience, encouragement and always open door. His readiness to help never once ran dry and I am forever grateful for all of his imparted knowledge on conducting high-standard research.

Furthermore, I would like to thank Prof. Dr. Peter Robin Hiesinger for valuable input and advice throughout my graduate work and for being my second supervisor and part of my thesis committee.

I am very much grateful for my colleagues as all of them contributed to this work by sharing their scientific ideas, providing moral support and helping with every day lab problems. They made long incubation waiting times and lunch breaks a lot more fun! Our former and present lab technicians Liana Kosizki and Isabelle Werner have been essential in keeping the lab running smoothly and making sure I had the equipment and reagents needed to do my experiments. Jasmin Bonkowski always readily helped me with all the administrative bureaucracy and her constant good mood was contagious! I am particularly grateful to Sophie Skarlatou, whose readiness to help and high spirits were incredible. Daily lab life would not have been the same without her! In addition, I would like to thank Sofia Pimpinella, with whom I was fortunate to cooperate with on parts of the afadin project.

But above all, I would like to express my infinite gratitude to all the persons that have always believed in me, listened to me when I needed them to listen and helping me find motivation: my family, Tabea Linnemann, Sophie Skarlatou, David Biermann and Anthea Wirges. Only with their unconditional support was I able to accomplish this work. Moreover, I highly appreciate their time and energy invested to review, format and comment this manuscript.

Table of Contents

Abbreviations

2D	two-dimensional
3D	three-dimensional
°C	degree Celsius
AF	alexa fluor
A/G	adductor/gracilis
ATCC	american type culture collection
BDNF	brain-derived neurotrophic factor
Bmp	bone morphogenetic proteins
Bp	base pair
Cad	cadherin
CAM	cell adhesion molecule
CHO	chinese hamster ovary
Cmn	common
CNS	central nervous system
Cy	cyanin
DAPI	4',6-diamidino-2-phenylindole
DMEM	dulbecco's modified eagle's medium
DMSO	dimethyl sulfoxide
DNA	deoxyribonucleic acid
dNTP	deoxynucleotide triphosphate
DsRed	discosoma red
DTT	dithiothreitol
e	embryonic day
EC	extracellular cadherin
EDTA	ethylenediaminetetra-acetic acid
Et al.	et alia
ETS	erythroblast transformation-specific
FBS	fetal bovine serum
FGF	fibroblast growth factor
FL	flox
FoxP1	Forkhead box p1

Fwd	forward
GDNF	glial cell line-derived neurotrophic factor
GFP	green fluorescent protein
H	hamstring
HCMF	HEPES calcium and magnesium free
HEK	human embryonic kidney
HEPES	4-(2-hydroxyethyl)-piperazin-1-ethan-sulfonic acid
HMC	hypaxial motor column
HMF	HEPES magnesium free
Hox	homeobox family of genes
HRP	horseradish peroxidase
HSD	honest significant test
IN	interneuron
KO	knock out
LDS	lithium dodecyl sulfate
Lhx1	Lim homeobox 1
LMC	lateral motor column
LMCl	lateral LMC
LMCm	medial LMC
min	minutes
MMC	median motor column
MN	motor neuron
NOA	neurite outgrowth assay
p	probability value
PBS	phosphate-buffered saline
PCR	polymerase chain reaction
Pen Strep	penicillin-streptomycin
PFA	paraformaldehyde
PGC	preganglionic motor column
pH	potential of hydrogen
pMN	motor neuron progenitor domain
PZ	progenitor zone
r	coefficient of correlation
RA	retinoic acid

Raldh2	retinaldehyde dehydrogenase 2
Rev	reverse
Rpm	rounds per minute
R/T	rectus femoris/tensor fasciae latae
scg	sympathetic chain ganglia
SD	standard deviation
SDS	sodium dodecyl sulfate
sec	seconds
SEM	standard error of the mean
Shh	sonic hedgehog
s-m	self-made
TRIS	tris(hydroxymethl)aminomethane
UV	ultraviolet
V	vasti
WT	wild type

List of Figures

List of Tables

Summary

Motor neurons in the spinal cord are found grouped in nuclear structures termed pools, whose position is precisely orchestrated during development. Despite the emerging role of pool organization in the assembly of spinal circuits, little is known about the morphogenetic programs underlying the patterning of motor neuron subtypes. Type I and type II classical cadherins constitute a family of cell adhesion molecules expressed in complex combinatorial profiles in the nervous system, suggesting the hypothesis that a cadherin-based adhesive code controls neuronal recognition at the basis of the development of neuronal structures and circuits. In addition, cadherin location at cell-cell contact sites is known to be regulated by the nectin-afadin cell adhesion complex. Thus, to test the impact of cell surface proteins on motor neuron organization, three-dimensional analysis of motor neuron positioning was established to reveal roles and contributions of classical cadherins function. The results uncovered that nuclear organization of motor neurons is dependent on inside-out positioning orchestrated by N-cadherin (a type I cadherin), catenins and afadin activities, controlling cell body layering on the medio-lateral axis. In addition to this lamination-like program, motor neurons undergo a secondary, independent phase of organization. This process results in segregation of motor neurons along the dorso-ventral axis of the spinal cord and relies on type II cadherin function, which is only revealed by concomitant elimination of N-cadherin.

Zusammenfassung

Motoneurone werden während ihrer Entwicklung im Rückenmark präzise in Motorpool-Kernarealen positioniert und organisiert. Obwohl die Positionierung dieser Motorpools eine wichtige Rolle während des Aufbaus des Nervensystems spielt, ist wenig über die der Organisation zugrunde liegenden morphogenetischen Programme bekannt.
Klassische Typ I und Typ II Cadherine gehören zu einer Familie der Zell-Adhäsionsmoleküle welche in komplexen, kombinatorischen Mustern im Nervensystem exprimiert werden und die Abgrenzung unterschiedlicher neuronaler Strukturen kontrollieren. Dies führt zu der Hypothese, dass ein Cadherin-basierter Code die Erkennung von Nervenzellen kontrolliert und somit den Grundstein zur Entwicklung korrekter neuronaler Netzwerke darstellt. Darüber hinaus ist bekannt, dass die Lokalisierung von Cadherinen an Zell-Zell-Kontakten durch den Zell-Zell-Adhäsionskomplex Nectin-Afadin reguliert wird. In dieser Arbeit wurde daher der Einfluss von Zell-Oberflächenproteinen auf die Organisation von Motoneuronen getestet. Dafür wurde eine Methode zur dreidimensionalen Untersuchung der Positionen von Motoneuronen etabliert. Anschließend wurde der Einfluss und die Beteiligung unterschiedlicher Zell-Adhäsionsproteine nach Inaktivierung von klassischen Cadherinen und Afadin auf die Positionierung der Motoneurone analysiert. Die Ergebnisse zeigen, dass die Organisation von Motorpools durch eine schrittweise verlaufende Schichtung entlang der medio-lateralen Achse entsteht, für welche die Funktionen von N-Cadherin (ein Typ I Cadherin), Catenine und Afadin entscheidend sind. Zusätzlich zu diesem Prozess der Zell-Schichtungen, durchlaufen die Motoneurone eine zweite, unabhängige Organisierungsphase, bei der sich die Zellkörper entlang der dorso-ventralen Achse im Rückenmark auftrennen. Dieser zweite, für die Entstehung von Motorpool-Kernarealen essentielle Schritt, beruht auf den Funktionen von Typ II Cadherinen, welche allerdings nur im Zusammenspiel mit N-Cadherin ihre Wirkung zeigen.

1. Introduction

1.1 Organization of the nervous system

A fundamental question in neuroscience regards the mechanisms used during development to assemble highly ordered and specific neuronal networks from a diverse array of neuronal cell types. Neuronal subtypes are often assigned highly stereotyped positions, where neurons grouped together not only share positional coordinates but also receive connections from similar inputs and send projections to common targets. Thus, precise spatial organization appears to represent a major strategy to simplify the problem of wiring neurons during development. To define the mechanisms governing these processes, it is is important to understand the developmental steps of neuronal circuit assembly.

1.1.1 Neurons are organized into nuclei and laminae

The existence of neuronal organization into functional and structurally distinct regions has long been evident in the central nervous system (CNS). During development, precise positioning of neurons is a tightly regulated process controlled by neurogenesis and migration, and is an important determinant of identity, connectivity and ultimately function (Leone et al., 2008; Sürmeli et al., 2011; Bikoff et al., 2016; Oishi et al., 2016). In the CNS, most neurons are organized along two main anatomical schemes (Ramon y Cajal, 1894). In the neo-cortex, cerebellum or the dorsal spinal cord for example, the predominant mode of organization is as stratified layers or laminae of neurons. However, in more evolutionary ancient regions of the CNS, the primary mode of organization clusters neurons with related functions into so called neuronal nuclei. Neurons that are organized within laminae or nuclei share several features like morphological properties, innervation targets and patterns of inputs. The cellular and molecular underpinnings of neuronal positioning have been mostly studied in the developing cortex, where signaling pathways controlling lamination and ordered distribution of neuronal populations have been identified (Rakic, 1974; Hatten, 1999; Bielas and Gleeson, 2004; Marin et al., 2010). In the developing cortex, inside-out positioning of neurons tightly links neuronal birth date and migratory pattern, controlling the laminar organization of neurons (Hatten, 1999; Marin et al., 2010). Neurons exiting the cell cycle at early time points populate deep

cortical layers, whereas neurons generated at later time points settle in more superficial layers. In contrast, it is unknown what processes drive neuronal nucleus formation; however, experimental evidence points to a multi-step process that involves switching between distinct migration modes (Kawauchi et al., 2006; Watanabe and Murakami, 2009; Shi et al., 2017). A striking example of nuclear organization in the CNS is apparent in the arrangement of motor neurons in the ventral horn of the spinal cord, which can be used as a model system to investigate the developmental processes of nuclear organization due to its well-studied anatomy and physiology and relative simplicity of its circuitry.

1.1.2 Nuclear organization of motor neurons in the spinal cord

At a general level, motor neuron nuclei are clearly separated from other spinal neurons, such as interneurons and projection neurons, as they assume characteristic ventro-lateral and ventro-medial positions within the Redex area IX in the spinal cord and project axons into the periphery. In addition, spinal motor neurons are further organized in a hierarchical fashion according to their target connectivity during development (Figure 1; Dasen and Jessell, 2009). Along the rostro-caudal axis motor neurons are organized in longitudinal columns, which correspond to segmentally distinct peripheral targets. Four major columnar classes have been described: at thoracic levels visceral preganglionic column (PGC) motor neurons project to sympathetic ganglia, while hypaxial motor column (HMC) neurons innervate intercostal and abdominal wall musculature (Dasen and Jessell, 2009). At limb levels, the lateral motor column (LMC) contains neurons that innervate limb muscles (Figure 1; Romanes, 1951). In contrast to these segmentally restricted motor columns, motor neurons in the median motor column (MMC) are present along the whole rostro-caudal axis of the spinal cord and innervate dorsal epaxial musculature. In addition, higher levels of anatomical organization are present within the LMC: LMC neurons can be further divided into medial (LMCm) and lateral (LMCl) divisions based on their projections to ventral and dorsal muscle targets, respectively (Tosney and Landmesser, 1985; Jessell, 2000; Dasen and Jessell, 2009). At the highest level of organization, all motor neurons innervating a single muscle target are segregated and clustered into pools, whose position is stereotyped and conserved across individuals (Figure 1; Romanes 1964; Vanderhorst and Holstege, 1997). In addition, motor pools that innervate limb muscles exerting synergistic functions are themselves grouped together forming columels that run along the rostro-caudal axis of the lumbar and brachial spinal cord (Romanes, 1964).

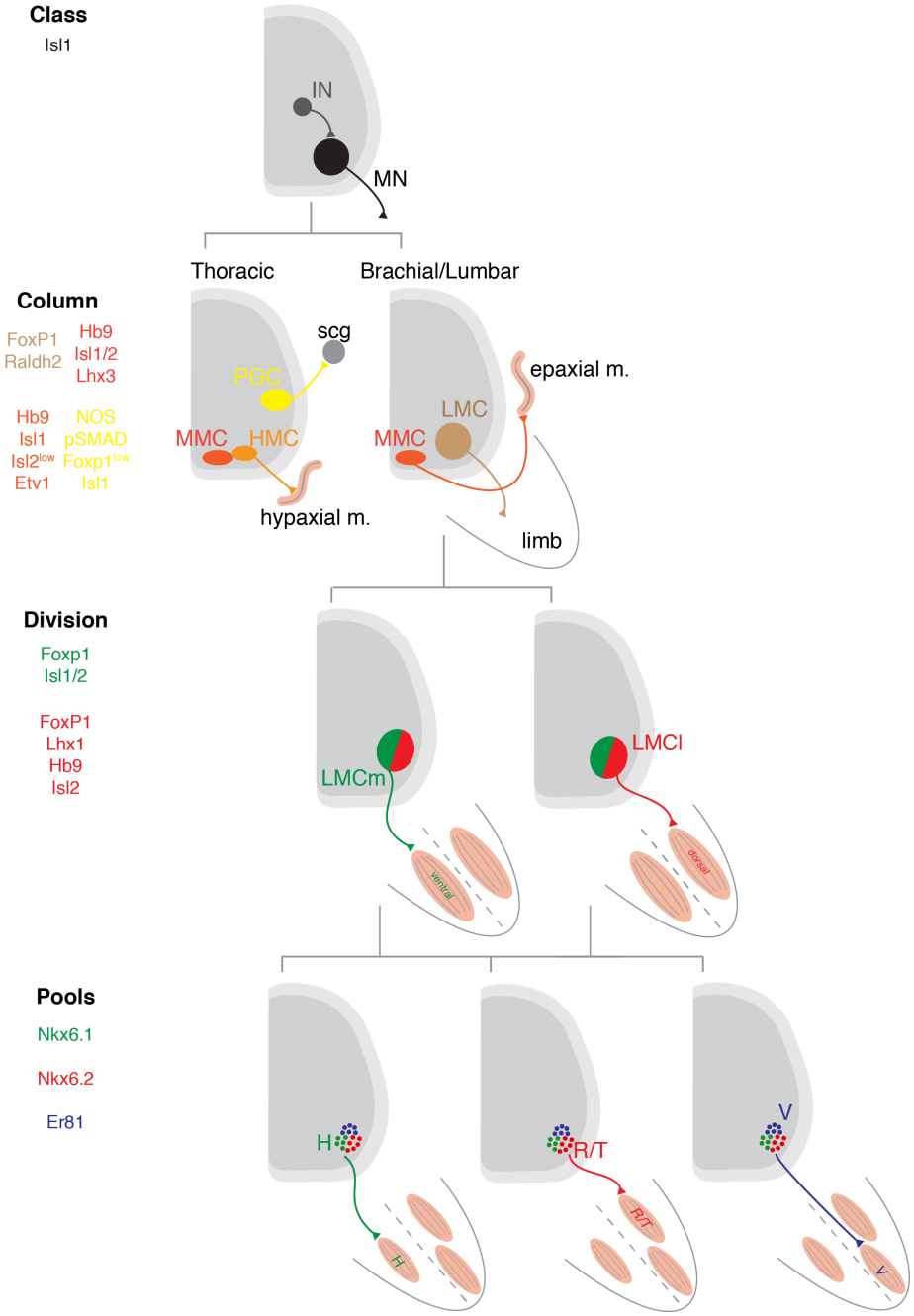

Figure 1: Hierarchical organization of spinal motor neuron subtypes.
Motor neurons (MNs) project axons out of the spinal cord, which distinguishes them from interneurons (INs). Sets of motor neurons are arrayed into longitudinal columns along the rostro-caudal axis and project to distinct regions in the periphery. Motor neurons within the median motor column (MMC) are generated at all rostro-caudal levels of the spinal cord and project to axial musculature (epaxial). Preganglionic column (PGC) motor neurons and hypaxial motor column (HMC) neurons are found at thoracic levels, projecting to sympathetic chain ganglia (sgc), and intercostal and body wall muscles (hypaxial), respectively. The lateral motor column (LMC) is located at brachial and lumbar levels of the spinal cord and sends axons into the limb mesenchyme. The LMC can further be divided into a medial (m) and lateral (l) division based on projections to the ventral and dorsal half of the limb mesenchyme, respectively. At the highest level of organization, motor pools occupy specific rostro-caudal positions within the LMC, with each pool innervating a dedicated target muscle. Proteins expressed by each motor neuron subtype are depicted with their respective color code (adapted from Jessell, 2000; Dasen and Jessell, 2009; Stifani, 2014).

Columels exhibit a positional plan that conforms, in remarkably precise fashion, to the three major axes of limb organization. 1) The rostro-caudal positioning of columels correlates to the antero-posterior coordinates of the limb muscle position (Landmesser, 1978; Hollyday and Jacobson, 1990). 2) The ventro-dorsal position of motor columels mirrors the proximo-distal position of limb muscles (Romanes, 1964; McHanwell and Biscoe, 1981; Vanderhorst and Holstege, 1997). 3) The medio-lateral positioning of columels reflects flexor-extensor function of limb muscles. However, what is the purpose of constructing such an elaborate and multilayered program of motor neuron organization?

1.2 Significance of motor pool positioning

The evolutionary conservation of motor neuron spatial organization in higher vertebrates emphasizes the importance of precise cell body positioning, but its significance has remained unclear. There are several anatomical features shared by all motor neurons within a pool. First, all motor neurons within a pool project axons to a single muscle target in the limb (Landmesser, 1978). Second, motor neurons within a pool receive monosynaptic inputs from proprioceptive sensory neurons that supply the same muscle target (Frank et al., 1988). Third, motor neurons within a pool are linked by transient coupling through gap junctions early during development (Brenowitz et al., 1983). Fourth, motor neurons within a pool possess characteristic dendritic arborization patterns (Vrieseling and Arber, 2006).

1.2.1 Muscle connectivity

What is the developmental relationship between motor pool position and muscle innervation pattern? One hypothesis that supports the need to construct such an elaborated motor neuron organization during development is that motor pool position could contribute to the precision and fidelity of muscle target innervation. Interestingly, despite the scrambling of motor neuron position through inactivation of cadherin signaling via elimination of catenins, motor neurons still target muscles appropriate for their molecular identity, indicating that motor neuron clustering and muscle-specific connectivity are controlled through independent processes (Demireva et al., 2011; Bello et al., 2012). Presumably, expression and activity profiles of many known axon guidance molecules like netrins, semaphorins, ephrins and slits are established in a manner independent of motor neuron cell body position (Bonanomi and Pfaff, 2010). For example, the dorso-ventral

axon trajectory in the limb is regulated by the expression of axonal Eph tyrosine kinase receptors that enable LMC growth cones to respond to ephrin ligands in the limb mesenchyme (see Introduction section 1.4.2.2; Eberhart et al., 2000; Luria et al., 2008). In addition, neuropilins, the secreted co-receptors of plexins, expressed by motor neurons, interact with semaphorin ligands provided by the limb to control axon entry into the limb mesenchyme and perturbation of neuropilin-semaphorin signaling has been shown to result in defects of dorso-ventral axonal projections (Huber et al., 2005).

Interestingly, studies on the role of reelin also indicate independent events of motor neuron position and axon guidance. Reelin is a large secreted extracellular matrix glycoprotein and expressed in dorso-medial LMC neurons in contrast to its intracellular adaptor protein Dab1, which is found at high levels in LMCl neurons. Both reelin and Dab1 mutant mice display impaired LMCl and LMCm positioning, however, their appropriate target selection is not impaired (Palmesino et al., 2010). Thus, these findings argue against the idea that the clustering and settling position of motor neurons helps to assign patterns of muscle target connectivity, but support the view that the molecular identity rather than position of an individual motor neuron determines its muscle target selectivity (Demireva et al., 2011).

1.2.2 Sensory input

If motor neuron organization is not important for overall pattern of neuromuscular innervation, may one function be to provide a positional logic that helps to establish the precise pattern of sensory-motor connectivity? The connections formed between proprioceptive sensory and motor neurons convey feedback signals that coordinate motor output (Hultborn, 2006). Proprioceptive sensory afferents that innervate a given muscle project to the cell bodies and dendrites of spinal motor neurons with exquisite specificity: they form strong connections with “self” motor neurons that innervate the same muscle and weaker connections with motor neurons that innervate muscles with synergistic functions. In contrast, motor neurons do not receive proprioceptive input from muscles with antagonistic or unrelated function (“non-self”). Instead, proprioceptive sensory afferents contact inhibitory 1a interneurons that silence motor neurons with antagonistic function to ensure alternation of flexor-extensor muscle activity at the basis of coordinated motor movement (Eccles et al., 1957). This triangulation of motor, muscle and sensory coordinates raises the question whether motor neuron position is a crucial element in the wiring of sensory connections. Indeed, recent studies in mice have shown that elimination

of a motor neuron transcriptional co-factor for homebox (Hox) family of genes, FoxP1, results in the loss of motor pool identity and the scrambling of settling position. As a consequence, a degraded specificity of sensory-motor connections is observed resulting in sensory afferents innervating "self" and "non-self" motor neurons at similar incidences. In addition, sensory afferents supplying an individual muscle exhibit a striking preference for motor neurons occupying a dorso-ventral position that coincides with the normal tier location of their "self" motor pool. Most strikingly, sensory axons continue to project to the appropriate dorso-ventral tiers within the spinal cord even when motor neurons are no longer present at that location (Dasen et al., 2008; Sürmeli et al., 2011). In contrast, inversion of motor pool positions in the cervical spinal cord does not alter specificity of sensory stimulation (Vrieseling and Arber, 2006). These findings suggest, that positioning of motor pools and columels constitutes part of a spatial logic that helps to establish precise patterns of monosynaptic connectivity, however, also motor neuron position-independent programs contribute to sensory input specificity.

1.2.3 Synchronous firing and neuromuscular stability

Does the clustering of motor neurons into pools have relevance for enhancing the coherence of motor neuron firing? At embryonic stages, motor neurons within a pool are connected by gap junction channels and active junctional communication has been argued to promote coherence in the firing of motor neurons that innervate a particular muscle target, and thus stabilizing neuromuscular connections (Chang et al., 1999). Indeed, the coherence of motor neuron firing is decreased in mutant mice in which gap junctional communication has been prevented by targeted inactivation of the connexin subunit Cx40 and fewer neuromuscular synapses are maintained at postnatal stages in these mutants (Personius et al., 2007). Furthermore, recent findings in the chick brainstem suggest that manipulation of gap junction coupling disrupts coordinated spontaneous activity during formation of nuclei and in turn, pharmacological disruption of spontaneous activity impairs nucleogenesis, demonstrating a functional role for activity (Montague et al., 2017). Thus, these findings suggest that clustering of motor neurons into pools might promote the stability of synaptic connections with target muscles and that gap junctions facilitate spontaneous activity crucial for nucleogenesis.

1.3 Developmental time course of motor and sensory neuron generation

In mouse, spinal motor neurons are generated within the neural tube at the motor neuron progenitor domain (pMN) between embryonic day (e) 9.0 and e11.5, with the peak of neurogenesis occurring around e9.5-e10.5 (Nornes and Das, 1974; Hollyday and Hamburger, 1977; Nornes and Carry, 1978). After exiting the cell cycle, motor neurons migrate from the progenitor zone to the lateral region of the ventral horn of the spinal cord. First, LMCm neurons are generated; then, later-born LMCl neurons migrate through LMCm neurons to reach their final settling position in the lateral ventral horn (Hollyday and Hamburger, 1977; Sockanathan and Jessell, 1998). The migration and segregation of the lateral and medial division of LMC occurs over the period of e11.0-e12.5 with projections of motor axons into the limb mesenchyme first occurring as early as e12.5. Last, defined subsets of motor neurons within each division coalesce to form motor pools with their final settling position achieved by e13.5 (Lin et al., 1998). Globally, spinal motor neuron specification follows a temporal gradient along the ventro-dorsal and rostro-caudal axes: motor neurons located in a more ventral and more rostral position are generated earlier reflecting the progressive expansion of the total volume of the neural tissue and the generation of specific cell types along the rostro-caudal axis (Stifani, 2014).

Sensory neurons arise from neural crest cells around e9.0-e10.0 and delaminate from the dorsal neural tube upon specific inductive signals. Subsequently, they migrate along ventral pathways in chain-like structures and coalesce into ganglia adjacent to the neural tube. Early differentiation processes and peripheral innervation occur between e11.5 and e15.5, while during the last embryonic week central innervation patterns and sensory neuron subtypes can be first identified. Presumably, direct sensory-motor connections are established between e16.0-e18.0. In addition, further sensory neuron subtype specifications and functional connectivity refinements occur during the first postnatal weeks (Lallemend and Ernfors, 2012).

Thus, the well-established positioning of motor neurons long before sensory axonal invasion underscores the hypothesis of a connectivity logic based on motor neuron position.

1.4 Molecular control of motor neuron development and specification

Motor neurons acquire divisional and pool identities through a process of extrinsic signals and transcription factor mediated specification that directs the innervation of target muscle in the periphery (Dasen, 2009). Limb-derived factors play a later role in motor neuron specification by inducing transcription factors that mediate pool clustering and arborization of motor terminals within muscle. The factors that contribute to the specification and diversification of motor neuron subtypes, as well as the down-stream effectors that facilitate the guidance of motor axons to their peripheral targets are well known and briefly described in the following sections.

1.4.1 Spinal motor neuron generation

Spinal progenitor cells are arrayed into different domains at conserved dorso-ventral positions along the midline of the neural tube and give rise to post-mitotic neurons during temporally restricted periods. In the ventral spinal cord, patterning of neural progenitor domains is governed mainly through a gradient of sonic hedgehog (Shh) along the dorso-ventral axis, secreted from the notochord and cells of the floor plate that provides topographic information by regulating the expression of homeodomain and basic helix-loop-helix transcription factors (Alaynick et al., 2011). Five ventral progenitor domains (p0, p1, p2, pMN, p3) give rise to four cardinal interneuron subtypes (V0, V1, V2 and V3) and motor neurons that will provide the main cellular substrate of spinal motor circuits (Figure 2A; Davis-Dusenbery et al., 2014). In the dorsal spinal cord, dorsal bone morphogenetic proteins (Bmps), secreted from the roof plate and surface ectoderm are responsible for producing dorsal cell types, which are typically associated with sensory relay circuits (Jessell, 2000). The ventral part of the neural tube is protected from the dorsalizing effects of Bmps by expression of its antagonist Noggin, which is secreted by the notochord (McMahon et al., 1998).

Shh acts via Gli family of transcription factors to regulate the expression profile of two classes of homeodomain transcription factors in the ventral spinal cord (Shirasaki and Pfaff, 2002). These transcription factors can be roughly divided into two classes based on their regulation in response to Shh signaling: ventrally expressed class II proteins, including Nkx6.1, Olig2 and Nkx2.2 are activated by Shh. Dorsally expressed class I proteins, including Pax6, Pax7, Irx3, Dbx1 and Dbx2 are repressed by Shh (Briscoe et al., 2000; Jessell, 2000; Alaynick et al., 2011). Class I and class II proteins have reciprocal

repressive activities (Pax6 versus Nkx2.2; Dbx2 versus Nkx6.1) that define and maintain the sharp boundaries of the five ventral progenitor domains and ensure the production of defined classes of post-mitotic cells (Briscoe et al., 2000; Jessell, 2000). Specifically, the combined actions of Nkx6.1, Nkx2.2 and Irx3 restrict the generation of motor neurons to a single progenitor domain (Tanabe et al., 1998; Briscoe et al., 2000). The activity of Nkx6.1, when unconstrained by the inhibitory effects of Irx3 and Nkx2.2, is sufficient to induce the expression of the homeodomain protein MNR2, which is first expressed during the final division cycle of motor neuron progenitors and induces the expression of the downstream transcription factors involved in motor neuron specification, including Lim3, Isl1, Isl2 and Hb9 (Figure 2A). This patterning, however, remains constant along the anterior-posterior axis, thus dorso-ventral signaling alone cannot explain the specification of motor neurons into subtypes along the rostro-caudal axis.

1.4.2 Subtype diversification of spinal motor neurons

All spinal motor neurons arise from a single ventral progenitor domain, but how is the further specification of motor neurons into subtypes achieved? Similar to dorso-ventral Shh/Bmps signaling, secreted fibroblast growth factor (FGF) and retinoic acid (RA) form opposing concentration gradients along the rostro-caudal axis to establish broad domains of homeodomain protein expression that are subsequently refined through selective cross-repressive interaction (Figure 2B). Notably, dorso-ventral signaling acts on neural progenitor cells whereas along the rostro-caudal axis, patterning programs are confined to post-mitotic motor neurons (Dasen et al., 2003).

Acquisition of columnar identity

A motor neuron transcriptional network that engages the actions of nearly two dozen of vertebrate Hox proteins has been shown to regulate motor neuron columnar identity and position (Lance-Jones et al., 2001). Hox genes are a large family of chromosomally arrayed genes encoding transcription factors that are instrumental in patterning along the rostro-caudal axis of most animal species (Alexander et al., 2000). In vertebrates, they comprise 39 genes organized in four clusters. In addition, the expression of Hox genes is closely aligned with their position within the Hox cluster: Hox genes located at the 3' end of the cluster are expressed more anteriorly than genes at the 5' end, thus resulting in a relationship between chromosomal location and spatial location (Lemons and McGinnis, 2006). The expression of these chromosomally arrayed Hox

genes is controlled by FGFs and RA signaling: within the neural tube, RA, secreted from the paraxial mesoderm, acts as a rostralizing signal, whereas FGF, derived from the primitive streak, acts as a caudalizing signal, along with the TGFβ family member Gdf11 (Bel-Vialar et al., 2002; Dasen et al., 2003; Liu et al., 2001). Expression and cross-repressive interactions of Hox proteins is closely aligned with the position in which molecularly defined columnar subtypes are generated: at brachial and lumbar levels, motor neurons that express Hox6 and Hox10 proteins, respectively, acquire a LMC identity. Whereas, at thoracic levels, Hox9 gene is essential for the assignment of HMC and PGC motor neuron fates (Figure 2B; Liu et al., 2001; Dasen et al., 2003).

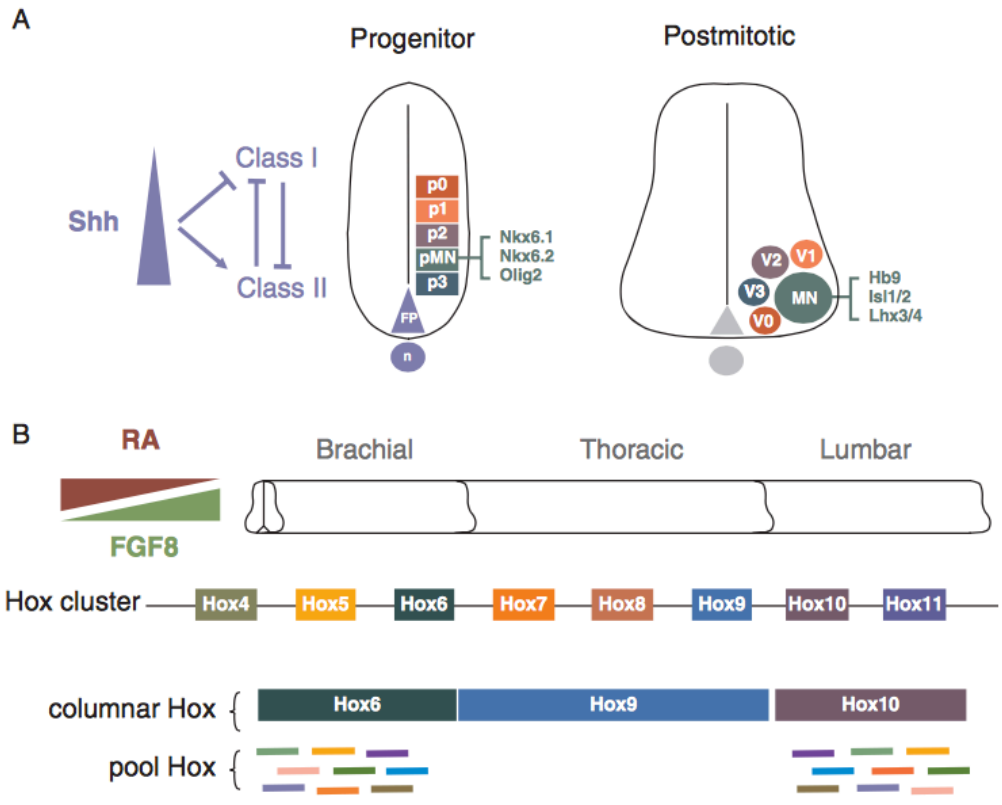

Figure 2: Generation of ventral neuronal subtypes in the spinal cord.
(**A**) A gradient of the secreted protein Sonic hedgehog (Shh) induces the patterned expression of different transcription factors in ventral progenitor domains, which are generated along the dorso-ventral axis of the neural tube. Class I transcription factors are induced while Class II proteins are repressed by Shh signaling. Selective cross-repressive interactions between these two classes sharpen the boundaries between progenitor domains. Each of these progenitor domains gives rise to postmitotic neurons, including motor neurons and several classes of interneurons, expressing specific sets of transcription factors. (**B**) Opposing gradients of retinoic acid (RA) and fibroblast growth factor (FGF) along the rostro-caudal axis of the neural tube induce Hox genes expression. Hox patterns are further refined through cross-repressive interactions giving rise to specific Hox expression profiles in motor columns and pools. From Dasen, 2009.

Misexpression of Hox9 at brachial levels is sufficient to convert LMC to PGC motor neurons, while expression of Hox6 and Hox10 at thoracic levels convert PGC and HMC neurons to a LMC character (Dasen et al., 2003). However, how do MMC motor neurons, which are found all along the body axis, escape Hox rostro-caudal patterning? MMC neuron specification has been associated with a ventral to dorsal decreasing gradient of Wnt4/5 signaling permitting the persistence of Lhx3/4 expression in the most ventral region, which in turn makes MMC neurons unresponsive to Hox patterning (Briscoe and Ericson, 2001; Dasen et al., 2005; Agalliu et al., 2009).

Although Hox protein activities appear to be critical in the generation of motor neuron subtype diversification, several lines of evidence suggest that an additional factor is required to gate their actions in motor neurons (Dasen and Jessell, 2009). Indeed, the network of Hox proteins driving motor neuron diversification depends on the actions of a single accessory factor, the forkhead class homeodomain protein FoxP1. In vertebrates, the FoxP1 protein is selectively expressed by PGC neurons (at low levels) and in LMC neurons (at high levels). The differences in FoxP1 levels is Hox-expression dependent, as misexpression of brachial or lumbar Hox proteins, like Hox6 and Hox10, switches HMC and PGC neurons to FoxP1^{high} LMC motor neurons at thoracic levels (Dasen et al., 2008). Furthermore, inactivating FoxP1 in mice results in the loss of all Hox-dependent steps of LMC motor neurons differentiation and motor neuron identities revert to an ancestral state, consisting of two continuous motor columns, HMCs and MMCs (Dasen et al., 2008; Rousso et al., 2008).

Establishment of divisional identity

An early step of Hox-dependent specification of LMC identity is to direct the expression of RA-synthesizing enzyme retinaldehyde dehydrogenase 2 (Raldh2) and to trigger a series of downstream signaling events that govern the pattern of motor neuron connectivity in the developing limb (Dasen and Jessell, 2009). However, the first step in establishing the acquisition of divisional identity originates as a consequence of the difference in birthdates between motor neurons of the medial and lateral LMC (see Introduction section 1.3). Earlier-born LMCm neurons co-express Isl1/2 and the Raldh2. As a consequence, the secretion of RA by LMCm neurons induces the down-regulation of Isl1 to the profit of the Lim homeobox 1 (Lhx1) in later born LMC neurons, generating LMCl subtype character (Sockanathan and Jessell, 1998). Lhx1 expression in turn, has been shown to direct the projection of LMC motor axons in the dorsal developing limb

through its ability to induce expression of the receptor EphA4, a guidance receptor required for axons to avoid ephrin-a5 repulsive signals originating from the ventral mesenchyme (Eberhart et al., 2002; Kania and Jessell, 2003). Conversely, EphB1 receptor expression, induced by Isl1, directs LMCm axons to the ventral limb mesenchyme by sensitizing them to repulsive signals from the dorsal cells containing ephrinB2 (Luria et al., 2008). Furthermore, local retinoid signaling also serves to suppress PGC and HMC fate (Dasen et al., 2003).

Control of motor pool identity

Two Hox-dependent programs appear to control motor pool fates: one, restricting rostro-caudal pool position, and a second controlling the assignment of transcriptional motor pool identities at intrasegmental levels (Dasen et al., 2005). Patterns of Hox expression that determine motor pool identity along the rostro-caudal axis of the LMC is mainly achieved through a series of cross-repressive interactions, which restrict the complement of Hox genes expressed by motor neuron subsets (Figure 2B). However, how does the motor pool-specific Hox gene expression profile translate into the acquisition of intrasegmental pool subtypes? Hox gene activities impose the pool-restricted expression of two sets of downstream transcription factors: an early limb-independent one, and a second one consisting of transcription factors induced by muscle target. The early intrinsic set of transcription factors, including members of the Runx, POU and Nkx homeodomain proteins, are expressed by motor neurons prior to their axons approaching muscle targets and are important for the selection of certain muscle-specific trajectories (Landmesser, 2001; Dasen et a., 2005, 2008). Nkx6 homeodomain proteins are expressed by subsets of LMC neurons in a pool-specific manner and altering Nkx6.1 expression in motor pools results in a failure of normal target innervation (Dasen et al., 2003; De Marco Garcia and Jessell, 2008). Thus, Nkx6.1 has two sequential roles in motor neuron development: first, it takes part in the specification of motor neuron progenitors in response to Shh signaling and second, it contributes to the specification of discrete motor pools.

The second set of transcription factors are extrinsically induced and expressed in developing motor neurons upon reception of limb-dependent signals. Studies of limb ablation and spinal cord inversion studies in the chick spinal cord have shown that the expression of the ETS genes Er81 and Pea3 depends on peripherally derived signals (Price et al., 2002; Lin et al., 1998). However, so far only one such extrinsic factor has been unambiguously identified: the glial cell derived neurotrophic factor (GDNF) is secreted by

specific cervical muscles inducing the expression of Pea3 in corresponding motor pools and several studies of Pea3 mutant mice have shown the requirement of these later signals for cell body position, axonal arborization and dendritic pattern (Haase et al., 2002; Livet et al., 2002; Vrieseling and Arber, 2006).

What are the mechanisms by which transcription factor identity is translated into precise positional organization of motor pools? To date, the main cell-surface molecules shown to be involved in motor neuron organization are members of the classical cadherin family of adhesion molecules, whose expression is known to be regulated by ETS proteins (Price et al., 2002; Demireva et al., 2011; Bello et al., 2012; Astick et al., 2014).

1.5 The cadherin family of cell-cell adhesion molecules

Cadherins (>100 in mammals) constitute a large family of cell surface glycoproteins, which are defined by the presence of calcium binding, extracellular cadherin (EC) repeats (Shapiro and Weis, 2009). Cadherins can be grouped into several main classes based on sequence homology, protein structure and domain organization and include the classical cadherins, protocadherins, desmosomal, Fat and 7-pass transmembrane cadherins (Takeichi 1995). They are conserved across species and most are expressed in the nervous system where they function in several aspects of neuronal development from neurogenesis and cell migration to synapse formation and plasticity (Takeichi, 2007). By far the best understood members of the cadherin family are the vertebrate classical cadherins.

1.5.1 Classical cadherins

Classical cadherins are defined by five tandem β-sandwich fold EC domains (EC1-5) in the extracellular portion, followed by a single-pass transmembrane domain and two well-conserved catenin binding domains in the cytoplasmic portion (Figure 3A; Brasch et al., 2012, Nollet et al., 2000). The cytoplasmic domain of classical cadherins presents two main motifs: a juxtamembrane region containing a p120 binding binding site and a C-terminal domain containing a catenin binding sequence motif for binding β-catenin and γ-catenin (also know as plakoglobulin). β-catenin and γ-catenin in turn are known to bind to α-catenin, which has a number of binding partners including F-actin (Figure 3A; Ozawa et al., 1989; Thoreson et al., 2000; Kobielak and Fuchs, 2004). The impairment of β-catenin

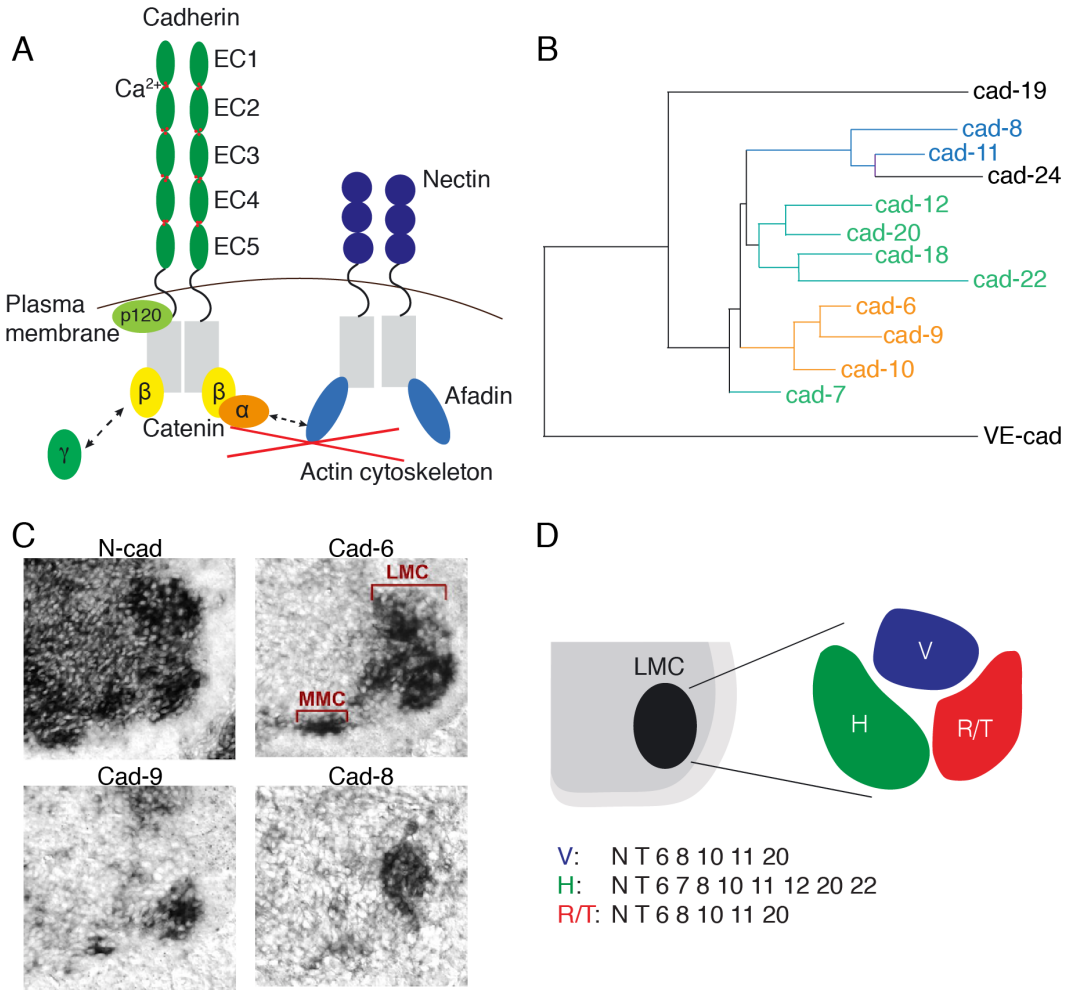

Figure 3: Classical cadherins expression in motor neurons.
(**A**) Classical cadherins have ectodomains composed of five extracellular cadherin (EC) repeats, a single transmembrane region and a cytoplasmic domain that interacts with β- and γ-catenin which in turn bind to the actin-binding α-catenin. In addition, the protein p120 catenin binds to the juxtamembrane portion of the cadherin cytoplasmic domain. Cell adhesion by cadherins depends on the presence of Ca^{2+}, which rigidifies the connections between successive ECs. Nectins consist of three IgG-like loops, a single transmembrane region and a cytoplasmic domain with a C-terminal PDZ binding motif. Nectins bind to the adaptor protein afadin, which in turn directly binds to the actin cytoskeleton. The nectin-afadin complex is thought to provide the first scaffold for adherens junctions and interacts with the cadherin-catenin complex (adapted from Niessen, 2007). (**B**) Phylogram of the type II cadherin family computed from alignment of amino acid sequences of adhesive EC1 and EC2 domain regions using a maximum likelihood method. Branches are colored according to specificity groups. Notably, cadherin-24 may belong to the specificity group of cadherin-8,-11, as it belongs to the same phylogenetic branch, however, shared binding affinities have not been confirmed yet (adapted from Brasch et al., 2018). (**C**) N-cadherin, cadherin-6, cadherin-9 and cadherin-8 expression in e13.5 lumbar spinal cord. N-cadherin and cadherin-6 are expressed by all motor neurons, whereas cadherin-8 and -9 have pool specific expression patterns. Note that cadherin-9 is only expressed at L4-5 lumbar spinal levels (adapted from Demireva et al., 2011). (**D**) Classical cadherin expression by motor pools at lumbar levels L1-L3 (adapted from Demireva et al., 2011).

binding has been shown to result in proteosomal degradation of classical cadherins (Chen et al., 1999).

Based on sequence homology and structural basis of their adhesive dimer interaction, 18 classical cadherins can be subdivided into two closely related families: type I and type II cadherins (Nollet et al., 2000). Type I cadherins include E-cadherin, N-cadherin, P-cadherin, R-cadherin and M-cadherin (cadherin-1-4 and 15, respectively) and are involved in strong cell-cell adhesion. They typically show broad distribution patterns that are segregated by embryonic germ layer or tissue type (Nishimura et al., 1999). Members of type II cadherins include cadherin-6-12, 18-20, 22 and 24, which are associated with less robust cell-cell adhesion and expression patterns are restricted to specific subsets of functionally or anatomically related cell types. Furthermore, type II cadherins appear to be more likely involved in heterophilic binding in contrast to type I cadherins, even though weak binding preferences between N-cadherin and E- and R-cadherin have been observed (Inuzuka et al., 1991; Matsunami et al., 1993). Recent studies have shown that cadherin-8, -11; cadherin-6, -9, -10; cadherin-7, -12, -18, -20, -22 can be organized into three specificity groups according to phylogenetic analyses and binding affinities (Figure 3B; Shimoyama et al., 2000; Brasch et al., 2018).

Several studies suggest that cadherin mediated intercellular adhesion occurs via stereotyped strand-swap binding in their membrane-distal EC1 domains (Zhang et al., 2009, Patel et al., 2006). The amino-terminal β-strands of paired EC1 domains (the A strands) "swap", so that the A strand of one monomer replaces the A strand of the other (Shapiro and Weis, 2009). Here, a key element is the insertion of the side chain from the conserved Trp-2 of the A strand of one protomer into a pocket extending into hydrophobic core of the adhesive partner. Importantly, current data suggest that type I and type II cadherins cannot interact, as they show substantial differences in these binding interfaces. Type II cadherins include two conserved Trp anchor residues, rather than one, and form a hydrophobic interface that runs the length of the EC1 domain (Shaprio and Weis, 2009). Indeed, this proposed lack of adhesive interactions between type I and type II cadherins based on structural analyses has been proven in transfected cell experiments, where cells transfected with a type I cadherin sort out from type II cadherin transfectants, indicating differences in binding affinities (Patel et al., 2006).

1.5.2 Classical cadherins expression and function in the nervous system

Based on expression patterns in developing and mature subdivisions of the nervous system such as brain nuclei, neuronal layers and fiber, classical cadherins have been proposed to play numerous roles in the development and maintenance of the CNS (Krishna-K et al., 2011; Bekirov et al., 2008; Yamagata and Sanes, 1995). Most studies have investigated N-cadherin function and expression in the nervous system as it has been implicated in many early steps in neural development including formation of the neural tube, neuronal migration and neurite outgrowth during axon guidance (Hirano and Takeichi, 2012). In zebrafish and chick, N-cadherin has been shown to be required for correct innervation of specific laminae by retinal optic nerves (Inoue and Sanes, 1997; Masai et al., 2003). One classical example of N-cadherin function during early neuronal development can be found during neurolation, where the invaginating neural plate expresses N-cadherin, while the overlapping ectoderm expresses E-cadherin, separating the two tissues.

In contrast, very few studies have addressed the function of type II cadherins, even though they are differentially expressed in complex combinatorial patterns demarcating neuronal structures and circuits. In the retina it was shown, that cadherin-8 and cadherin-9 play instructive roles in targeting bipolar cells to appropriate sublaminae (Duan et al., 2014). In addition, cadherin-8 mutant mice have been shown to display defects in the physiological detection of cold sensation, most likely due to the loss of cadherin-8 homophilic interactions between cold sensing afferents and their targets. However, no anatomical changes in synaptic morphology or connectivity were detected (Suzuki et al., 2007). In addition, cadherin-6 expression by a subset of in retinal ganglion cells mediates axon target matching in a specific non-image-forming circuit (Osterhout et al., 2011). Lastly, loss of cadherin-11 enhances plastic changes in hippocampal synapses and results in behavioral deficits in fear conditioning (Manabe et al., 2000).

Recent studies indicate that redundancy in the adhesive function of type II cadherin specificity groups is at the basis of neuronal recognition properties as only elimination of all members of a type II cadherin specificity group results in connectivity and functional defects in the retina and hippocampus, respectively, providing an explanation for the small numbers of phenotypes observed in single type II cadherin mutants (Basu et al., 2017; Duan et al., 2018). In addition, classical cadherins have been shown to be important mediators of motor pool sorting in the spinal cord, as it will be briefly described in the following section (Demireva et al, 2011; Patel et al., 2006; Price et al., 2002).

1.5.3 Roles of classical cadherins in motor neuron organization

The remarkable property of type II cadherins expression patterns to highlight anatomical features of the nervous system is clearly evident in motor pools of the spinal cord (Figure 3C; Romanes, 1964; Vanderhost and Holstage, 1997). Combinatorial expression profiles of type II cadherins define motor pools at a molecular level in mouse and chick and genetic manipulation in chick motor neurons has been shown to perturb pools morphogenesis (Figure 3D; Price et al., 2002, Patel et al., 2006; Demireva et al., 2011; Astick et al., 2014). In mouse embryos, inactivation of N-cadherin, expressed by all motor neurons, as well as perturbation of all classical cadherin function through β- and γ-catenin elimination, have been shown to prevent divisional segregation and pool clustering (Demireva et al., 2011). However, because catenin mutations likely affect multiple intracellular signaling pathways and motor neuron disorganization has been reported only in N-cadherin mutants in mouse, the role and contributions of type I and type II cadherins and the nature of the morphogenetic events that lead to motor pool formation remains to be fully understood. In addition, catenin adhesive signaling has been shown to cooperate with nectins, a family of Ca^{2+}-independent immunoglobulin-like CAMs, via direct interaction with afadin (Figure 3A; Mandai et al., 1997; Takai and Nakanishi, 2003; Takai et al., 2008; Harris and Tepass, 2010).

1.6 The afadin/nectin cell adhesive system

The nectin family comprises four members: nectin-1, -2, -3 and -4, which are encoded by the PVRL1, PVRL2, PVRL3 and PVRL4 genes, respectively. Interestingly, their heterophilic trans-interactions are stronger than their homophilic ones in the following order: nectin-1-3 > nectin-2-3 > nectin-1-1, 2-2, and 3-3 (Harrison et al., 2012). Furthermore, they can heterophilically interact in *trans* with the extracellular regions of other Ig-like molecules, including nectin-like molecules (Ikeda 2003). Examples of nectins mediated cell-adhesions can be found in numerous tissues and cell types including mossy-fiber-CA3 synapses in the hippocampus (Mizoguchi et al., 2002), contacts between commissural axons and floor plate cells in the neural tube (Okabe et al., 2004) and the formation of a checkerboard-like mosaic pattern in auditory hair cells (Togashi et al., 2011). Nectins contain an extracellular region with three immunoglobulin-like loops, a single membrane-spanning region and a cytoplasmic tail through which they directly bind afadin, an F-actin-binding protein, via the PDZ domain (Figure 3A). Afadin, α-catenin and

their binding proteins are known to physically mediate the association between nectin and cadherin molecules (Pokutta et al., 2002, Takai et al., 2008). Furthermore, afadin controls nectin adhesive function in similar ways as catenins regulate cadherin activity and cross-talk between nectin/afadin and cadherin/catenin signaling is believed to be an important regulator of cell adhesive function (Takai and Nakanishi, 2003). Afadin links nectins and cadherins by binding to the cytoplasmic domains of nectins and associating with p120-catenin and α-catenin, which in turn interact with the cytoplasmic domains of cadherins (Ozawe et al., 1989, Pokutta et al., 2002). Mice lacking nectins are viable and show relatively moderate phenotypes and no life-threatening disorders most likely due to functional redundancy. In contrast, afadin knock-out mice show embryonic lethality due to impairments in formation of cell-cell junctions, cell movement and cell differentiation (Ikeda et al., 1999). Interestingly, in the developing brain, conditional elimination of afadin has been shown to impair synapse formation and neuronal migration (Beaudoin et al., 2012; Gil-Sanz et al., 2014; Yamamoto et al., 2013; Miyata et al., 2017). However, a potential role for nectin/afadin signaling in motor neuron organization in the spinal cord has not been explored.

2. Aims of the thesis

Motor neurons in the spinal cord are found grouped in nuclear structures termed pools, whose position is precisely orchestrated during development. Despite the emerging role of pool organization in the assembly of spinal circuits, little is known about the morphogenetic programs underlying the positioning of motor neuron subtypes. Thus, in this thesis, spinal motor neurons were used as a prototypic example of the CNS nuclear organization to ask how these nuclei arise during spinal cord development by focusing on the role of cell adhesion molecules.

Aim 1: Establishing and validating a three-dimensional positional analysis to evaluate motor neuron organization.

Aim 2: Assessing the impact of nectin/afadin signaling in the control of motor neuron positional organization.

Aim 3: Testing the roles of type II cadherin specificity groups in motor neuron positional organization.

Aim 4: Evaluating combined function of type I and type II cadherins in motor neuron positional organization.

3. Material

3.1 Antibodies

Table 1: Primary antibodies that were used for immunohistochemistry.

"Self-made" antibodies were generated and used as previously described (Agalliu et al., 2009; Dasen et al., 2008; De Marco Garcia and Jessell, 2008).

Target	Host	Source	Dilution
Afadin	Guinea-Pig	T. Jessell lab, s-m	1:20.000
β-catenin	Rabbit	T. Jessell lab, s-m	1:1000
DsRed	Rabbit	Clonetech 632496	1:1000
Er81	Rabbit	T. Jessell lab, s-m	1:30.000
FoxP1	Rabbit	T. Jessell lab, s-m	1:64.000
γ-catenin	Rabbit	T. Jessell lab, s-m	1:1000
GFP	Chicken	Abcam ab13970	1:1000
Hb9	Rabbit	T. Jessell lab, s-m	1:8000
Isl1	Guinea-Pig	T. Jessell lab, s-m	1:30.000
Lhx3	Mouse	T. Jessell lab, s-m	1:20.000
N-cadherin	Mouse	BD Bioscience 610921	1:1000
Nectin-1	Rat	MBL D146-3	1:200
Nectin-2	Rat	MBL D083-3	1:200
Nectin-3	Rat	MBL D084-3	1:200
Nectin-4	Rabbit	Abcam ab155692	1:200
Nkx6.1	Rat	T. Jessell lab, s-m	1:3000
Nkx6.2	Guinea-Pig	T. Jessell lab, s-m	1:15.000
nNos	Rabbit	T. Jessell lab, s-m	1:16.000
pSMAD	Rabbit	T. Jessell lab, s-m	1:2000

Discosoma red fluorescent protein (DsRed), forkhead box protein P1 (FoxP1), green fluorescent protein (GFP), homebox gene 9 (Hb9), Islet 1 (Isl1), self-made (s-m)

Table 2: Secondary antibodies that were used for immunohistochemistry.

All antibodies were obtained from Jackson ImmunoResearch.

Target	Host	Conjugate	Dilution
Chicken	Donkey	Cy3 Cy5 AF-488	1:1000 1:500 1:1000
Guinea-Pig	Donkey	Cy3 Cy5 AF-488	1:1000 1:500 1:1000
Mouse	Donkey	Cy3 Cy5 AF-488	1:1000 1:500 1:1000
Rabbit	Donkey	Cy3 Cy5 AF-488	1:1000 1:500 1:1000
Rat	Donkey	Cy3 Cy5 AF-488	1:1000 1:500 1:1000

Alexa Fluor (AF), cyanin (Cy)

Table 3: Antibodies that were used for western blots.

Target	Host	Conjugate	Source	Dilution
β-actin	Mouse	-	Merk A5441	1:20.000
Mouse	Goat	HRP	Jackson ImmunoResearch 115-035-003	1:20.000
N-cadherin	Mouse	-	BD Bioscience 610921	1:1000
Pan-Cadherin	Rabbit	-	Abcam ab6529	1:500
Rabbit	Goat	HRP	Jackson ImmunoResearch 111-035-045	1:20.000

Horseradish peroxidase (HRP)

3.2 Plasmids

Table 4: Plasmids that were used for transfections of cell lines.

Name	Source
Cadherin-2-mCherry pCAG	M. Williams lab, s-m
Cadherin-6-EGFP pCAG	M. Williams lab, s-m
Cadherin-6-mCherry pCAG	M. Williams lab, s-m
Cadherin-8-EGFP pCAG	M. Williams lab, s-m
Cadherin-8-mCherry pCAG	M. Williams lab, s-m
Cadherin-9-EGFP pCAG	M. Williams lab, s-m
Cadherin-9-mCherry pCAG	M. Williams lab, s-m
Cadherin-10-EGFP pCAG	M. Williams lab, s-m
Cadherin-10-mCherry pCAG	M. Williams lab, s-m
Cadherin-11-EGFP pCAG	M. Williams lab, s-m
Cadherin-11-mCherry pCAG	M. Williams lab, s-m

3.3 Cell lines

Table 5: Cell lines that were used for *in vitro* experiments.

Cell line	Source	Description
CHO-K1	ATCC	CCL-61
HEK293T	ATCC	CRL-3216

American Type Culture Collection (ATCC), chinese hamster ovary cell line (CHO), human embryonic kidney cell line (HEK)

3.4 Oligonucleotides and PCR programs

Table 6: Oligonucleotides, annealing temperature and extension time used for genotyping mouse lines.

Name	Primers	Ann. temp. (°C)	Extension time (sec)	Fragment length (bp)
Afadin FL	Fwd: TCA GTA CAG GGG AAC AAC AGG Rev: TCA GTA CAG GGG AAC AAC AGG	60	20	WT allele 188bp; FL allele 315 bp
Afadin KO	Fwd: GCC TTA GAG TTA GGA GGA ACA TG Rev: TCA GTA CAG GGG AAC AAC AGG	62	30	WT allele 1482bp; KO allele 238bp
β-catenin FL	Cmn Fw: AAG GTA GAG TGA TGA AAG TTG TT Rev WT: CAC CAT GTC CTC TGT CTA TTC Rev FL: TAC ACT ATT GAA TCA CAG GGA CTT	60	40	WT allele 221bp; FL allele 324bp
Cad-6	Cmn Fw: CATTCTTGCTCCTGCCTATTTGCT Rev WT: CGTACTGATAATCGGATCCCGTGT Rev KO: GAACCTGGTCGAAATCAGTGCGTT	61	90	WT allele 400bp; KO allele 900pb

Cad-8	Fwd WT: GCT AGC TGA GAC GCT CAT GGA CCT CTG GAC Rev WT: AAT GAA GCT TAC CCG GCC AAC GAG AAT CGG Fwd KO: TGT ACT GGA GGC TGA AGT TCA GAT GTG CGG Rev KO: TCC ATG ACC TGA CCA TGC AGA GGA TGA TGC	60	60	WT allele 252bp; KO allele 390bp
Cad-9	Fwd: TGCAGAATTTCAGTGGTTTGG Rev: AGAGTCTAGCAAAGTATTCCAAGCA	60	30	WT allele 740bp; KO allele 700bp
Cad-10	Cmn Fwd: CTGATGAAGTGCTGGAAGCCAGTT Rev WT: CCACGTTTTTGACGGTGAAGGATT Rev KO: GCCGCATAACCAGTGAAACAGCAT	61	90	WT allele 250bp; KO allele 850bp
Cad-11	Cmn Fwd: TTC AGT CGG CAG AAG CAG GAC Rev WT: GTG TAT TGG TTG CAC CAT G Rev KO: TCT ATC GCC TTC TTG ACG AGT TC	55	60	WT allele 270bp; KO allele 420bp
eGFP	Fwd: TCG AGC TGG ACG GCG ACG TAA A Rev: TAG TGG TTG TCG GGC AAG CAG CA	55	60	KO allele 550bp
γ-catenin FL	Fwd: CTT CTG GGA TCT CAG GAG TGT AC Rev: GTC ATG TGC TAG CCC AGT CTA AG	53	30	WT allele 170bp; FL allele 200bp

γ-catenin KO	Cmn Fwd: CGG CCA TCG TCC ATC TCA TC Rev WT: CCT CCT TCT TGG ACA GCT GG Rev KO: CTT CTA TCG CCT TCT TGA CG	53	30	WT allele 300bp; KO allele 150bp
N-cad FL	Fwd: CCA AAG CTG AGT GTG ACT TG Rev: TAC AAG TTT GGG TGA CAA GC	60	10	WT allele 290bp; FL allele 260bp
N-cad KO	Fwd: TGC TGG TAG CAT TCC TAT GG Rev: GTA TGG CCA AGT AAT GGG GAC	60	40	KO allele 450bp
Olig2-cre	Fwd: CGA CGG TGA CTT GAG CAG Rev: TCT GGA TTC ATC GAC TGT GG	60	45	Cre allele 360bp

Base pairs (bp), cadherin (cad), common (Cmn), flox (FL), forward (Fwd), knockout (KO), polymerase chain reaction (PCR), reverse (Rev), wild-type (WT)

3.5 Mouse strains

Table 7: Mouse strains that were used for *in vivo* experiments.

Detailed information on construct design and PCR genotyping strategy has been published as listed below.

Lab name	Official nomenclature	Published by	Source
Afadin FL	*Afdn$^{tm1.1Lfr}$*	Beaudoin III et al., 2012	Jackson Laboratory
Afadin KO	Not registered yet, obtained by crossing *Afdn$^{tm1.1Lfr}$* to *Protamine::cre mice*	O'Gorman et al., 1997	Niccolò Zampieri

β-cat FL	*B6.129-Ctnnb1^{tm2Kem}/KnwJ*	Brault et al., 2001	Jackson Laboratory
Cad-8 KO	*Cdh8^{tm1Mta}/JrsJ*	Suzuki et al., 2007	Jackson Laboratory
Cad-11 KO	*Cdh11^{tm1Mta}/HensJ*	Horikawa et al., 1999	Jackson Laboratory
γ-cat FL	*Jup$^{tm1.1Glr}$/J*	Demireva et al., 2011	Jackson Laboratory
γ-cat KO	*B6.129-Jup^{tm1Ruiz}/J*	Ruiz et al., 1996	Jackson Laboratory
Hlxb9-GFP	*B6.Cg-Tg(Hlxb9-GFP)1Tmj/J*	Wichterle et al., 2002	Jackson Laboratory
KO6910 CAD +/-	*Cdh6$^{-/-}$; cdh9$^{-/-}$; cdh10$^{-/-}$*	Duan et al., 2018	Xin Duan lab
N-cad FL	*B6.129S6(SJL)-Cdh2^{tm1Glr}/J*	Kostetskii et al., 2005	Jackson Laboratory
N-cad KO	*Cdh2^{tm1Hyn}*/J	Radice et al., 1997	Jackson Laboratory
Olig2-cre	*Olig2$^{tm1.1(cre)Wdr}$*	Dessaud et al., 2007	Jackson Laboratory

3.6 Devices and chemicals

Table 8: Devices and equipment that were used to perform the experiments.

Description	Model	Brand
Basic Power/Voltage Supply	Power Pac 200	Bio-Rad
Binocular	MZ8	Leica
Cell Culture Hood	SAFE2020	Thermo Scientific
Centrifuge	Sorvali RC 6+ Centrifuge	Thermo Scientific
Confocal	LSM 800	ZEISS
Cryostat	CM3050 S	Leica
Flaming/Brown Micropipette puller	Model P97, B	Sutter Instrument
Fluid aspiration system	Professional vacuubrand	BVC
Fluorescence Microscope	DFC3000 G	Leica
Fluorescence lamp	HXP 120V	ZEISS
Gel Electrophoresis System	Owl Easycast B1 and B2	Thermo Scientific
Gel imager	C150	azure biosystems
High speed centrifuge	5804	eppendorf
Hotplate stirrer	VMS-C7 advanced	VWR
Incubator	Series CB	Binder
Infrared lamp	SIL06	Sanitas
Inverted microscope	Eclipse TS100	Nikon
Lamp for Binocular	KL1500LCD	Leica
Mercury lamp	Ebq100 isolated	LEJ
Microcentrifuge	PerfectSpin Mini	peqlab
Nanodrop	Spectrophotometer ND-1000	peqlab
Orbital Shaker	Sky Line	ELMI
PCR Cycler	Mastercycler nexus GX2	eppendorf
Pipettes	Research plus	eppendorf
Platform shaker	Polymax1040	Heidolph Instruments
Scale	PF	Shinko Denish
Tabletop Centrifuge	Centrifuge 5415D	eppendorf
Thermomixer	Thermomixer comfort	eppendorf

UV Table	TFX-35	Vilber Lourmat
Vortex Mixer	Vortex-Genie2	Specific Industries
Water bath	Alpha A6	Lauda
Water bath	AQUAline AL12	Lauda

Table 9: Chemicals and kits that were used to perform the experiments.

Name	Company
Agarose Standard	Roth
Ampicilin	Roth
Bovine Serum Albumin	Sigma
B27 Supplement	gibco
Calcium chloride dihydrate	Roth
DAPI, 4',6-Diamidino-2-phenylindole	Sigma
DMEM	gibco
D(+)-Glucose	Roth
Dimethylsulfoxid	Roth
Di-sodium hydrogen phosphate heptahydrate	Roth
dNTP, Deoxynucleotide, Mix	Promega
DPBS with Calcium and Magnesium	PAN Biotech
D(+)-Saccharose	Roth
DTT, Dithiothreitol	Thermo Scientific
ECL Western Blotting Detection Reagents	GE Healthcare
0.5 M EDTA pH 8.0	Ambion
Ethanol	Roth
Ethidium Bromide	Roth
Fetal Bovine Serum Premium	PAN Biotech
F-12K Nutrient Mixture (1x)	gibco
Formamide	Sigma
GeneRuler 1kb Plus	Thermo Scientific
Geneticin, G418	gibco
Glycine	Sigma
GoTagG2 DNA Polymerase	Promega

5x Green GoTaq Reaction Buffer	Promega
Ham's F-12K (Kaighn's) Medium	Thermo Fischer
Hepes buffered saline	Fluka
Heat inactivated horse serum	life technology
Hydrochloric acid (1N)	Roth
KAPA2G Fast ReadyMix + dye (2x)	KAPA Biosystems
Laminin	Sigma
LB-Agar (granulated)	Roth
LB-Medium (granulated)	Roth
Leibovitz L-15 Medium	Thermo Fisher
Lipofectamine 2000	Thermo Fisher
Magnesium chloride hexahydrate	Roth
Methanol	Roth
Neurobasal Medium (1x)	gibco
Nonfat Dry Milk	Cell Signaling Technology
NuPAGE LDS Sample Buffer (4x)	Novex
NuPAGE Tris-Acetate Mini Gels 3-8%	novex
N-2 Supplement (100x)	gibco
Opti-MEM I Reduced Serum Medium (1x)	gibco
Optimum cutting temperature compound	Tissue-Tek
Papain dissociation System	Worthington
Paraformaldehyde	Roth
10x PBS Liquid Concentrate	Merk Millipore
Penicillin Streptomycin	gibco
Poly-L-Lysine	Sigma
Potassium chloride	Roth
2-Propanol	Roth
Protease inhibitor complete ULTRA Tablets, EDTA-free, glass vials	Roche
Proteinase K	Sigma
QIAquick Gel Extraction Kit	QIAgen

QIAquick PCR Purification Kit	QIAgen
QIAprep Spin Maxiprep Kit	QIAgen
QIAprep Spin Miniprep Kit	QIAgen
Recombinant Human BDNF	Merk Millipore
Recombinant Human GDNF	Merk Millipore
Recombinant mouse Cadherin-11/Fc Chimera	R&D Systems
Recombinant mouse N-Cadherin/Fc Chimera	R&D Systems
Restriction Enzymes and Buffers	BioLabs
RIPA buffer	Sigma
Rotiphorese 10x TAE-Buffer	Roth
SeeBlue Plus2 Pre-stained Protein Standard	invitrogen
Sodium acetate	Roth
Sodium carbonate monohydrate	Roth
Sodium chloride	Roth
Sodium dihydrogen phosphate dihydrate	Roth
Sodium hydrogen carbonate	Roth
Sodium hydroxide solution (1N)	Roth
Supersignal West Femto	Thermo Scientific
Sylgard 184	Dow Corning
TRIS	Roth
TRIS-Acetate SDS Running Buffer	novex
Triton X 100	Roth
Trypsin (0.25%), phenol red (1x)	gibco
Trypsin (0.25%), phenol red, without EDTA (1x)	gibco
Tween-20	Sigma
Vectashield (+DAPI)	Vector

3.7 Software

Table 10: Software that was used for analyses.

Name	Description
Adobe Illustrator	CS6
Adobe Photoshop	CS6
Fiji	ImageJ 2.0.0-rc-68/1.52e
GraphPad	Prism 7
IMARIS	Bitplane IMARIS 9.4
Microsoft Office	Excel, PowerPoint, Word, 2011
R	R.app GUI 1.68 R Foundation for Statistical Computing, 2016
R studio	1.0.136 2009 -2016 RStudio, Inc.
ZEN	ZEN 2.3 (blue edition)

4. Methods

4.1 *In vivo* experiments

4.1.1 Spinal cord dissection

The pregnant female mouse was sacrificed via cervical dislocation and embryos were dissected into a petri dish with ice cold PBS (1x). After the placenta and yolk sac were removed, the head was cut off and the rib cage was opened. Heart, lungs and guts were carefully pulled out in order to expose the spinal cord. Embryos were then pinned down (with small pins in shoulders and legs) with the ventral side up, in a dish coated with sylgard gel. Tail biopsies were taken for genotyping.

4.1.2 Genotyping

For *afadin*$^{\Delta MN}$ and *N*$^{\Delta MN}$ mutant mice: Tail biopsies were incubated in 50 µl tail lysis buffer with proteinase K (at 0.1 mg/ml final concentration) over night or for 3 hours at 56°C on a shaking heating block. Samples were then vortexed briefly and centrifuged at 13000 rpm for 2 min. Subsequently, samples were diluted 1:20 in ddH_2O and used for PCR.

Tail lysis buffer

- 50 ml 1 M Tris HCl pH 8.5
- 20 ml 5 M NaCl
- 10 ml 10 % SDS
- 5 ml 0.5 M EDTA
- fill up to 500 ml with ddH_2O and store at room temperature

For *8/11*$^{-/-}$, *6/9/10*$^{-/-}$, *βγ*$^{\Delta MN}$, *N*$^{\Delta MN}$*8*$^{-/-}$ and *N*$^{\Delta MN}$*11*$^{-/-}$ mutant mice: 200 µl of 0.5 M NaOH were added to the tail biopsies and centrifuged briefly. After incubation for 30 min at 95°C on a heating block, 20 µl of 1 M Tris/HCl pH 7.5 were added. Samples were vortexed, centrifuged at 13000 rpm for 5 min and then used for PCR. Oligonucleotides were used according to the mouse line as listed in Materials section 3.4, Table 6. The following protocol was used:

For *afadin*$^{\Delta MN}$ and *N*$^{\Delta MN}$ mutant mice:

5x Green GoTaq Reaction Buffer	5 µl
50x Primer mix (20 µM of each primer)	0.5 µl (0.4 µM each final)
dNTPs (10 µM each)	0.5 µl
GoTagG2 DNA Polymerase	0.125 µl
DNA	1.5 µl
Milli-Q H_2O	to 25 µl

For *8/11*$^{-/-}$, *6/9/10*$^{-/-}$, *βγ*$^{\Delta MN}$, *N*$^{\Delta MN}$*8*$^{-/-}$ and *N*$^{\Delta MN}$*11*$^{-/-}$ mutant mice:

KAPA2G Fast ReadyMix	12.5 µl
50x Primer mix (20 µM of each primer)	0.5 µl (0.4 µM each final)
DNA	1.5 µl
Milli-Q H_2O	to 25 µl

The following PCR program was used:

1.	94°C	3 min	
2.	94°C	30 sec	repeat 40x
3.	Annealing temperature according to Table 6	30 sec	
4.	72°C	Extension time according to Table 6	
5.	72°C	10 min	
6.	10°C	forever	

PCR products were then loaded next to a DNA ladder onto a 1.5-2 % agarose gel containing ethidium bromide for 45 min at 100 V and imaged via UV light at a basic gel documentation system.

4.1.3 Immunohistochemistry

After spinal cord dissection, embryonic spinal cords were fixed with 4 % paraformaldehyde (PFA) for 90 min on ice, cryoprotected by equilibration with 30 % sucrose over night at 4°C and frozen in optimum cutting temperature compound. Lumbar cords were then sectioned at 16 µm using a Leica cryostat. Sections were collected on superfrost plus microscope slides (VWR) and rehydrated with PBS (1x) for 10 min. Immunohistochemistry on cryosections was performed as previously described (Tsuchida et al., 1994). In brief, primary antibodies (in PBX, dilutions according to Materials section 3.1, Table 1) were carefully added for 3 hours at room temperature or over night at 4°C. After three washes with PBX for 5 min each, secondary antibodies (in PBX, dilutions according to Materials section 3.1, Table 2) were added for 1 hour at room temperature. Sections were then washed twice with PBX for 5 min each and once with 1x PBS for 10 min. Slides were cover-slipped using Vectashield (with or without DAPI) as a mounting medium. Immediately afterwards, images were acquired with a 20x objective on a Zeiss LSM 800 confocal microscope.

4 % PFA (100 ml)

- add 20 µl 10 N NaOH to 50 ml of ddH_2O
- microwave for 30 sec
- add 4 g PFA and stir under hood until dissolved
- add 50 ml of 0.2 M PB
- mix and filter
- store at 4°C and use within 48 hrs

PBX

- 0.1 % v/v Triton X 100 in PBS (1x)
- stir and store at room temperature

0.2 M PB (1 L)

- 6.2 g NaH_2PO_4 * $2H_2O$
- 42.88 g Na_2HPO_4 * $7H_2O$
- filter and store at room temperature

30 % sucrose

- 30 % w/v saccharose in 0.1 M PB
- filter and store at 4°C

4.1.4 Motor neuron subtype identification

Median motor column (MMC) neurons were identified by expression of the homeodomain transcription factor Lhx3 or coexpression of Isl1 and Hb9 (Dasen et al., 2008; Rousso et al., 2008). Motor neurons belonging to the PGC were identified by expression of pSMAD and nNOS. At lumbar levels, FoxP1 can be used to identify LMC neurons. Motor neuron divisional subtypes were identified by the expression of homeobox transcription factors Isl1/2 (LMCm) and Hb9 (LMCl; Sockanathan and Jessell, 1998). Motor pools occupying different medio-lateral and dorso-ventral positions at lumbar spinal levels were identified by expression of homeobox and ETS transcription factors (De Marco Garcia and Jessell, 2008). The adductor/gracilis (A/G) pool was identified by expression of Er81 and Nkx6.1; the rectus femoris/tensor fasciae latae (R/T) complex was identified by expression of Nkx6.2; the hamstrings (H) complex was identified by expression of Nkx6.1 and the vasti (V) motor pool was identified by expression of Er81.

4.2 *In vitro* experiments

4.2.1 Cultivation and cryo-preservation of cell lines

Cells were cultured at 37°C, 5 % CO_2 and a relative humidity of 95 % in a Binder CB incubator. Adherent cells were passaged depending on their growth rate at a confluency of about 90 %. For this purpose, medium was removed, cells were washed with 1x PBS and treated with 0.05 % trypsin-EDTA for 5 min at 37°C. Cells were centrifuged at 1000 rpm for 5 min and the required number of resuspended cells was added into a culture dish with fresh serum-containing medium. For cryo-preservation, cells were resuspended in 90 % FBS and 10 % DMSO, transferred to cryotubes and stored for 48 hours at -80°C in cryotube vials (Thermo Fisher). For longtime storage, cells were transferred into liquid nitrogen. Cells were thawed again by incubation at 37°C for 2 min. Thawed cells were taken up into 10 ml cold medium, centrifuged at 1000 rpm for 5 min and seeded in fresh serum-containing medium into appropriate culture dishes.

Culture medium for CHO cells

- F-12 K media
- 10 % FBS Premium
- 1 % Pen Strep
- filter sterilized and stored at 4°C

Culture medium for HEK293 cells

- DMEM without pyruvate
- 10 % FBS Premium
- 1 % Pen Strep
- filter sterilized and stored at 4°C

4.2.2 Transfection of cell lines

Twenty-four hours before transfection, cells were seeded into cell culture dishes to obtain 70-90 % of confluency on the day of transfection. Culture medium was changed to Opti-MEM I Reduced Serum Medium (Opti-MEM) 30 min prior to transfection. DNA and Lipofectamine 2000 were diluted in Opti-MEM, respectively, mixed gently and incubated for 5 min at room temperature. Then, diluted DNA was combined with diluted Lipofectamine 2000, mixed gently and incubated for 20 min at room temperature. DNA-Lipofectamine 2000 complexes were added to cell culture dishes containing cells and Opti-MEM and mixed gently by rocking the plate or slides back and forth. Cells were then incubated at 37°C in an incubator for 24 - 48 hours before testing for transgene expression. Medium was changed back to normal culture medium 4-6 hours post-transfection. The following amounts of DNA and Lipofectamine 200 were used in the experiments:

Cell aggregation assay: 5 µg DNA and 8 µl Lipofectamine 2000 each in 250 µl Opti-MEM; 60 mm cell culture dishes
NOA: 1 µg DNA and 2 µl Lipofectamine 2000 each in 25 µl Opti-MEM; 8-well slides
Stable N-cadherin expressing cell line: 4 µg DNA and 8 µl Lipofectamine 2000 each in 250 µl Opti-MEM; 60 mm cell culture dishes
Co-culture assay: 13.75 µg DNA and 25 µl Lipofectamine 2000 each in 680 µl Opti-MEM; 10 cm cell culture dishes

4.2.3 Generation of a stable cell line expressing N-cadherin

CHO cells, which express no endogenous cadherins (Ginsberg et al., 1991; Figure 27A), were used to generate a N-cadherin-expressing stable cell line.

Killing curve

First, a dose-response curve (killing curve) was established to determine the selective conditions for CHO cells. Cells were seeded into wells of a 24-well plate containing various concentrations of Geneticin (G418 sulfate, a commonly used selection antibiotic for stable cell transfection). The different concentrations ranged from 0 µg/ml to 3000 µg/ml and selection medium was changed every second day for 2 weeks. Wells were examined for viable cells and a concentration of 1500 µg/ml of Geneticin was determined as the most appropriate selective drug concentration required to kill all cells in a well and subsequently added to the media during all steps of the stable cell line generation.

Stable transfection

Cells were seeded into 6 cm dishes and then transfected with an N-cadherin expression vector using Lipofectamine 2000 (according to manufacture's protocol, for details see section 4.3.2). A neomycin selectable marker was included on the DNA construct used for transfection, so that only cells that had acquired the DNA vector would survive. Twenty-four hours after transfection, cells were passaged at different dilutions (1:5 to 1:100) in medium containing Geneticin. For the next three weeks, Geneticin-containing medium was replaced every 2-3 days and cells were passaged at high dilutions to avoid confluency as confluent, non-growing cells are resistant to the effects of antibiotics like Geneticin. During the third week, cells were monitored for distinct "islands" of surviving cells. Using a Nikon Self Inking Object Marker, circles were placed around cell clones of interest on the microscope, which were then picked from the cell culture dishes after one wash with PBS and adding a drop of trypsin on top using a pipette tip. 24 clones were picked in total and added into a 24-well plate containing Geneticin. Clones were then cultured for several days and screened for N-cadherin expression via western blot and immunohistochemistry and called N-cad CHO cells thereafter (Figures 27B and 27C).

4.2.4 Cell aggregation assay (adapted from Basu et al., 2017)

CHO cells or N-cad CHO cells were transfected with different type II cadherins labeled at their C termini with either GFP or mCherry (see Material section 3.2, Table 4) and medium was changed 4-6 hours after transfection to F-12K medium to restrict cell division (see Methods section 4.3.2). 48 hours post transfection cells were washed three times with warm HMF buffer and dissociated with 0.01 % trypsin in HMF buffer for 30 min at 37°C. Cells were subsequently detached, spun down at 1500 rpm for 5 min. Supernatant was discarded and the cell pellet was resuspended in HMF and kept on ice. Cells were then counted using a counting chamber (Neubauer Imroved, Blaubrand) and 75.000 cells expressing a GFP-tagged cadherin were mixed with 75.000 cells expressing a mCherry-tagged cadherin. Cells were plated on HCMF + 1 % BSA coated 8-well glass slides and supplemented to obtain final concentrations of 4 mM $CaCl_2$, 20 mg/ml DNase I, and 1 mM $MgCl_2$ and brought to a final volume of 500 µl. Cells were then shaken in a nutating shaker for 90 min and subsequently fixed by addition of 500 µl of 8% PFA in PBS pH 7.4 and DAPI to label all cell nuclei and kept at 4°C. 12 hours later cells aggregates were carefully transferred with a cut-off p1000 pipette tip to a 8-well glass bottom slide and cell aggregates were imaged using a Zeiss LSM 800 confocal microscope with a 5x magnification lens.

HEPES Mg^{2+} free (HMF) buffer (1 L)

- 137 mM NaCl
- 5.4 mM KCl
- 1 mM $CaCl_2$
- 0.34 mM Na_2HPO_4
- 10 mM HEPES
- 1 g Glucose
- pH 7.4 and filter and store at 4°C
- HCMF is HMF buffer without adding $CaCl_2$

4.2.5 Co-culture assay (adapted from Brasch et al., 2018)

CHO cells or N-cad CHO cells were transfected with different type II cadherins labeled at their C termini with either GFP or mCherry (see Material section 3.2, Table 4) and medium was changed 4-6 hours after transfection to F-12K medium to restrict cell division (see Methods section 4.3.2). 24 hours post transfection cells were washed with

PBS (1x) and dissociated with 0.05 % trypsin for 5 min at 37°C. Cells were subsequently detached and spun down at 1000 rpm for 5 min. Supernatant was discarded and the cell pellet was resuspended in culture medium and kept on ice. Cells were then counted using a counting chamber (Neubauer Imroved, Blaubrand) and equal amounts of cells (25.000) expressing a GFP-tagged cadherin were mixed with cells expressing a mCherry-tagged cadherin. Cell-mixtures were plated on 8-well glass slides (pre-coated with Poly-L-Lysine) and co-cultured over night in an incubator. Cells were then imaged using a Zeiss LSM 800 confocal microscope with a 20x or 40x magnification lens and screened for homotypic cell contacts between cells of the same cell line and heterotypic contacts between cells from different cell lines.

4.2.6 Neurite outgrowth assay (NOA) of primary motor neuron cultures (adapted from Demireva et al., 2011)

Two sets of experiments were performed: 1) Motor neurons were dissociated from e10.5 control (*afadin*$^{fl/+}$*; olig2::Cre+/- ; rosa-lsl-tdTomato*$^{fl/+}$) or *afadin*$^{\Delta MN}$ (*afadin*$^{fl/-}$*; olig2::Cre+/- ; rosa-lsl-tdTomato*$^{fl/+}$) embryos and plated on dishes coated with laminin (15 µg/ml) or N-cadherin protein substrate (15 µg/ml). 2) Motor neurons were dissociated from Hb9:GFP^{+} e10.5 embryos and plated either on CHO cells expressing different sets of classical cadherins (CHO cells or N-cad CHO cells were transfected with cadherin-11 prior to NOA; see Methods section 4.3.2) or on purified protein substrate (N-cadherin and Cadherin-11; 15 µg/ml).

Shortly, embryos were dissected in L-15 medium and kept on ice at all times. Spinal cords were microdissected and isolated from all other tissue. tdTomato or GFP^{+} cords were then selected by visualizing direct fluorescence and dissociated using papain enzymatic treatment as per manufacturer's protocol. In brief, spinal cords were incubated in 400 µl of EBSS medium containing papain powder (with 25 µl DNase) for 45 min in an incubator at 37°C. The caps of the vials were left open to allow gas equilibration during incubation. After incubation, tissue was triturated vigorously until it was completely dissociated and centrifuged for 5 min at 800 rpm. The supernatant was removed and the cell pellet was resuspended in MN media. 20.000 cells were plated per well on 8-well slides (pre-coated with Poly-L-Lysine) coated with different protein substrates or CHO cells. Motor neurons were cultured in MN media between 16 and 20 hours and subsequently fixed in ice-cold PFA for 5 min. Cells were then stained for 2 hours at room temperature with rabbit-anti-GFP or rabbit anti-DsRed antibody, washed three times with

PBS and treated with secondary donkey anti-rabbit antibody conjugated to Alexa-488 or Cy3. After three washes, slides were coverslipped and entire wells were imaged at the confocal microscope. Number of neurites, length, and total number of motor neurons per well were quantified using ImageJ and IMARIS.

MN medium (100ml)

- 50 % Neurobasal medium (without L-Glutamine)
- 50 % DMEM/F12 (with 15mM HEPES, L-Glutamine, pyridoxine)
- 2 % Heat-inactivated horse serum
- 1 x Pen Strep
- filter sterilize the above before adding the following supplements (on day of experiment):
- 1x B27 Supplement
- 1x N2 Supplement
- 100 pg/ml GDNF
- 1 ng/ml BDNF

4.3 Western Blots

4.3.1 Preparation of cell lysate and immunological protein detection

CHO cells, HEK293 cells and N-cad CHO cells were used for western blots. Generation of cell lysates for detection of protein expression was done by resuspension of cells in RIPA lysis buffer freshly supplemented with the protease inhibitors (1x) and dithiothreitol (DTT; 1 M). After 15 min of incubation on a rotating mixer at 4°C, lysates were centrifuged (13000 rpm, 10 min, 4°C) to remove cellular debris. The supernatant was either stored at -20°C or immediately used for protein estimation via Bradford Protein Quantification (according to manufactures instructions). Equal amounts of protein were then prepared with LDS sample buffer and DTT and heated at 72°C for 10 min. For protein separation, a NuPAGE 3-8 % Tris-Acetate 10-well gel was used. As a standard for the molecular weight, the "SeeBlue Plus2 Prestained Standard" was applied. The electrophoresis was performed in Tris-Acetate SDS running buffer (novex) running at 80 V for 15-20 min followed by 150 V.

4.3.2 Protein transfer and immunological protein detection

Separated proteins on gel were transferred via electroblotting onto a PVDF membrane (Immobilon-P, Merck) at 110 V for 60 min in transfer buffer. After transfer, the non-specific protein binding sites were blocked by incubation of the membrane in PBS-T supplemented with 5% milk powder for 1 hour under agitation at room temperature. For antibody staining, the membrane was incubated with an uncoupled protein specific primary antibody in blocking solution over night under agitation at 4°C. The membrane was then washed three times for 10 min with PBS-T and incubated with an HRP-coupled secondary antibody in blocking solution for 1 h under agitation at room temperature (see Materials section 3.1, Table 3). The membrane was then washed three times and protein detection was performed by treating the membrane with the ”ECL western blotting detection reagents” or “SuperSignal West Femto” according to the manufacturers instructions. HRP activity resulted in chemiluminescence signals that were detected using the ChemiDoc.

PBS-T

- 0.1 % Tween-20 in PBS (1x)

Transfer buffer (2 L)

- 6 g TRIS
- 28.8 g Glycine
- 400 ml Methanol
- 1600 ml ddH_2O

4.4 Statistical Analysis

Positional datasets were analyzed using custom scripts in ‘‘R project’’ (R Foundation for Statistical Computing, Vienna, Austria, 2005). Contour and density plots were generated using "ggplot2" package by estimating the Gaussian kernel density for the distribution of neuron positions. Contour plots were calculated from 2D density estimates of neuron positions using a bivariate normal kernel on a 100x100 grid. These calculations rely on the "kde2D" function in the MASS library. Correlation heat maps were used to compare the 2D spatial distribution of neurons across experiments. In order to produce the heat maps, we first computed 2D density estimates of positions on a 100x100 grid. The similarity between pairs of experiments was measured by the Pearson correlation

coefficient of the 2D density estimates on the 100x100 grid. The heat map was then ordered using hierarchical clustering with complete linkage method and the distance metric as *1-r*, where *r* is the Pearson correlation coefficient. The package "corrplot" was used for plotting and ordering the heat map.

Table 11: Genotypes, number of embryos and number of sections per embryo analyzed for three-dimensional positional analysis

Experiment	MN Subtype	Genotype	# of embryos	# of sections/embryo
"control"	Divisions	*afadin fl/+*	3	33 27 30
"control"	Pools	*afadin fl/+*	3	31 29 30
"afadin$^{\Delta MN}$"	Divisions	*afadin fl/-;* *Olig2::Cre+/-*	3	27 26 24
"8/11$^{-/-}$"	Division	*cadherin-8 -/-;* *cadherin-11 -/-*	3	27 32 27
"8/11$^{-/-}$"	Pools	*cadherin-8 -/-;* *cadherin-11 -/-*	3	26 30 24
"6/9/10$^{-/-}$"	Pools	*cadherin-6 -/-;* *cadherin-9 -/-;* *cadherin-10 -/-*	3	19 23 17
"N$^{\Delta MN}$"	Divisions	*N-cadherin fl/-;* *Olig2::Cre +/-*	3	20 30 31
"N$^{\Delta MN}$"	Pools	*N-cadherin fl/-;* *Olig2::Cre +/-*	3	30 26 31
"βγ$^{\Delta MN}$"	Divisions	*β-catenin fl/fl;* *γ-catenin fl/-;* *Olig2::Cre +/-*	3	31 32 30
"βγ$^{\Delta MN}$"	Pools	*β-catenin fl/fl;* *γ-catenin fl/-;* *Olig2::Cre +/-*	3	25 28 28
"N$^{\Delta MN}$8$^{-/-}$"	Divisions	*N-cadherin fl/-;* *cadherin-8 -/-;* *Olig2::Cre +/-*	3	29 31 31
"N$^{\Delta MN}$8$^{-/-}$"	Pools	*N-cadherin fl/-;* *cadherin-8 -/-;* *Olig2::Cre +/-*	3	24 26 26
"N$^{\Delta MN}$11$^{-/-}$"	Pools	*N-cadherin fl/-;* *cadherin-11 -/-;* *Olig2::Cre +/-*	4	24 28 21 19

5. Results

The first part of this doctoral thesis (Results section 5.1 to 5.4) was published in February 2018 in Cell Reports, as listed below. Control and *afadin*$^{\Delta MN}$ motor pool datasets were generated by my colleague Sofia Pimpinella. All other data was generated by me, unless stated otherwise.

Dewitz, C., Pimpinella, S., Hackel, P., Akalin, A., Jessell, T.M., and Zampieri, N. (2018). Nuclear Organization in the Spinal Cord Depends on Motor Neuron Lamination Orchestrated by Catenin and Afadin Function. Cell Rep. 22, 1681–1694

Aim1: Establishing and validating a three-dimensional positional analysis to evaluate motor neuron organization.

5.1 Establishment of a three-dimensional positional analysis to evaluate motor neuron organization

Previous studies performed qualitative analyses to detect defects in motor neuron organization informing about intermixing of different motor neuron subtypes at a local level in the ventral horn (Price et al., 2002; Demireva et al., 2011). These methods share the principle of being designed to measure the segregation or degree of intermixing of two neuronal populations on the basis of their relative position, locally, in the ventral horn. However, they failed to provide any information on the actual position of motor neurons in the spinal cord. Therefore, a different approach to quantitatively analyze motor neuron subtype positioning in three dimensions (3D) was crucial to reveal the cellular and molecular mechanisms controlling motor pool formation (Stepien et al., 2010; Bikoff et al., 2016). Thus, the first aim of this thesis was to generate 3D maps of motor neuron positions using Cartesian coordinates obtained from immunohistochemistry experiments performed on consecutive sections of mouse spinal cord (see Methods section 4.1.3).

5.1.1 Development of three-dimensional analysis of motor neuron positioning

Lumbar levels at e13.5, the earliest point in development when motor neurons have settled in their final position, were analyzed by cutting 16 µm consecutive cryosections and performing immunostaining with specific antibodies recognizing transcriptions factors expressed by motor neuron divisions (Isl1/2 for LMCm neurons; Hb9 for LMCl neurons; Figure 4A) and motor pools (Nkx6.1 for H neurons, Nkx6.2 for R/T neurons, Er81 for V neurons). See Materials section 3.1, Table 1 for more details on antibody concentrations and sources and Methods section 4.1.4 for motor neuron subtype identifications. After acquisition of high-resolution images at the confocal microscope (with wide-field microscopy settings), motor neuron positional coordinates were obtained in an automated and unbiased manner using the "spots" function of the imaging software IMARIS, which assigns x and y values to motor neurons belonging to each divisional or pool subtype. To account for experimental variability in spinal cord size, orientation and shape between embryos sections were rotated and normalized to a standardized spinal cord whose

dimensions were empirically calculated by averaging experimental measurements of e13.5 wild type lumbar spinal cords (midline to the lateral edge: 365 μm; midpoint of the midline to the ventral edge: 340 μm). The rostro-caudal position (z) of each neuron was derived by tracking the order of histological sections. Datasets were aligned on the z axis by starting analysis from the section (z = 0) where either the first Isl1/2$^+$ (for divisional analysis) or Nkx6.1$^+$ motor neuron (for pool analysis) appeared and analysis progressed caudally for 512 μm (for a maximum of 33 sections, 16 μm each), covering approximately the rostral half of the lumbar spinal. These datasets, composed of x, y and z coordinates, were then used to digitally reconstruct 3D motor neuron positions via density and distribution maps as well as correlation analyses with the statistic software R. See Methods section 4.5, Table 11 for genotypes, number of embryos and number of sections analyzed.

5.1.2 Validation of three-dimensional positional analysis

In order to validate the three-dimensional positional analysis, it was first fundamental to test the reproducibility of motor neuron positions belonging to different datasets. Thus, LMC divisional datasets of e13.5 wild type mouse embryos were generated. Transverse and longitudinal projections of cell body position coordinates were plotted to visualize motor neuron distributions on the medio-lateral, dorso-ventral and rostro-caudal axes for three biological replicates (Figures 5). LMCm and LMCl neurons were found in distinct medio-lateral positions in the ventral horn, segregated from each other, as expected by stereotyped positioning of motor neuron divisional subtypes (Figure 4B and 4C; Romanes, 1964; Vanderhorst and Holstege, 1997). Accordingly, overall average medio-lateral/dorso-ventral settling positions of LMCm and LMCl neurons did not reveal obvious differences between replicates, indicating that motor neuron positioning is highly conserved across individuals (Figure 4C). Moreover, both medio-lateral and dorso-ventral distributions were highly reproducible (Figures 4D and 4E). Finally, to assess variability in motor neuron positioning, divisional datasets of individual embryos were compared using correlation analysis. We found that the position of motor neurons sharing the same subtype identity highly correlated with each other (LMCm versus LMCm and LMCl versus LMCl, $r \geq 0.9$), in contrast to datasets of motor neurons residing in different divisions (LMCm versus LMCl and LMCl versus LMCm, $r \leq 0.3$; Figure 4F).

Thus, these findings show that three-dimensional positional analysis is a reliable and reproducible tool required and suitable to quantitatively assess and compare motor neuron organization in the embryonic spinal cord.

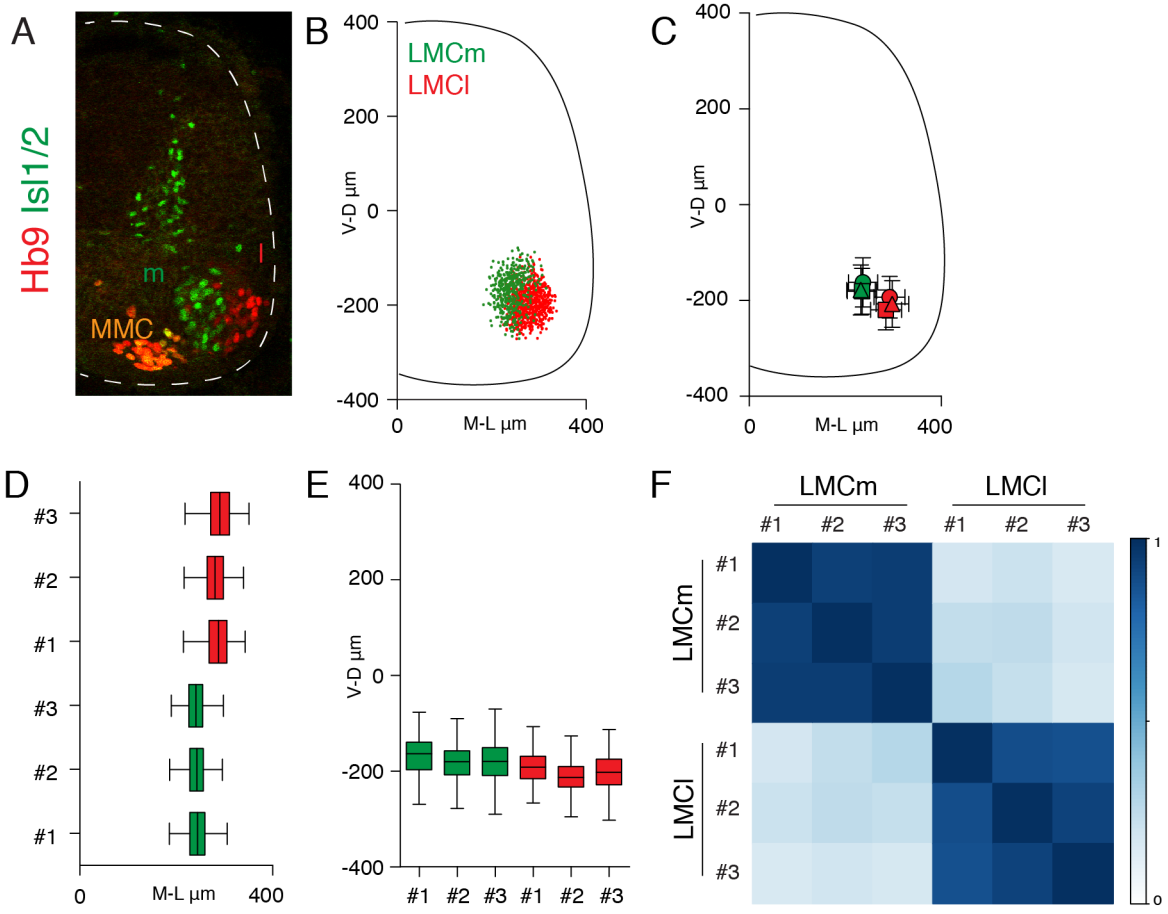

Figure 4: Three-dimensional analysis of motor neuron positions in the developing spinal cord is reproducible.
(**A**) Motor neuron organization in an e13.5 control embryo at lumbar spinal level. Isl1/2^{+} LMCm neurons; Hb9^{+} LMCl neurons; Isl1/2^{+}, Hb9^{+} MMC neurons. (**B**) Digitally reconstructed distribution of LMC neurons at L1-L3, shown as transverse projection. (**C**) Medio-lateral and dorso-ventral positions (mean position ± standard deviation (SD) of LMCm (green) and LMCl (red) neurons (#1 ○; #2 □ ; #3 △). (**D** and **E**) Boxplots showing distributions of LMCm (green) and LMCl (red) neurons along the medio-lateral (**D**) and dorso-ventral (**E**) axes. (**F**) Correlation analysis of LMC positional coordinates. The scale bar indicates correlation values.

5.2 Analysis of motor neuron organization after β- and γ-catenin elimination

Previous work showed that genetic inactivation of β- and γ-catenin, and, to an extent, also of N-cadherin, disrupts divisional segregation of LMC neurons and leads to intermixing of motor pools (Demireva et al., 2011). However, since the actual position of motor neurons in the spinal cord was neglected in those studies, the first set of experiments of this thesis aimed at taking advantage of the three-dimensional positional analysis to perform quantitative analysis of positional defects in β- and γ-catenin mutant embryos before carrying out analyses of individual cadherins and the role of the interactions among

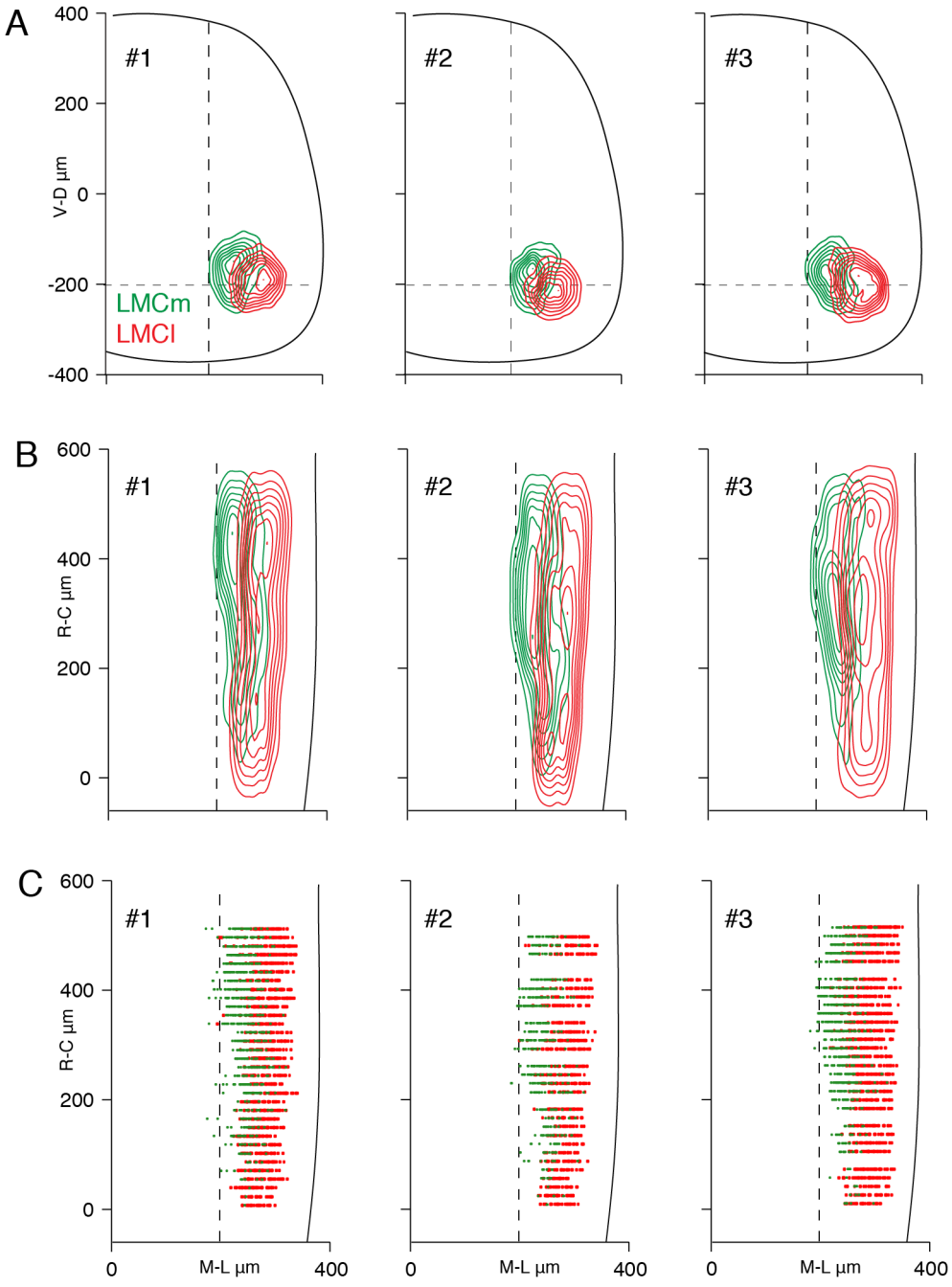

Figure 5: Divisional organization is conserved across individual e13.5 control embryos along all three axes.

(**A**) Transverse contour density plots of LMCm (green) and LMCl (red) neurons (n=3). (**B**) Longitudinal contour density plots of LMCm (green) and LMCl (red) neurons (n=3). (**C**) Longitudinal digital reconstruction of LMCm (green) and LMCl (red) neuronal positions (n=3).

members of the family at a higher resolution. Catenins were eliminated from motor neurons by crossing *olig2::Cre* mice with conditional β- and γ-catenin alleles to generate $\beta^{f/f}$, $\gamma^{f/-}$, *olig2::Cre* mutant mice ($\beta\gamma^{\Delta MN}$; Demireva et al., 2011).

5.2.1 Effects of β- and γ-catenin inactivation on divisional organization

First, divisional organization of motor neurons in $\beta\gamma^{\Delta MN}$ mutant embryos was assessed. Motor neuron subtypes were identified as described in Methods section 4.1.4. Transverse and longitudinal contour plots from control and $\beta\gamma^{\Delta MN}$ embryos revealed clear differences in medio-lateral and dorso-ventral organization (Figures 6A-6F). In $\beta\gamma^{\Delta MN}$ embryos, an overlap in the distribution of LMCm and LMCl neurons could be observed on the medio-lateral axis (Figures 6E and 6F; Figures 7A and 7B). Notably, no local variation in the rostro-caudal distribution of motor neurons was detected, with LMCl neurons from $\beta\gamma^{\Delta MN}$ embryos consistently being found in a medial position at all levels analyzed (Figures 6E and 6F). Surprisingly, the medio-lateral distribution and average position of LMCm neurons in control and $\beta\gamma^{\Delta MN}$ embryos was not significantly different, whereas $\beta\gamma^{\Delta MN}$ LMCl neurons were found in medial positions, causing intermixing with LMCm neurons (Figures 7C and 7D). On the dorso-ventral axis, a ventral shift in the location of both LMCm and LMCl neurons was detected (Figures 7F–7I). To provide an overall assessment of divisional organization in catenin mutants, correlation analysis was used. LMCl neuron positions of $\beta\gamma^{\Delta MN}$ and control embryos were no longer correlated ($\beta\gamma^{\Delta MN}$ versus control LMCl, $r < 0.1$; Figure 6H). In contrast, LMCm neuron positions were still partially correlated despite the ventral shift of the whole motor column in $\beta\gamma^{\Delta MN}$ mutant embryos ($\beta\gamma^{\Delta MN}$ versus control LMCm, $r = 0.58$; Figure 6H). Accordingly, datasets from LMCm neurons of $\beta\gamma^{\Delta MN}$ and control embryos were still highly correlated when only medio-lateral coordinates were considered ($\beta\gamma^{\Delta MN}$ versus control LMCm, $r > 0.9$, $\beta\gamma^{\Delta MN}$ versus control LMCl, $r < 0.3$; Figure 7E).

Thus, in contrast to previous studies, which simply detected a disruption of motor neuron organization after catenin elimination, three-dimensional positional analysis uncovers that inactivation of β- and γ-catenin function perturbs divisional organization in two ways: on the medio-lateral axis by preventing lateral positioning of LMCl neurons and on the dorso-ventral axis by shifting ventrally the location of the whole column (Figure 6G).

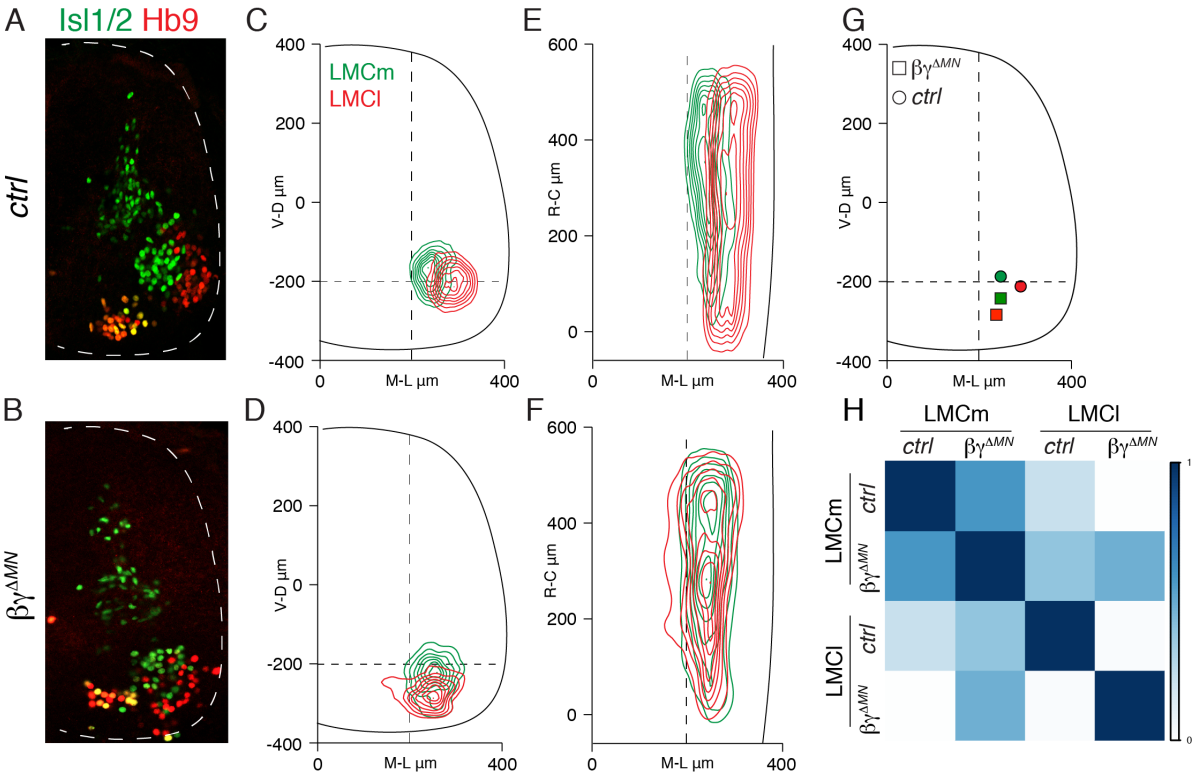

Figure 6: Catenin inactivation perturbs divisional motor neuron organization.
(**A** and **B**) Organization of Isl1/2^{+} medial and Hb9^{+} lateral LMC neurons at lumbar spinal levels in e13.5 control (**A**) and $\beta\gamma^{\Delta MN}$ (**B**) embryos. (**C** and **D**) Transverse contour density plots of LMCm (green) and LMCl (red) neurons in control (**C**) and $\beta\gamma^{\Delta MN}$ (**B**) embryos. (**E** and **F**) Longitudinal contour density plots of LMCm (green) and LMCl (red) neurons in control (**E**) and $\beta\gamma^{\Delta MN}$ (**F**) embryos. (**G**) Average medio-lateral and dorso-ventral positions of LMCm (green) and LMCl (red) neurons in control and $\beta\gamma^{\Delta MN}$ embryos (mean). (**H**) Correlation analysis of LMC neuron positional coordinates in control and $\beta\gamma^{\Delta MN}$ embryos. The scale bar indicates correlation values.

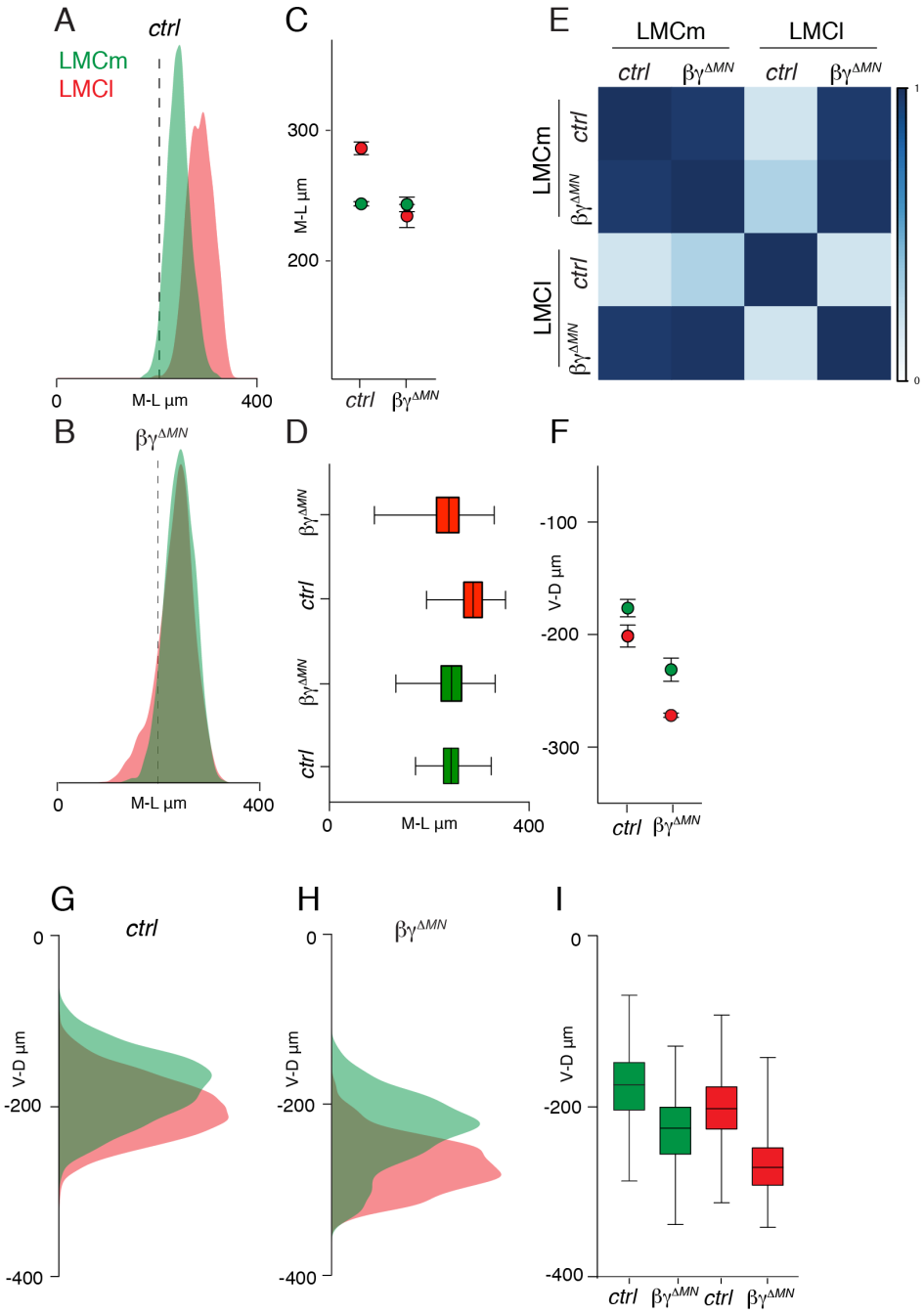

Figure 7: Catenin inactivation impairs LMCl medio-lateral and columnar dorso-ventral motor neuron positioning.

(**A** and **B**) Medio-lateral density plots of LMCm (green) and LMCl (red) neurons in control (**A**) and $\beta\gamma^{\Delta MN}$ (**B**) embryos. (**C**) Average medio-lateral position of LMCm (green) and LMCl (red) neurons in control and $\beta\gamma^{\Delta MN}$ embryos (mean ± SD; differences significant for LMCl neurons; t-test, $p < 0.001$). (**D**) Box-plots showing medio-lateral distributions of LMCm (green) and LMCl (red) neurons in control and $\beta\gamma^{\Delta MN}$ embryos. (**E**) Correlation analysis of LMC positional coordinates on the medio-lateral axis in control and $\beta\gamma^{\Delta MN}$ embryos. Scale bar indicates correlation values. (**F**) Average dorso-ventral position of LMCm (green) and LMCl (red) neurons in control and $\beta\gamma^{\Delta MN}$ embryos (mean ± SD; differences significant for LMCm and LMCl neurons; t-test: LMCm $p < 0.01$; LMCl $p < 0.001$). (**G** and **H**) Dorso-ventral density plots of LMCm (green) and LMCl (red) neurons in control (**G**) and $\beta\gamma^{\Delta MN}$ (**H**) embryos. (**I**) Box-plots showing dorso-ventral distributions of LMCm (green) and LMCl (red) neurons in control and $\beta\gamma^{\Delta MN}$ embryos.

5.2.2 Effects of β- and γ-catenin inactivation on motor pool organization

To test whether three-dimensional positional analysis could also reveal more details about the specific nature of the pool segregation defects in $\beta\gamma^{\Delta MN}$ embryos, the next set of experiments focused on differences in motor neuron subtype position within divisions (Figures 8A and 8B). Motor neuron subtypes were identified as described in section 4.1.4.

First, the effect of β- and γ-catenin inactivation on the positioning of pools that normally reside in different LMC divisions was assessed by analyzing the medio-lateral segregation of medial (hamstring, H) from lateral pools (rectus femoris/tensor fasciae latae, R/T; De Marco Garcia and Jessell, 2008). In control embryos, H neurons were found clearly separated from R/T neurons in medial and lateral positions, respectively (Figures 8C and 8E). In $\beta\gamma^{\Delta MN}$ embryos, motor pool organization is disrupted with H and R/T pools being no longer segregated and occupying largely overlapping areas (Figures 8D and 8F). Distribution and average positional analyses on the medio-lateral axis showed that, consistent with the LMCl phenotype, lateral R/T neurons were found in a medial position (Figures 8G–8I).

Next, the dorso-ventral organization of motor neurons was investigated by analyzing the segregation of dorsal (vasti, V) from ventral pools (H and R/T). Contour, density, and average position analyses showed that segregation of pools on the dorso-ventral axis was lost in $\beta\gamma^{\Delta MN}$ embryos (Figures 8C, 8D, 8J and 8K). Importantly, detailed contour density plots of dorsal and ventral pools showed that, in addition to the overall ventral shift in LMC location, the relative position between dorsal (V) and ventral (H and R/T) neurons was changed, with dorsal V neurons now occupying more ventral positions resulting in a positional overlap with ventral H and R/T neurons (Figures 8L and 9A-F).

Thus, the three-dimensional position analysis reveals that β- and γ-catenin inactivation disrupts motor pool segregation both on the medio-lateral and the dorso-ventral axes.

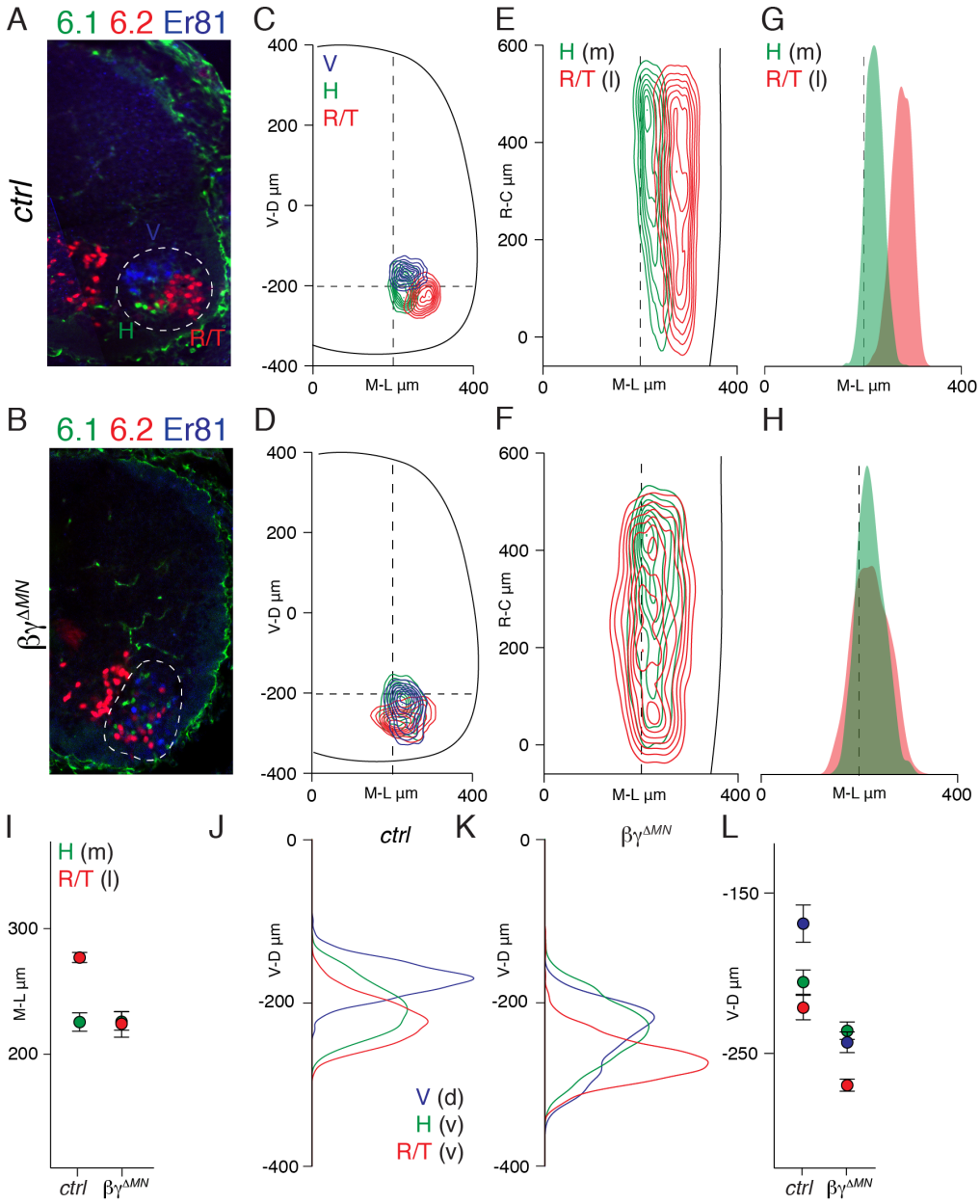

Figure 8: Catenin inactivation disrupts motor pool organization.
(**A** and **B**) Organization of H (Nkx6.1^{+}), R/T (Nkx6.2^{+}) and V (Er81^{+}) motor pools in e13.5 control (**A**) and $\beta\gamma^{\Delta MN}$ (**B**) embryos. The motor neuron area is delimited by a dashed line. (**C** and **D**) Transverse contour density plots of H (green), R/T (red) and V (blue) motor pools in control (**C**) and $\beta\gamma^{\Delta MN}$ (**D**) embryos. (**E** and **F**) Longitudinal contour density plots of H (green, medial) and R/T (red, lateral) neurons in control (**E**) and $\beta\gamma^{\Delta MN}$ (**F**) embryos. (**G** and **H**) Medio-lateral density plots of H (green, medial) and R/T (red, lateral) neurons in control (**G**) and $\beta\gamma^{\Delta MN}$ (**H**) embryos. (**I**) Average medio-lateral position of H (green, medial) and R/T (red) neurons in control and $\beta\gamma^{\Delta MN}$ embryos (mean ± SD; differences significant for H neurons; t-test, $p < 0.01$). (**J** and **K**) Dorso-ventral density plots of H (green, ventral), R/T (red, ventral) and V (blue, dorsal) neurons in control (**J**) and $\beta\gamma^{\Delta MN}$ (**K**) embryos. (**L**) Average dorso-ventral position of H (green), R/T (red) and V (blue) neurons in control and $\beta\gamma^{\Delta MN}$ embryos (mean ± SD; differences significant for H, RT and V neurons; t-test: H $p < 0.05$; R/T and V $p < 0.001$).

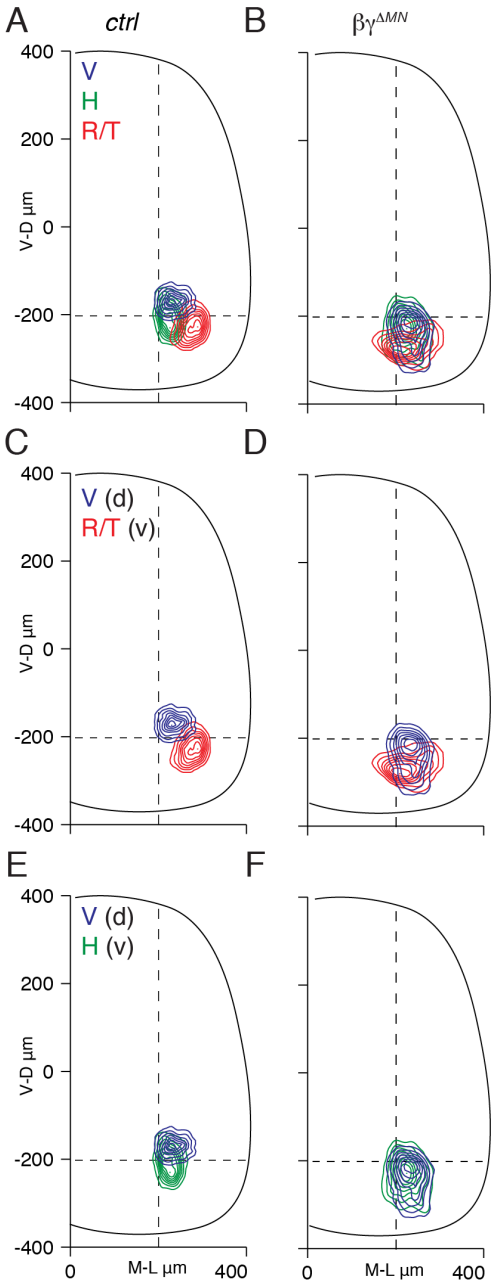

Figure 9: Catenin inactivation impairs dorso-ventral motor pool segregation.
(**A** and **B**) Transverse contour density plots of H (green), R/T (red) and V (blue) motor pools in control (**A**) and $\beta\gamma^{\Delta MN}$ (**B**) embryos. (**C** and **D**) Transverse contour density plots of V (blue, dorsal) and R/T (red, ventral) motor pools in control (**C**) and $\beta\gamma^{\Delta MN}$ (**D**) embryos. (**E** and **F**) Transverse contour density plots of V (blue, dorsal) and H (green, ventral) motor pools in control (**E**) and $\beta\gamma^{\Delta MN}$ (**F**) embryos.

5.3 Analysis of motor neuron organization after N-cadherin elimination

Previous motor neuron intermixing analysis suggested that the defects of N-cadherin mutants phenocopied the ones observed in β- and γ-catenin mutants, albeit less severely (Demireva et al., 2011). Thus, it was of high interest to test whether N-cadherin

elimination recapitulates the β- and γ-catenin inactivation phenotypes using the three-dimensional position assay.

5.3.1 Effects of N-cadherin inactivation on divisional organization

N-cadherin was eliminated from motor neurons by crossing an *olig2::Cre* driver line with mice carrying floxed N-cadherin alleles ($N^{\Delta MN}$; Demireva et al., 2011). The analysis revealed defects in the positioning of LMC neurons in $N^{\Delta MN}$ embryos (Figures 10A–10C). Divisional distribution on the medio-lateral axis showed that elimination of N-cadherin selectively impaired lateral positioning of LMCl neurons whereas LMCm neurons were not affected (Figures 10D and 10E). On the dorso-ventral axis, all LMC neurons were found in more ventral positions phenocopying the defects observed after β- and γ-catenin elimination (Figures 10F and 10G). However, although the medio-lateral defect in $N^{\Delta MN}$ embryos only partially recapitulates the one observed in $\beta\gamma^{\Delta MN}$ embryos, the dorso-ventral phenotype is nearly indistinguishable (Figures 10D-10G).

5.3.2 Effects of N-cadherin inactivation on motor pool organization

Next, motor pool organization was investigated in $N^{\Delta MN}$ mtant mice (Figures 11A and 11B). Analysis of medio-lateral distribution of medial (H) and lateral (R/T) pools confirmed divisional data that elimination of N-cadherin specifically impairs LMCl neuron subtype positioning (Figures 10C-11E; Figures 11C-11E). Surprisingly, on the dorso-ventral axis, transverse contour analysis indicated that, despite the ventral shift in columnar location, motor pool segregation in the absence of N-cadherin function was not completely eroded, as observed in $\beta\gamma^{\Delta MN}$ embryos (Figures 11A and 11B; Figures 8B and 8D). Density, distribution and average position analyses on the dorso-ventral axis confirmed that segregation of motor pool subtypes was mostly preserved (Figures 11F, 11H and 11I). As a consequence, the average distance between dorsal and ventral pools in $N^{\Delta MN}$ embryos was not significantly different from control embryos, as opposed to $\beta\gamma^{\Delta MN}$ embryos (Figure 11G).

Thus, three-dimensional positional analysis reveals that N-cadherin elimination, although accounting entirely for the columnar positioning defect and partially for the LMCl medio-lateral phenotype, does not recapitulate the dorso-ventral motor pool mixing phenotype of β- and γ-catenin mutants.

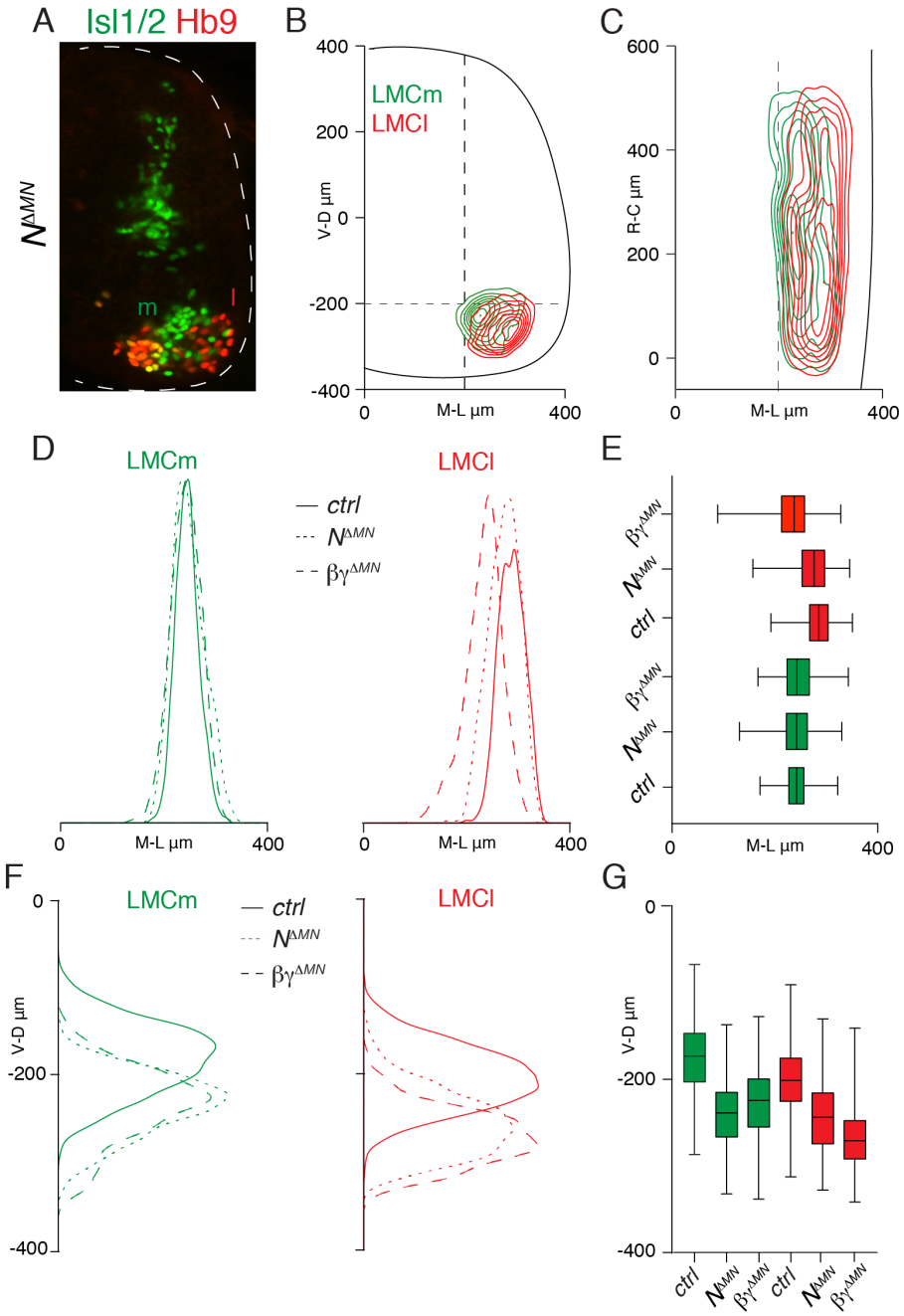

Figure 10: N-cadherin elimination perturbs divisional motor neuron organization.
(**A**) Organization of Isl1/2^{+} medial and Hb9^{+} lateral LMC neurons at lumbar spinal levels in e13.5 $N^{\Delta MN}$ embryos. (**B**) Transverse contour density plots of LMCm (green) and LMCl (red) neurons in $N^{\Delta MN}$ embryos. (**C**) Longitudinal contour density plots of LMCm (green) and LMCl (red) neurons in $N^{\Delta MN}$ embryos. (**D**) Medio-lateral density plots of LMCm (green) and LMCl (red) neurons in control (solid line), $N^{\Delta MN}$ (dotted line) and $\beta\gamma^{\Delta MN}$ (dashed line) embryos. (**E**) Box-plots showing medio-lateral distributions of LMCm (green) and LMCl (red) neurons in control, $N^{\Delta MN}$ and $\beta\gamma^{\Delta MN}$ embryos. (**F**) Dorso-ventral density plots of LMCm (green) and LMCl (red) neurons in control (solid line), $N^{\Delta MN}$ (dotted line) and $\beta\gamma^{\Delta MN}$ (dashed line) embryos. (**G**) Box-plots showing dorso-ventral distributions of LMCm (green) and LMCl (red) neurons in control, $N^{\Delta MN}$ and $\beta\gamma^{\Delta MN}$ embryos.

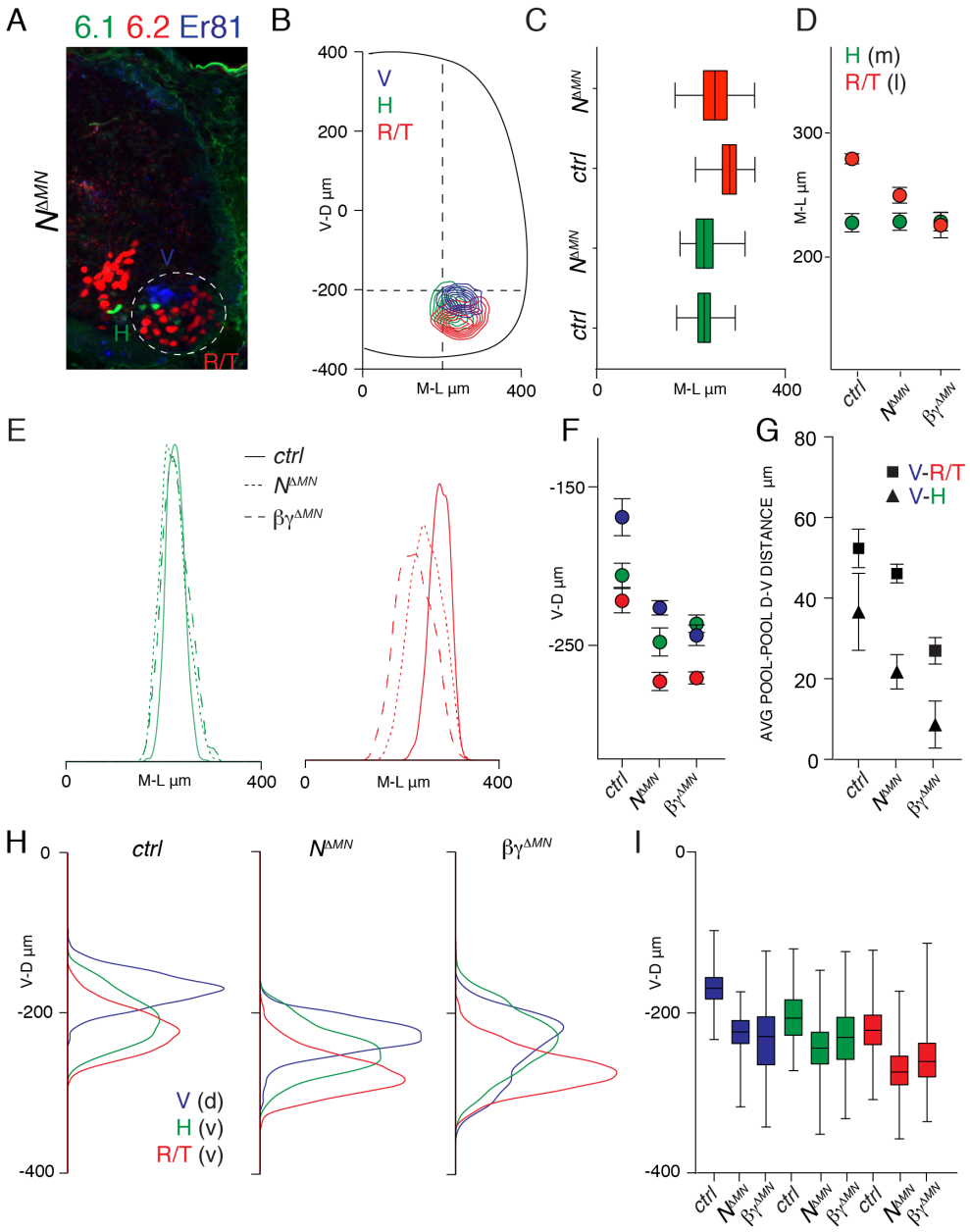

Figure 11: N-cadherin elimination does not perturb dorso-ventral pool segregation.
(**A**) Organization of H (Nkx6.1$^+$), R/T (Nkx6.2$^+$) and V (Er81$^+$) motor pools in e13.5 $N^{\Delta MN}$ embryos. The motor neuron area is delimited by a dashed line. (**B**) Transverse contour density plots of H (green), R/T (red) and V (blue) motor pools in $N^{\Delta MN}$ embryos. (**C**) Box-plots showing medio-lateral distributions of H (green), R/T (red) and V (blue) motor pools in control, $N^{\Delta MN}$ and $\beta\gamma^{\Delta MN}$ embryos. (**D**) Average medio-lateral position of H (green, medial) and R/T (red, lateral) neurons in control, $N^{\Delta MN}$ and $\beta\gamma^{\Delta MN}$ embryos (mean ± SD; differences significant for R/T neurons: control versus $N^{\Delta MN}$ $p < 0.01$; control versus $\beta\gamma^{\Delta MN}$ $p < 0.001$; $N^{\Delta MN}$ versus $\beta\gamma^{\Delta MN}$ $p < 0.05$; one-way ANOVA followed by post hoc Tuckey's honest significant test (HSD)). (**E**) Medio-lateral density plots of H (green, medial) and R/T (red, lateral) neurons in control (solid line), $N^{\Delta MN}$ (dotted line) and $\beta\gamma^{\Delta MN}$ (dashed line) embryos. (**F**) Average dorso-ventral position of H (green, ventral), R/T (red, ventral) and V (blue, dorsal) neurons in control, $N^{\Delta MN}$ and $\beta\gamma^{\Delta MN}$ embryos (mean ± SD; differences significant for V neurons: control versus $N^{\Delta MN}$ and $\beta\gamma^{\Delta MN}$ $p < 0.001$; for R/T neurons: control versus $N^{\Delta MN}$ and $\beta\gamma^{\Delta MN}$ $p < 0.001$; for H neurons: control versus $N^{\Delta MN}$ and $\beta\gamma^{\Delta MN}$ $p < 0.01$; one-way ANOVA and post hoc Tukey's HSD test). (**G**) Average distance between dorso-ventral positions of V-R/T (■) and V-H (▲) pools in control, $N^{\Delta MN}$ and $\beta\gamma^{\Delta MN}$ embryos. (**H**) Dorso-ventral density plots of H (green, ventral), R/T (red, ventral) and V (blue, dorsal) neurons in control, $N^{\Delta MN}$ and $\beta\gamma^{\Delta MN}$ embryos. (**I**) Box-plots showing dorso-ventral distributions of H (green, ventral), R/T (red, ventral) and V (blue, dorsal) motor pools in control, $N^{\Delta MN}$ and $\beta\gamma^{\Delta MN}$ embryos.

Aim 2: Assessing the impact of nectin/afadin signaling in the control of motor neuron positional organization.

5.4 Analysis of motor neuron organization after afadin elimination

The limited effect on dorso-ventral pool segregation observed after N-cadherin elimination suggests the involvement of additional catenin-dependent effectors. Type II cadherins are obvious candidates because motor neuron subtypes can be distinguished by their combinatorial expression and manipulations that equalize type II cadherin profiles disrupt motor pool segregation in chick spinal cord (Figure 3D, Price et al., 2002). However, genetic mouse models where type II cadherins have been eliminated either individually or in combination exhibit no defect in motor neuron positioning (N.Z., unpublished data). Thus, one hypothesis to test was whether catenins might regulate dorso-ventral motor neuron sorting by engaging the activity of nectins. To start studying a possible involvement of nectin signaling, the focus was set on afadin, an intracellular transducer molecule that is necessary for nectin-mediated adhesive function (Figure 3A; Takai and Nakanishi, 2003).

5.4.1 Motor neuron generation, differentiation and columnar organization in afadin mutant embryos

Nectins are not strongly expressed in the spinal cord during development (Figures 13C-13F), whereas afadin mRNA and protein are expressed in motor neurons throughout the developmental period encompassing their generation, migration, and final positioning in the ventral horn of the spinal cord (Figures 12A and 12B, 13A and 13B). Because afadin constitutive inactivation results in gross developmental defects and abortion by e10.5 due to its essential roles during gastrulation, afadin deletion was targeted to motor neurons by using a conditional approach (Ikeda et al., 1999). Afadin heterozygous mutants are indistinguishable from wild-type mice; thus, mice carrying one copy of a constitutive mutant allele (*afadin*$^{-}$) and one copy of a floxed allele (*afadin*^{fl}) were crossed with the *olig2::Cre* driver line to restrict recombination to motor neuron progenitors and generated *afadin*$^{fl/-}$; *olig2::Cre+/-* mice (*afadin*$^{\Delta MN}$; Beaudoin et al., 2012; Dessaud et al., 2007).

Afadin was effectively eliminated from spinal motor neurons in *afadin*$^{\Delta MN}$ embryos (Figures 12C–12F). The first step was then to evaluate whether afadin elimination has an

effect on motor neuron generation and subtype identity. Motor neuron columnar subtypes were distinguished using transcription factor expression profiles as described in Methods section 4.1.4. The total number of neurons generated was similar in control and *afadin*$^{\Delta MN}$ embryos and no significant differences in the numbers of LMC and MMC neurons were observed (Figures 12G–12I). Similarly, no differences in the generation, differentiation, and overall organization of motor columns were detected at thoracic levels (Figures 12J–12L).

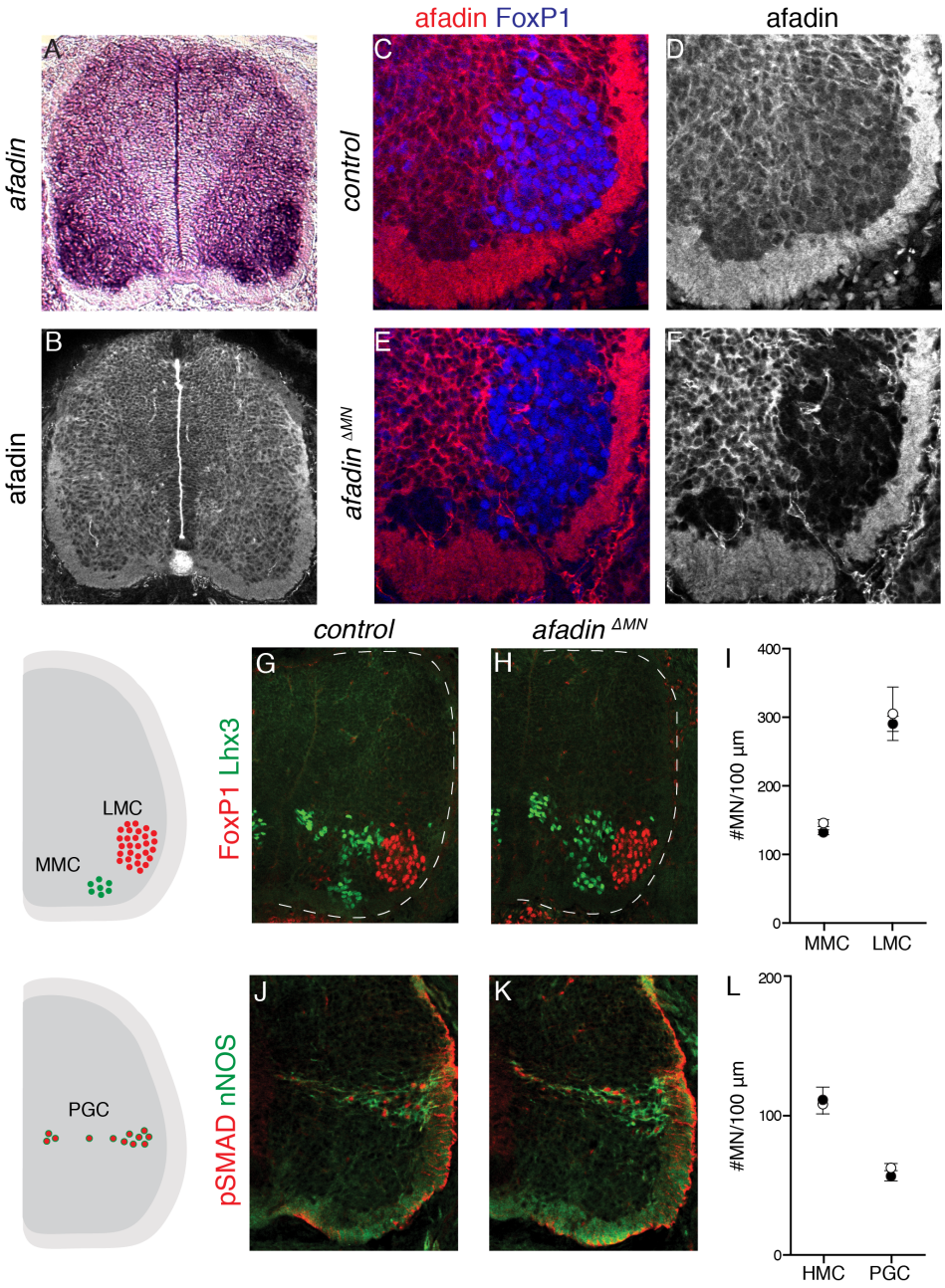

Figure 12: Afadin expression and motor neuron generation in the developing spinal cord.
(**A** and **B**) Afadin mRNA (**A**) and protein (**B**) expression in e13.5 lumbar spinal cord. (**C–F**) Afadin expression in e13.5 lumbar spinal cord in control (**C** and **D**) and *afadin*$^{\Delta MN}$ (**E** and **F**) embryos. FoxP1 identifies LMC neurons. (**G** and **H**) Segregation of Lhx3^{+} MMC and FoxP1^{+} LMC neurons in e13.5 lumbar spinal cord of control (**G**) and *afadin*$^{\Delta MN}$ (**H**) embryos. (**I**) Number of MMC and LMC neurons found in e13.5 lumbar spinal cord of control (○) and *afadin*$^{\Delta MN}$ (●) embryos. Motor neurons/100 µm, mean ± SD. (**J** and **K**) pSMAD^{+}, nNOS^{+} preganglionic column (PGC) neurons in e13.5 thoracic spinal cord of control (**J**) and *afadin*$^{\Delta MN}$ (**K**) embryos. (**L**) Number of hypaxial motor column (HMC) and PGC neurons in e13.5 thoracic spinal cord of control (○) and *afadin*$^{\Delta MN}$ (●) embryos. Motor neurons/100 µm, mean ± SD.
In situ hybridization experiment for Afadin mRNA expression was performed by Niccolò Zampieri. HMC and PGC neuron immunostaining and counts were performed by Sofia Pimpinella.

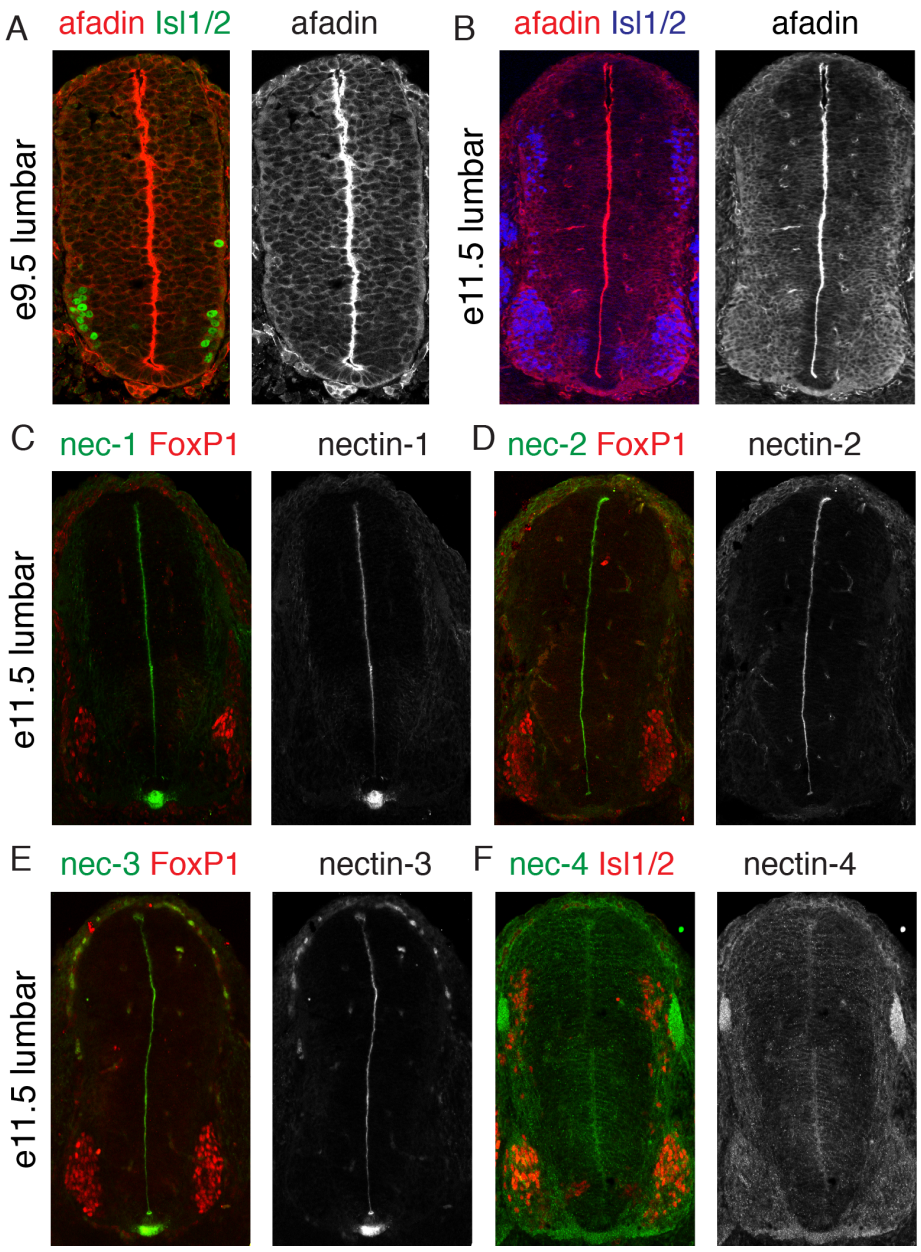

Figure 13: Afadin and nectins expression in the developing spinal cord.
(**A**) Afadin expression at lumbar spinal level of e9.5 wild type embryo. (**B**) Afadin expression at lumbar spinal level of e11.5 wild type embryo. (**C**) Nectin 1 expression at lumbar spinal level of e11.5 wild type embryo. (**D**) Nectin 2 expression at lumbar spinal level of e11.5 wild type embryo. (**E**) Nectin 3 expression at lumbar spinal level of e11.5 wild type embryo. (**F**) Nectin 4 expression at lumbar spinal level of e11.5 wild type embryos. FoxP1 identifies LMC neurons. Isl1/2 neurons identifies LMCm neurons.
Part of the nectin immunostainings were performed by Sofia Pimpinella.

5.4.2 Effects of afadin inactivation on motor neuron organization

Next, it was investigated whether divisional and pool organization is affected by the loss of afadin. In e13.5 *afadin*$^{\Delta MN}$ embryos, intermixing of medial and lateral LMC neurons was detected as well as defects in the clustering and segregation of motor pools

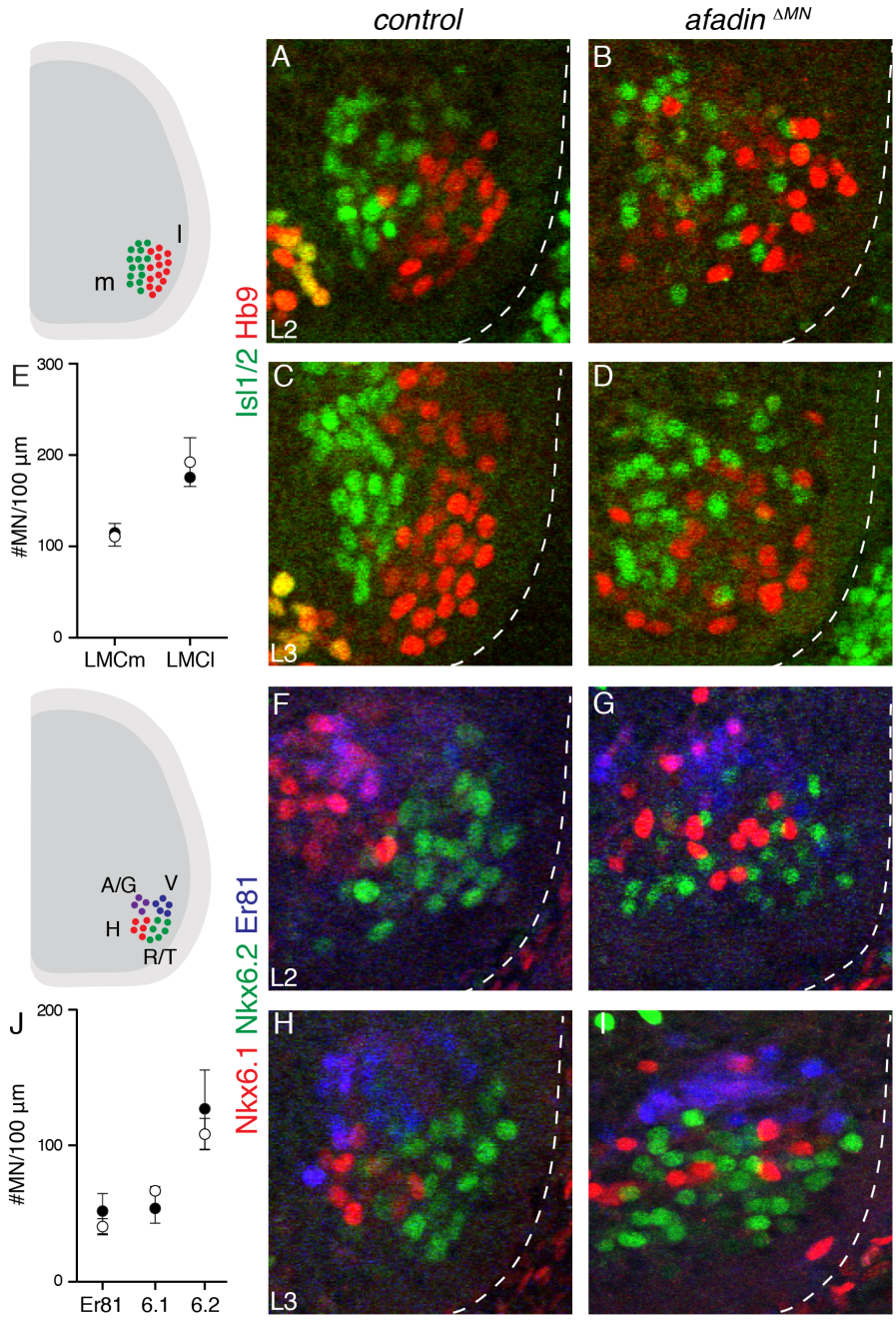

Figure 14: Perturbed divisional and pool organization in afadin mutant mice.
(**A-D**) Isl1/2^{+} medial and Hb9^{+} lateral LMC neurons at L2/L3 in e13.5 control (**A** and **C**) and *afadin*$^{\Delta MN}$ (**B** and **D**) embryos. (**E**) Number of LMCm and LMCl neurons in e13.5 lumbar spinal cord of control (○) and *afadin*$^{\Delta MN}$ (●) embryos. Motor neurons/100 µm, mean ± SD.(**F–I**) Motor pools at L2/L3 in e13.5 control (**F** and **H**) and *afadin*$^{\Delta MN}$ (**G** and **I**) embryos. Nkx6.1^{+}, Er81^{+} adductor/gracilis (A/G) neurons; Er81^{+}, Nkx6.1^{-} V neurons; Nkx6.2^{+} R/T neurons; Nkx6.1^{+}, Er81^{-} H neurons. (**J**) Number of Er81^{+}, Nkx6.1^{+}, and Nkx6.2^{+} motor neurons in e13.5 lumbar spinal cord of control (○) and *afadin*$^{\Delta MN}$ (●) embryos. Motor neurons/100 µm, mean ± SD. Motor pool counts were performed by Sofia Pimpinella.

(Figures 14A–14D and 14F–14I). However, no changes in the numbers of motor neurons allocated to the lateral and medial division or to the pool subtypes analyzed were observed (Figures 14E and 14J).

Thus, afadin elimination does not interfere with the acquisition of motor neuron divisional and pool identities but selectively abolishes their positional organization.

The next step was to use three-dimensional position analysis to assess motor neuron organization defects in *afadin*$^{\Delta MN}$ embryos in more detail. At a divisional level a perturbation in the segregation of LMCm and LMCl neurons could be observed (Figures 15A and 15B). Medio-lateral distribution and average position analyses indicated that afadin inactivation selectively impairs the ability of LMCl neurons to settle laterally to LMCm neurons (Figures 15D and 15E). On the dorso-ventral axis, a subtle ventral shift in columnar location was detected (Figure 15C). To provide a quantitative assessment of divisional organization in afadin mutants, correlation analysis was used (Figure 15F). LMCm neuron positions of *afadin*$^{\Delta MN}$ and control embryos were highly correlated (*afadin*$^{\Delta MN}$ versus control LMCm, r = 0.91), indicating that the overall spatial organization of these neurons is not affected by afadin elimination. In contrast, correlation of LMCl neuron positions of *afadin*$^{\Delta MN}$ and control embryos was reduced (*afadin*$^{\Delta MN}$ versus control LMCl, r = 0.65).

Next, the effect of afadin inactivation on motor pool organization was investigated. These data were generated by my colleague Sofia Pimpinella. Consistent with the divisional data, the pool position analysis indicated that afadin inactivation selectively impairs the ability of motor neurons with a lateral identity (R/T) to settle past motor neurons with a medial identity (H; Figure 15G, data not shown). She also analyzed the segregation and clustering of dorsal (V) and ventral (H and R/T) motor pools. Transverse contour density plots indicated that the relative dorso-ventral organization of motor pools was not affected by afadin inactivation (Figures 15G). Analyses of dorso-ventral distribution and average position did not reveal significant differences between control and afadin mutants (Figures 15H and 15I).

Thus, these data indicate that afadin signaling specifically controls motor neuron segregation on the medio-lateral axis by regulating LMCl positioning, but is not required for motor neuron organization on the dorso-ventral axis.

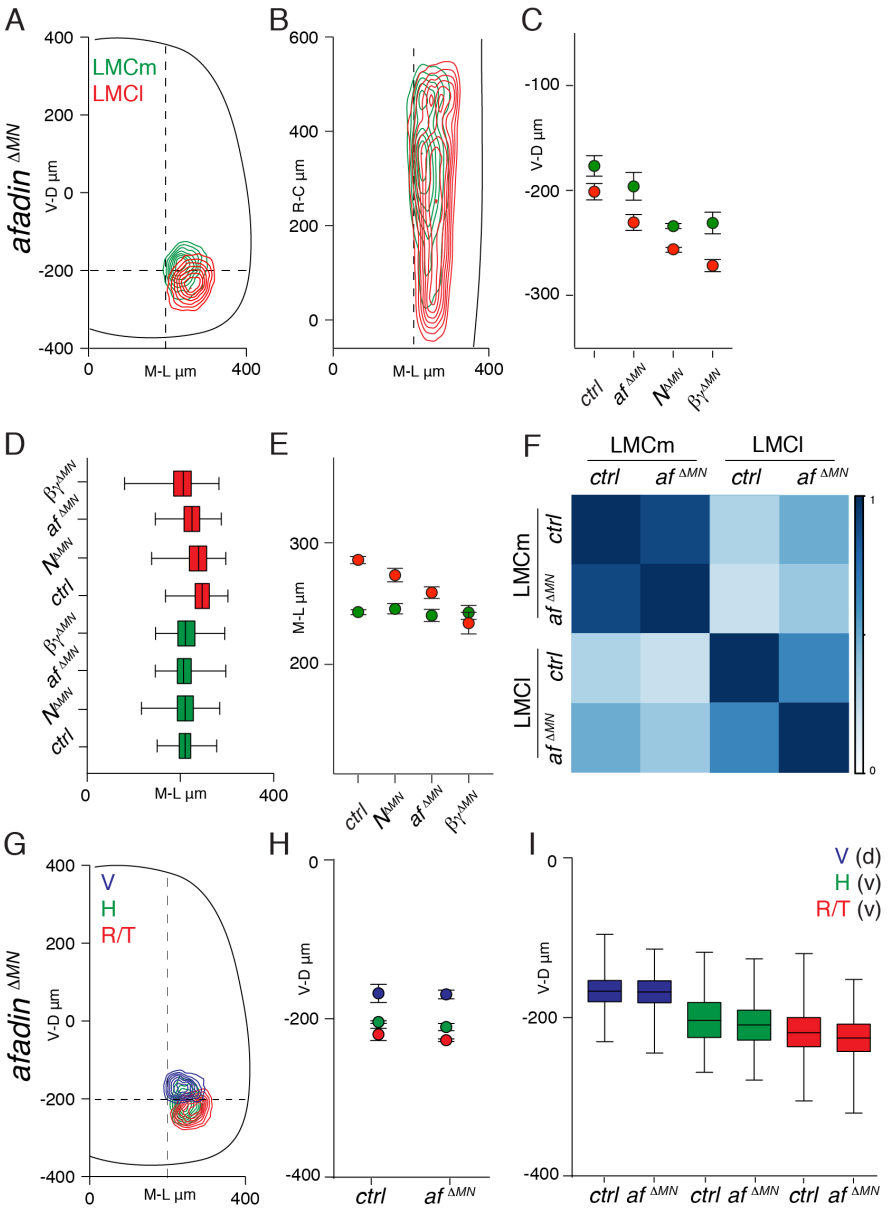

Figure 15: Afadin is required for medio-lateral but not dorso-ventral motor neuron positioning.
(**A** and **B**) Transverse (**A**) and longitudinal (**B**) contour density plots of LMCm (green) and LMCl (red) neurons in e13.5 *afadin*$^{\Delta MN}$ embryos. (**C**) Average dorso-ventral position of LMCm (green) and LMCl (red) neurons in control, *afadin*$^{\Delta MN}$, $N^{\Delta MN}$ and $\beta\gamma^{\Delta MN}$ embryos (mean ± SD; differences significant for LMCm neurons: control versus $N^{\Delta MN}$ p<0.001, control versus $\beta\gamma^{\Delta MN}$ p<0.001, *afadin*$^{\Delta MN}$ versus $\beta\gamma^{\Delta MN}$ p<0.01, *afadin*$^{\Delta MN}$ versus $N^{\Delta MN}$ p<0.01; for LMCl neurons: control versus *afadin*$^{\Delta MN}$ p<0.05, control versus $N^{\Delta MN}$ p<0.001, control versus $\beta\gamma^{\Delta MN}$ p<0.001, *afadin*$^{\Delta MN}$ versus $N^{\Delta MN}$ p<0.05, *afadin*$^{\Delta MN}$ versus $\beta\gamma^{\Delta MN}$ p<0.01; one-way ANOVA followed by post hoc Tukey's HSD test). (**D**) Box-plots showing medio-lateral distributions of LMCm (green, medial) and LMCl (red, lateral) neurons in control, *afadin*$^{\Delta MN}$ $N^{\Delta MN}$ and $\beta\gamma^{\Delta MN}$ embryos. (**E**) Average medio-lateral positions of LMCm (green) and LMCl (red) neurons in control, *afadin*$^{\Delta MN}$, $N^{\Delta MN}$ and $\beta\gamma^{\Delta MN}$ embryos (mean ± SD; differences significant for LMCl neurons: control versus *afadin*$^{\Delta MN}$ p<0.01, control versus $\beta\gamma^{\Delta MN}$ p<0.001, *afadin*$^{\Delta MN}$ versus $\beta\gamma^{\Delta MN}$ p<0.05, $N^{\Delta MN}$ versus $\beta\gamma^{\Delta MN}$ p<0.001; one-way ANOVA followed by post hoc Tukey's HSD test). (**F**) Correlation analysis of LMCm and LMCl positional coordinates in control and *afadin*$^{\Delta MN}$ embryos. Scale bar indicates correlation values. (**G**) Transverse contour density analyses of V (blue), H (green) and R/T (red) motor pools in control, *afadin*$^{\Delta MN}$, $N^{\Delta MN}$ and $\beta\gamma^{\Delta MN}$ embryos. (**H**) Average dorso-ventral position of H (green), R/T (red), and V (blue) neurons in control and *afadin*$^{\Delta MN}$ embryos (mean ± SD; differences not significant, t-test). (**I**) Box-plots showing dorso-ventral distributions of H (green, ventral), R/T (red, ventral), and V (blue, dorsal) neurons in control and *afadin*$^{\Delta MN}$ embryos.

5.4.3 N-cadherin expression and function in afadin mutants

The next question arising is whether afadin is required for cadherin/catenin expression and function. First, to test N-cadherin function, neurite outgrowth in motor neurons isolated from control and *afadin*$^{\Delta MN}$ embryos grown either on laminin- or N-cadherin-coated dishes was monitored (see Methods section 4.2.1). It has been shown previously that motor neurons undergo a 2-fold increase in neurite length and branching when grown on N-cadherin-presenting substrates and that these enhancements are completely abrogated in the absence of catenin function (Demireva et al., 2011). However, no significant difference in N-cadherin enhanced neurite outgrowth and branching were observed between control and *afadin*$^{\Delta MN}$ motor neurons (Figure 16). Second, the consequences of afadin elimination on the expression of N-cadherin and β-catenin were examined. No changes in the motor neuron area and in the motor neuron progenitor zone of *afadin*$^{\Delta MN}$ embryos were detected (Figure 17).

Altogether, these experiments indicate that motor neurons do not require afadin activity either for expression of N-cadherin/catenin or for functional interaction with an N-cadherin substrate.

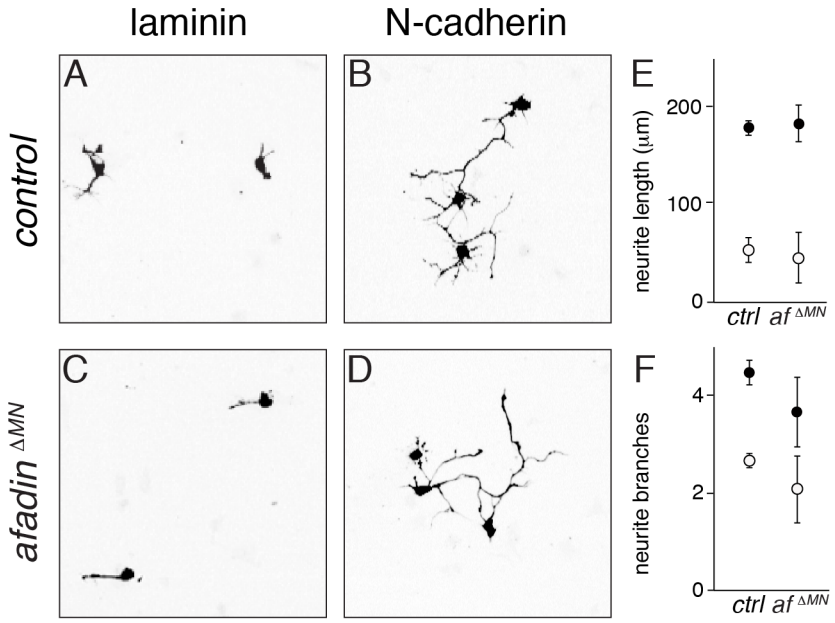

Figure 16: N-cadherin function in afadin mutant motor neurons.
(**A-D**) Neurite outgrowth of motor neurons, dissociated from control (*afadin*$^{fl/+}$*; olig2::Cre+/-*; *rosa-lsl-tdTomato*$^{fl/+}$) and *afadin*$^{\Delta MN}$ (*afadin*$^{fl/-}$*; olig2::Cre+/-*; *rosa-lsl-tdTomato*$^{fl/+}$) e10.5 embryos and seeded on dishes coated with laminin (**A** and **C**) or N-cadherin (**B** and **D**). Motor neurons visualized by tdTomato immunoreactivity depicted in black. (**E** and **F**) Average motor neuron neurite length (**E**) and branching (**F**) grown on laminin (○) or N-cadherin (●) for control and *afadin*$^{\Delta MN}$ mutant embryos (mean ± SEM for length; mean ± SD for branches, n=3).

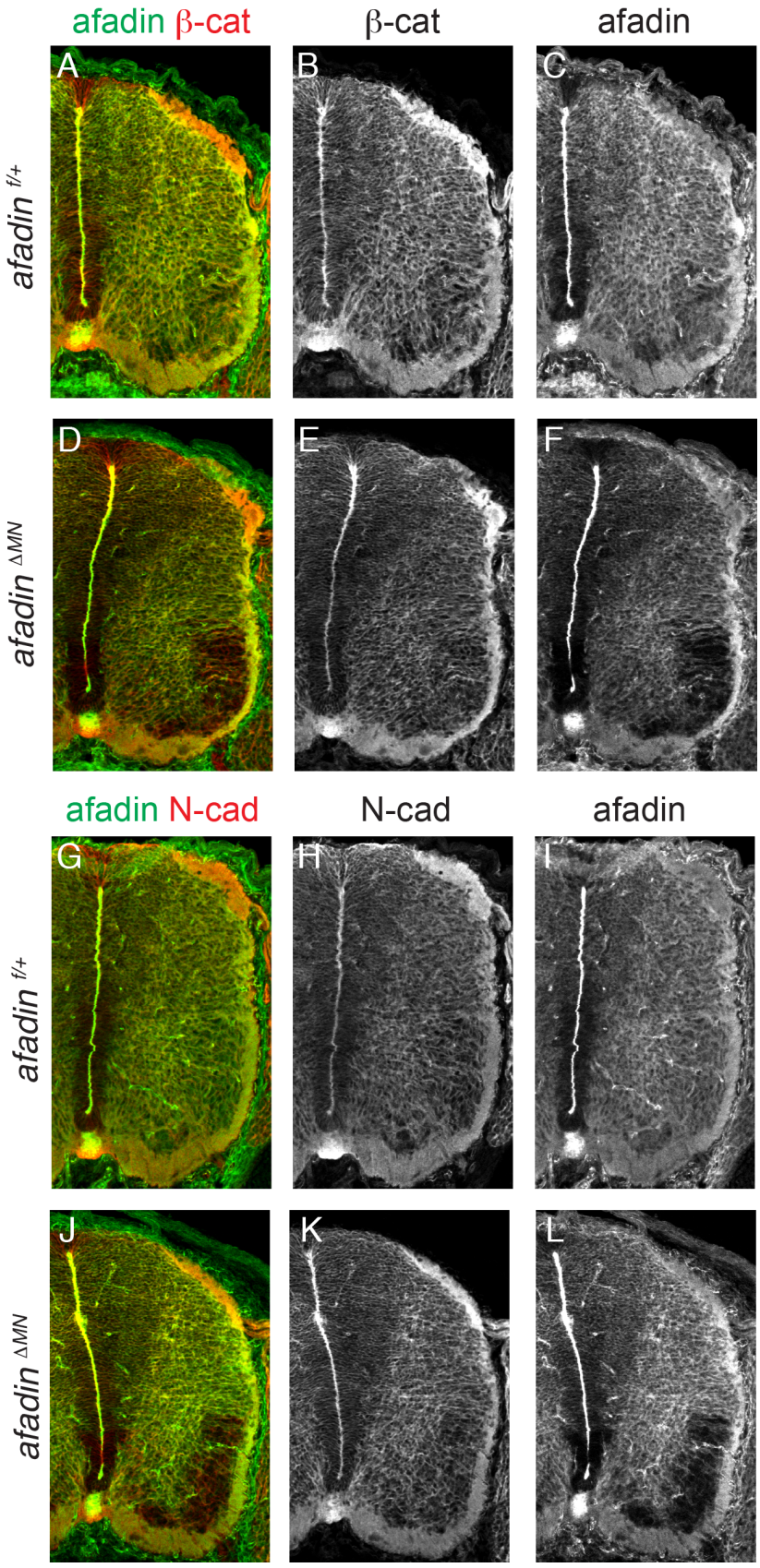

Figure 17: N-cadherin/catenin expression in afadin mutant mice.
(**A-F**) Afadin and β-catenin expression in e13.5 control and *afadin*$^{\Delta MN}$ lumbar spinal cords. (**G-L**) Afadin and N-cadherin expression in e13.5 control and *afadin*$^{\Delta MN}$ lumbar spinal cords.

Aim 3: Testing the roles of type II cadherin specificity groups in motor neuron positional organization.

5.5 Analysis of motor neuron organization after type II cadherins specificity group elimination

So far, the molecular underpinnings supporting motor pools segregation on the dorso-ventral axis are still unknown. Type II cadherins are obvious candidates because of their expression profiles and their dependency on catenins activity (Kemler, 1993; Nelson, 2008). However, elimination of individual type II cadherins using mouse genetics does not perturb motor neuron positioning, thus raising questions regarding their roles and contributions (Demireva et al., 2011). Recent studies indicate that redundancy in the adhesive function in groups of type II cadherins is at the basis of neuronal recognition properties in the retina and the hippocampus (Basu et al., 2017; Duan et al., 2018). Indeed, at a molecular level, type II cadherins can be divided into three different specificity groups according to pylogenetic analyses and their adhesive preferences (Figure 3B; Shimoyama et al., 2000; Brasch et al., 2018, see Introduction section 1.5.1). Thus, to start addressing whether functional redundancy in binding recognition properties of type II cadherins is an important determinant of motor neuron spatial organization, a mouse model lacking all the members of a specificity group by crossing cad-8 and cad-11 single knock-out mice was generated (*8/11*$^{-/-}$; Horikawa et al., 1999; Suzuki et al., 2007).

5.5.1 Effects of type II cadherins specificity group (8/11) inactivation on divisional organization

8/11$^{-/-}$ mice are born at expected Mendelian ratio and do not present any obvious phenotype. First, motor neuron generation and acquisition of subtype identities in *8/11*$^{-/-}$ mice was analyzed and similar numbers compared to control mice were found (Figure 21F). Next, motor neuron divisional organization was studied by applying three-dimensional positional analysis. Motor neuron subtypes were identified according to their specific transcription factor expression profiles (see Methods section 4.1.4). Transverse and longitudinal contour plots from control and *8/11*$^{-/-}$ embryos did not reveal any defects in medio-lateral and dorso-ventral positioning of LMCm and LMCl neurons (Figures 18A-18C). Accordingly, no changes neither in the distribution nor in the average position were

observed, both on the medio-lateral and dorso-ventral axis (Figures 18E-18H). In addition, correlation analysis was used to provide an overall assessment of LMCm and LMCl neurons spatial organization. Cartesian coordinates of motor neurons sharing the same subtype identity were highly correlated between control and *8/11*$^{-/-}$ embryos (control LMCm versus *8/11*$^{-/-}$ LMCm r > 0.8 and control LMCl versus *8/11*$^{-/-}$ LMCl r > 0.8; Figure 18D).

Thus, these data show that elimination of the type II cadherin specificity group comprising cad-8 and cad-11 does not affect motor neuron generation, identity and divisional organization.

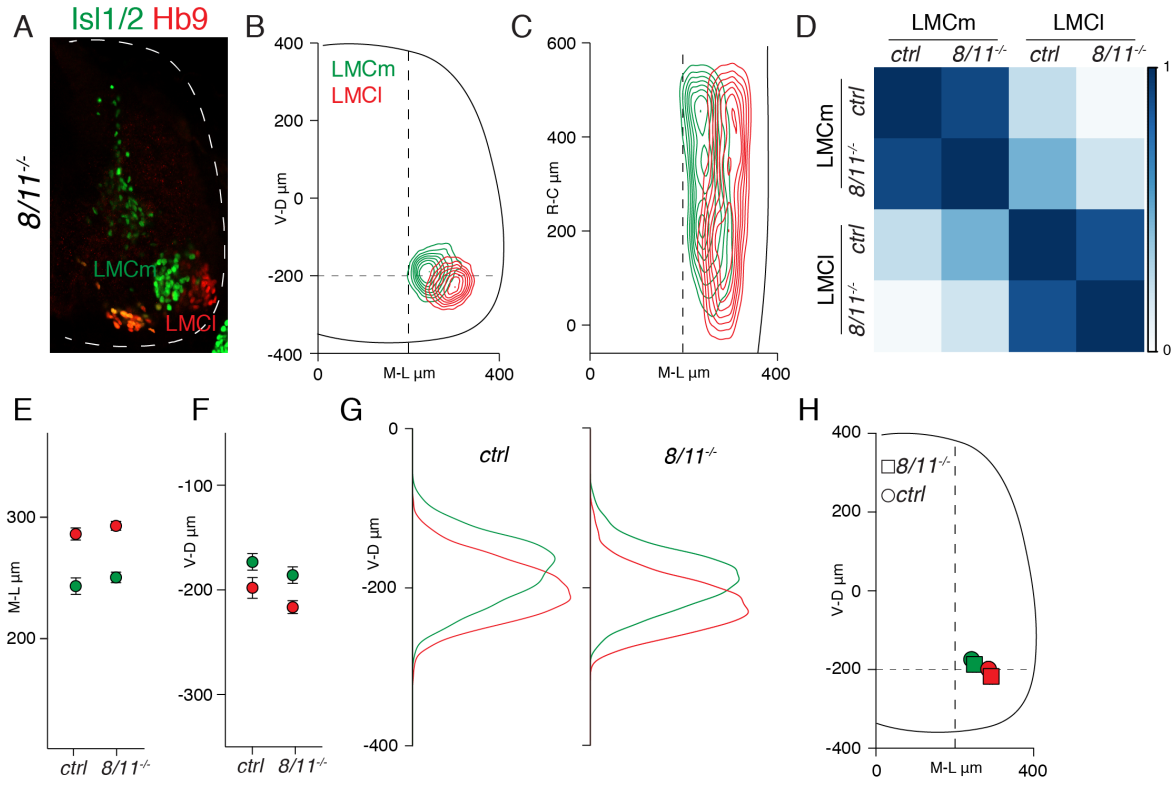

Figure 18: Elimination of cad-8, -11 specificity group does not perturb divisional organization.
(**A**) Organization of Isl1/2^{+} LMCm and Hb9^{+} LMCl neurons at lumbar spinal levels in e13.5 *8/11*$^{-/-}$embryos. (**B**) Transverse contour density plots of LMCm (green) and LMCl (red) neurons in *8/11*$^{-/-}$ embryos. (**C**) Longitudinal contour density plots of LMCm (green) and LMCl (red) neurons *8/11*$^{-/-}$ embryos. (**D**) Correlation analysis of LMC neurons medio-lateral and dorso-ventral Cartesian coordinates in control and *8/11*$^{-/-}$ embryos. The scale bar indicates correlation values. (**E**) Average medio-lateral position of LMCm (green) and LMCl (red) neurons in control and *8/11*$^{-/-}$ embryos (mean ± SD; differences not significant; t-test). (**F**) Average dorso-ventral position of LMCm (green) and LMCl (red) neurons in control and *8/11*$^{-/-}$ embryos (mean ± SD; differences not significant; t-test). (**G**) Dorso-ventral density plots of LMCm (green) and LMCl (red) neurons in control and *8/11*$^{-/-}$ embryos. (**H**) Average medio-lateral and dorso-ventral positions of LMCm (green) and LMCl (red) neurons in control and *8/11*$^{-/-}$ embryos (mean).

5.5.2 Effects of type II cadherin specificity group (8/11) inactivation on motor pool organization

Until now, N-cadherin/catenin and afadin signaling have been identified to control medio-lateral segregation of motor neuron divisions. However, the catenin-dependent effectors of motor neuron segregation into pools on the dorso-ventral axis are still unknown. Thus, it was next tested whether joint elimination of cad-8 and cad-11 could have a role in orchestrating dorso-ventral pool segregation despite not having an effect at divisional level. In order to test this hypothesis, segregation of dorsal (V, $Er81^{+}$) and ventral motor pools (H, $Nkx6.1^{+}$ and R/T, $Nkx6.2^{+}$) was analyzed (Figure 19A). Transverse contour analysis indicated that motor pool dorso-ventral organization was not affected in *8/11*$^{-/-}$ mutant embryos (Figure 19B). Density, distribution and average position analyses confirmed that segregation of motor pool subtypes was preserved (Figures 19C-19E). In addition, consistent with the divisional data no changes in pool organization on the medio-lateral axis were observed (Figures 21A-21D).

Thus, these data indicate that joint inactivation of cad-8 and -11 leaves motor pools segregation and positioning intact**.**

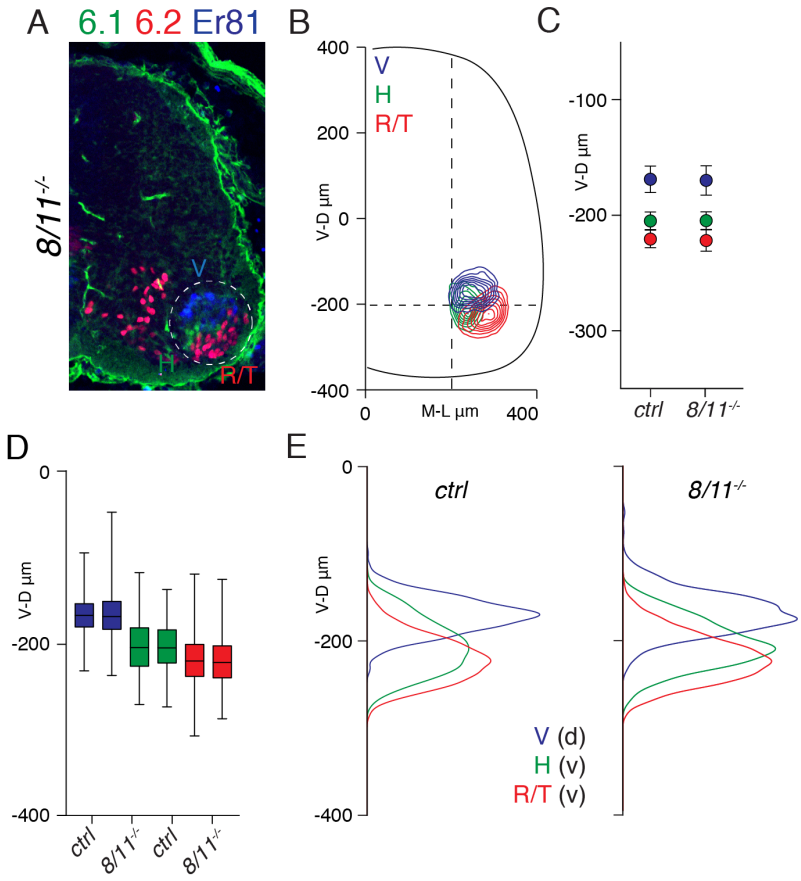

Figure 19: The type II cadherins specificity group cad-8, -11 is dispensable for motor pool organization.

(A) Organization of H (Nkx6.1^{+}), R/T (Nkx6.2^{+}), and V (Er81^{+}) motor pools at lumbar spinal levels in e13.5 *8/11*$^{-/-}$ embryos. The motor neuron area is delimited by a dashed line. (**B**) Transverse contour density plots of H (green), R/T (red), and V (blue) motor pools in *8/11*$^{-/-}$ embryos. (**C**) Average dorso-ventral position of H (green), R/T (red), and V (blue) neurons in control and *8/11*$^{-/-}$ embryos (mean ± SD; differences not significant; t-test). (**D**) Box-plots showing dorso-ventral distributions of H (green), R/T (red), and V (blue) neurons in control and *8/11*$^{-/-}$ embryos. (**E**) Dorso-ventral density plots of H (green, ventral), R/T (red, ventral), and V (blue, dorsal) neurons in control and *8/11*$^{-/-}$ embryos.

5.5.3 Effects of type II cadherins specificity group (6/9/10) inactivation on motor pool organization

In order to confirm and expand the observations of a lack of phenotype in *8/11*$^{-/-}$ mutant embryos, the effect of inactivating a second specificity group on motor neuron organization was next studied. Recent studies show that functional redundancy in cad-6, -9, -10 has important functions in controlling neuronal interactions in the hippocampus and the retina (Basu et al., 2017; Duan et al., 2018). Thus, triple cad-6, -9, -10 knock-out mice were generated using targeted genome editing as previously described (*6/9/10*$^{-/-}$; Duan et al., 2018). *6/9/10*$^{-/-}$ mice are viable and fertile and do not present any obvious phenotype. Moreover, motor neurons were present at expected numbers and acquired appropriate

subtype identities (Figure 21F). Next, motor pool organization in triple mutant embryos was investigated. Contour, average position, distribution and density analyses showed that segregation of pools on the dorso-ventral axis in *6/9/10*$^{-/-}$ embryos was similar to control and *8/11*$^{-/-}$ double mutants (Figures 20A-20E). As a consequence, positional coordinates of H, R/T and V neurons were highly correlated in control, *8/11*$^{-/-}$ and *6/9/10*$^{-/-}$ embryos (for all three pool comparisons r > 0.8; Figure 20F). Accordingly, positioning of motor pools along the medio-lateral axis was not affected (Figures 21C-21E).

Altogether, these experiments indicate that elimination of type II cadherin specificity groups does not affect motor neuron generation, diversification and spatial organization in the spinal cord.

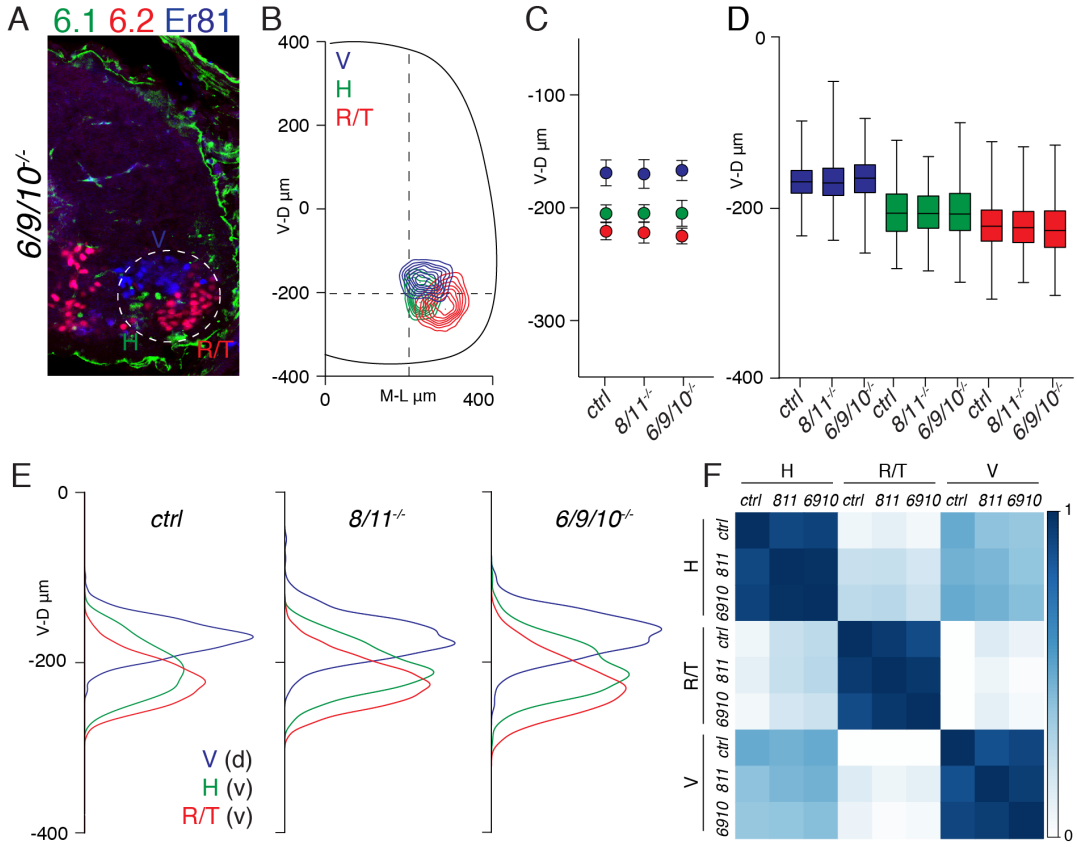

Figure 20: Elimination of type II cadherins specificity group cad-6, -9, -10 does not affect dorso-ventral pool segregation.

(**A**) Organization of H (Nkx6.1^{+}), R/T (Nkx6.2^{+}), and V (Er81^{+}) motor pools at lumbar spinal levels in e13.5 *6/9/10*$^{-/-}$ embryos. The motor neuron area is delimited by a dashed line. (**B**) Transverse contour density plots of H (green), R/T (red), and V (blue) motor pools in *6/9/10*$^{-/-}$ embryos. (**C**) Average dorso-ventral position of H (green), R/T (red), and V (blue) neurons in control, *8/11*$^{-/-}$ and *6/9/10*$^{-/-}$ embryos (mean ± SD; differences not significant; one-way ANOVA and post hoc Tukey's HSD test). (**D**) Box-plots showing dorso-ventral distributions of H (green), R/T (red), and V (blue) neurons in control, *8/11*$^{-/-}$ and *6/9/10*$^{-/-}$ embryos. (**E**) Dorso-ventral density plots of H (green, ventral), R/T (red, ventral), and V (blue, dorsal) neurons in control, *8/11*$^{-/-}$ and *6/9/10*$^{-/-}$ embryos. (**F**) Correlation analysis of H, R/T and V neurons medio-lateral and dorso-ventral Cartesian coordinates in control, *8/11*$^{-/-}$ and *6/9/10*$^{-/-}$ embryos. The scale bar indicates correlation values.

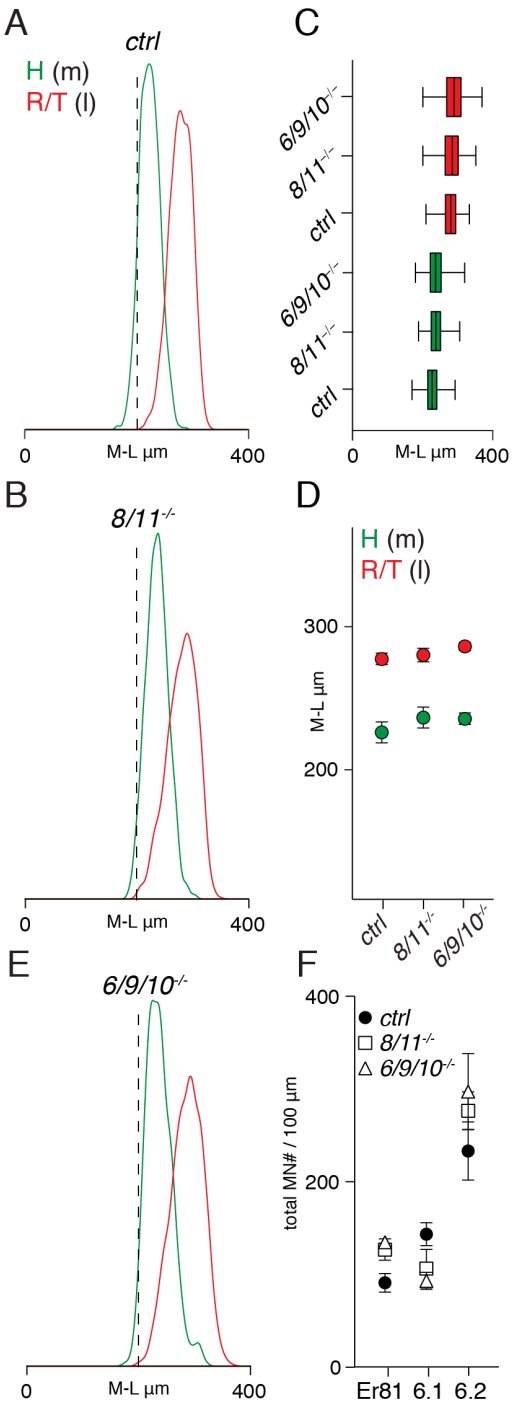

Figure 21: Medio-lateral pool organization is unchanged after elimination of type II cadherins specificity groups.

(**A** and **B**) Medio-lateral density plots of H (green) and R/T (red) neurons in control (**A**) and *8/11*$^{-/-}$ (**B**) embryos. (**C**) Box-plots showing medio-lateral distributions of H (green) and R/T (red) neurons in control, *8/11*$^{-/-}$ and *6/9/10*$^{-/-}$ embryos. (**D**) Average medio-lateral position of H (green) and R/T (red) neurons in control, *8/11*$^{-/-}$ and *6/9/10*$^{-/-}$ embryos (mean ± SD; differences not significant; one-way ANOVA and post hoc Tukey's HSD test). (**E**) Medio-lateral density plots of H (green) and R/T (red) neurons in 6/9/10$^{-/-}$ embryos. (**F**) Average total numbers of Er81^{+}, Nkx6.1^{+}, and Nkx6.2^{+} motor neurons in e13.5 lumbar spinal cords of control, *8/11*$^{-/-}$ and *6/9/10*$^{-/-}$ embryos (motor neurons/100 µm, mean ± SD; differences significant for H neurons: control versus *6/9/10*$^{-/-}$ embryos $p<0.05$; differences significant for V neurons: control versus *8/11*$^{-/-}$ and *6/9/10*$^{-/-}$ embryos $p<0.01$; one-way ANOVA and post hoc Tukey's HSD test).

Aim 4: Evaluating combined function of type I and type II cadherins in motor neuron positional organization.

5.6 Analysis of joint inactivation of N-cadherin and a type II cadherin

Type II cadherins expression profiles in motor neurons are highly suggestive of their involvement in pool organization. However, so far, any attempt to disrupt motor neuron positioning by eliminating type II cadherins function in mice has failed. Thus, a hypothesis was that another factor might be required to elicit type II cadherins activity. According to previous genetic results, such factor should be ubiquitously expressed in motor neurons and capable of interacting with catenin adhesive signaling (Demireva et al., 2011). N-cadherin, a type I cadherin expressed from early progenitor stages on, fulfills these requirements and its conditional elimination from motor neurons has been shown in previous experiments to cause a defect in LMCl medio-lateral migration as well as a ventralization of LMC positioning, but did not perturb segregation of pools on the dorso-ventral axis (Figures 10 and 11). Thus, either cad-8 or cad-11 mutant alleles, which do not present any positioning defect either alone or in combination, were combined with N-cadherin conditional deletion to generate $N^{\Delta MN}8^{-/-}$ and $N^{\Delta MN}11^{-/-}$ mice.

5.6.1 Motor neuron migration arrest in the progenitor area after joint elimination of N-cadherin and a type II cadherin

$N^{\Delta MN}8^{-/-}$ and $N^{\Delta MN}11^{-/-}$ mice are lethal at late embryonic stages as previously described for $N^{\Delta MN}$ mutants, thus allowing analysis of motor neuron development until positional organization is completed at e13.5 (Demireva et al., 2011). First, motor neuron generation was assessed and it was found that total number and identity of motor neuron subtypes in $N^{\Delta MN}8^{-/-}$ and $N^{\Delta MN}11^{-/-}$ embryos did not significantly differ from control embryos (Figures 21F and 26F). However, a striking defect in motor neuron migration, resulting in about 50% of post-mitotic motor neurons found arrested in the progenitor area, was observed, both in $N^{\Delta MN}8^{-/-}$ and $N^{\Delta MN}11^{-/-}$ embryos (Figures 22A and 22B, 22E and 22F). The same phenotype, at reduced penetrance, was previously observed in $N^{\Delta MN}$ embryos and after conditional inactivation of β- and γ-catenin in motor neurons (Figures 22B-22D; Demireva et al., 2011). The migration defect was comparable between $N^{\Delta MN}8^{-/-}$

and $N^{\Delta MN}11^{-/-}$ embryos and different motor neuron subtypes were found in the progenitor zone with similar frequencies (Figure 22B).

Thus, concomitant elimination of N-cadherin with a type II cadherin does not affect motor neuron generation and diversification, but results in a partial failure of motor neuron migration out of the progenitor area.

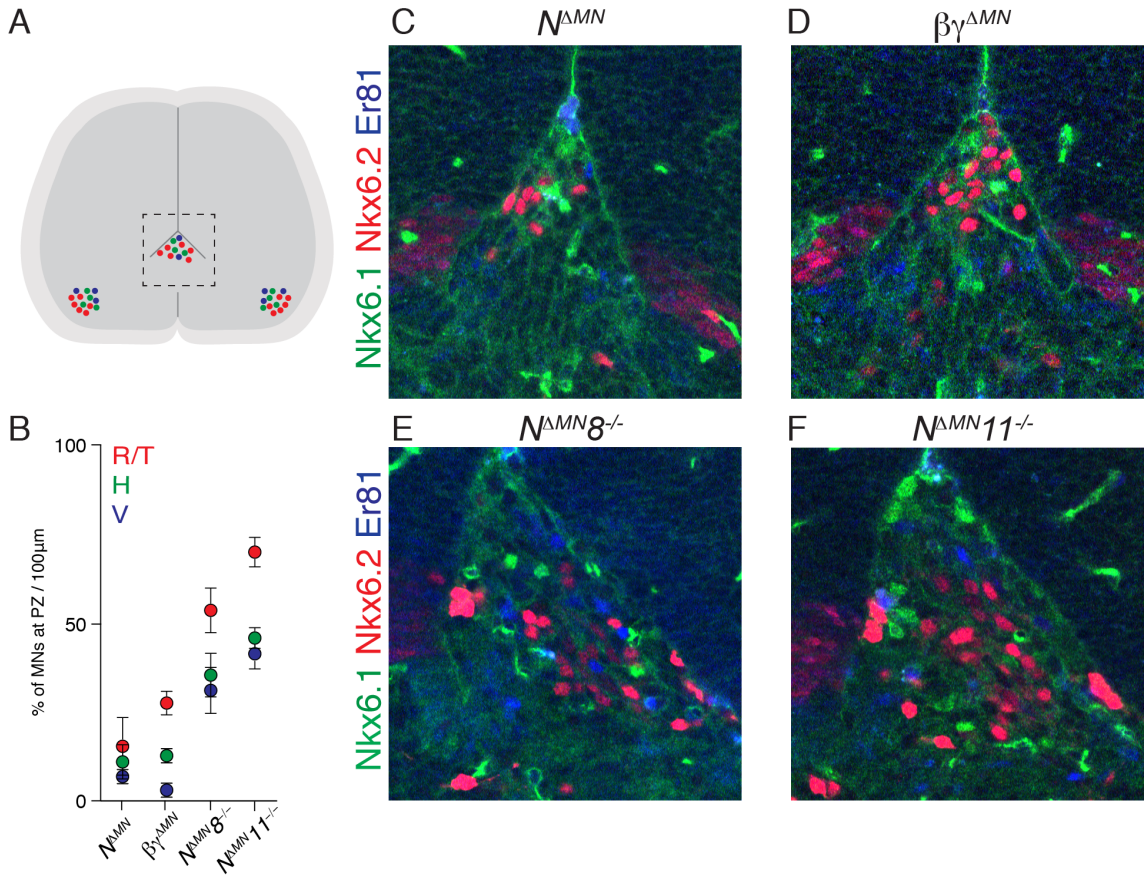

Figure 22: Motor neuron migration arrest at the progenitor zone after combined elimination of N-cadherin and a type II cadherin.

(**A**) Schematic showing motor neurons arrested at the progenitor zone (delimited by a dashed line) in lumbar spinal cord. (**B**) Average number of motor neurons found in the progenitor zone (PZ) expressed as percentage of total number of motor neurons of each motor pool identity in $N^{\Delta MN}$, $\beta\gamma^{\Delta MN}$, $N^{\Delta MN}8^{-/-}$ and $N^{\Delta MN}11^{-/-}$ embryos (mean ± SD; differences significant for Nkx6.1$^+$ neurons: $N^{\Delta MN}$ versus $N^{\Delta MN}8^{-/-}$ and $N^{\Delta MN}11^{-/-}$ embryos $p<0.01$; $\beta\gamma^{\Delta MN}$ versus $N^{\Delta MN}11^{-/-}$ embryos $p<0.01$; $\beta\gamma^{\Delta MN}$ versus $N^{\Delta MN}8^{-/-}$ embryos $p<0.05$; differences significant for Nkx6.2$^+$ neurons: $N^{\Delta MN}$ versus $N^{\Delta MN}8^{-/-}$ and $N^{\Delta MN}11^{-/-}$ embryos $p<0.01$; $\beta\gamma^{\Delta MN}$ versus $N^{\Delta MN}11^{-/-}$ embryos $p<0.01$; $\beta\gamma^{\Delta MN}$ versus $N^{\Delta MN}8^{-/-}$ embryos $p<0.05$; differences significant for Er81$^+$ neurons: $N^{\Delta MN}$ versus $N^{\Delta MN}8^{-/-}$ embryos $p<0.05$; $N^{\Delta MN}$ versus $N^{\Delta MN}11^{-/-}$ embryos $p<0.001$; $\beta\gamma^{\Delta MN}$ versus $N^{\Delta MN}8^{-/-}$ embryos $p<0.05$; $\beta\gamma^{\Delta MN}$ versus $N^{\Delta MN}11^{-/-}$ embryos $p<0.001$; $N^{\Delta MN}8^{-/-}$ versus $N^{\Delta MN}11^{-/-}$ embryos $p<0.05$; one-way ANOVA and post hoc Tukey's HSD test. Data are presented only for genotypes in which a significant medial arrest of motor neurons was observed with respect to controls). (**C-F**) Motor neurons arrested at the progenitor zone in $N^{\Delta MN}$ (**C**), $\beta\gamma^{\Delta MN}$ (**D**), $N^{\Delta MN}8^{-/-}$ (**E**) and $N^{\Delta MN}11^{-/-}$ (**F**) e13.5 embryos at lumbar spinal level.

5.6.2 Effects of joint elimination of N-cadherin and a type II cadherin on motor neuron organization

Next, motor neuron organization at divisional level in $N^{\Delta MN}8^{-/-}$ embryos was assessed and defects in the positioning of LMC neurons were observed consistent with the ones previously described after inactivation of N-cadherin (Figures 23A, 23B and 23I; Figures 10 and 11). Transverse and longitudinal contour density plots showed a medial shift in LMCl neurons position, which was further confirmed by correlation analysis (Figures 23B, 23C and 23F). LMCm neuron positions were highly correlated between control and $N^{\Delta MN}8^{-/-}$ embryos (control LMCm versus $N^{\Delta MN}8^{-/-}$ LMCm r = 0.87) in contrast to a decrease in correlation of the medio-lateral position of LMCl neurons (control LMCl versus $N^{\Delta MN}8^{-/-}$ LMCl r = 0.54; Figure 23F). In addition, density and average position analyses revealed that the medio-lateral positioning defect of LMCl neurons in $N^{\Delta MN}8^{-/-}$ embryos was significantly more severe than in single N-cadherin mutants (Figures 23D and 23E). In contrast, the observed ventralization in columnar location did not differ from $N^{\Delta MN}$ embryos (Figures 23G and 23H). Thus, these data indicate that, at divisional level, cad-8 selectively contributes to the control of LMCl medio-lateral positioning and removal of N-cadherin is required to reveal its involvement.

Next, motor pools segregation was analyzed on the dorso-ventral axis (Figures 24A and 24B). Interestingly, average dorso-ventral position and density analyses of V (dorsal), H and R/T (ventral) neurons showed that, unlike in $N^{\Delta MN}$ embryos, dorso-ventral segregation of pools was clearly impaired in $N^{\Delta MN}8^{-/-}$ embryos and now their positioning resembled the one previously observed after inactivation of βγ-catenin, with V and H pools found in mostly overlapping areas (Figures 24C and 24E). As a consequence, the average distance between dorsal and ventral pools (V-H and V-R/T) was significantly decreased in $N^{\Delta MN}8^{-/-}$ embryos compared to $N^{\Delta MN}$ and controls embryos, but not different from $\beta\gamma^{\Delta MN}$ embryos (Figure 24D).

The next question asked was whether the dorso-ventral segregation phenotype is specific for the removal of cad-8 in combination with N-cadherin. Thus, $N^{\Delta MN}11^{-/-}$ embryos were analyzed and it was found that motor neuron organization was also dramatically perturbed after concomitant elimination of N-cadherin and cad-11 (Figures 25A and 25B). Interestingly, dorso-ventral distributions, average and relative position analyses revealed that the removal of either cad-8 or cad-11 generated almost indistinguishable phenotypes (Figures 25C-25F). In addition, analysis of medio-lateral position of H (medial) and R/T (lateral) pools supported the observation made at divisional level, with elimination of

either cad-8 or cad-11 in combination with N-cadherin increasing the severity of LMCl neurons positioning defect observed in $N^{\Delta MN}$ embryos (Figures 26A-26E; Figure 11).

Altogether, these data reveal the contributions of type II cadherins to motor neuron positional organization, first in the control of medio-lateral migration of LMCl neurons and second in mediating dorso-ventral segregation of pools, however their impact is only exposed in absence of N-cadherin.

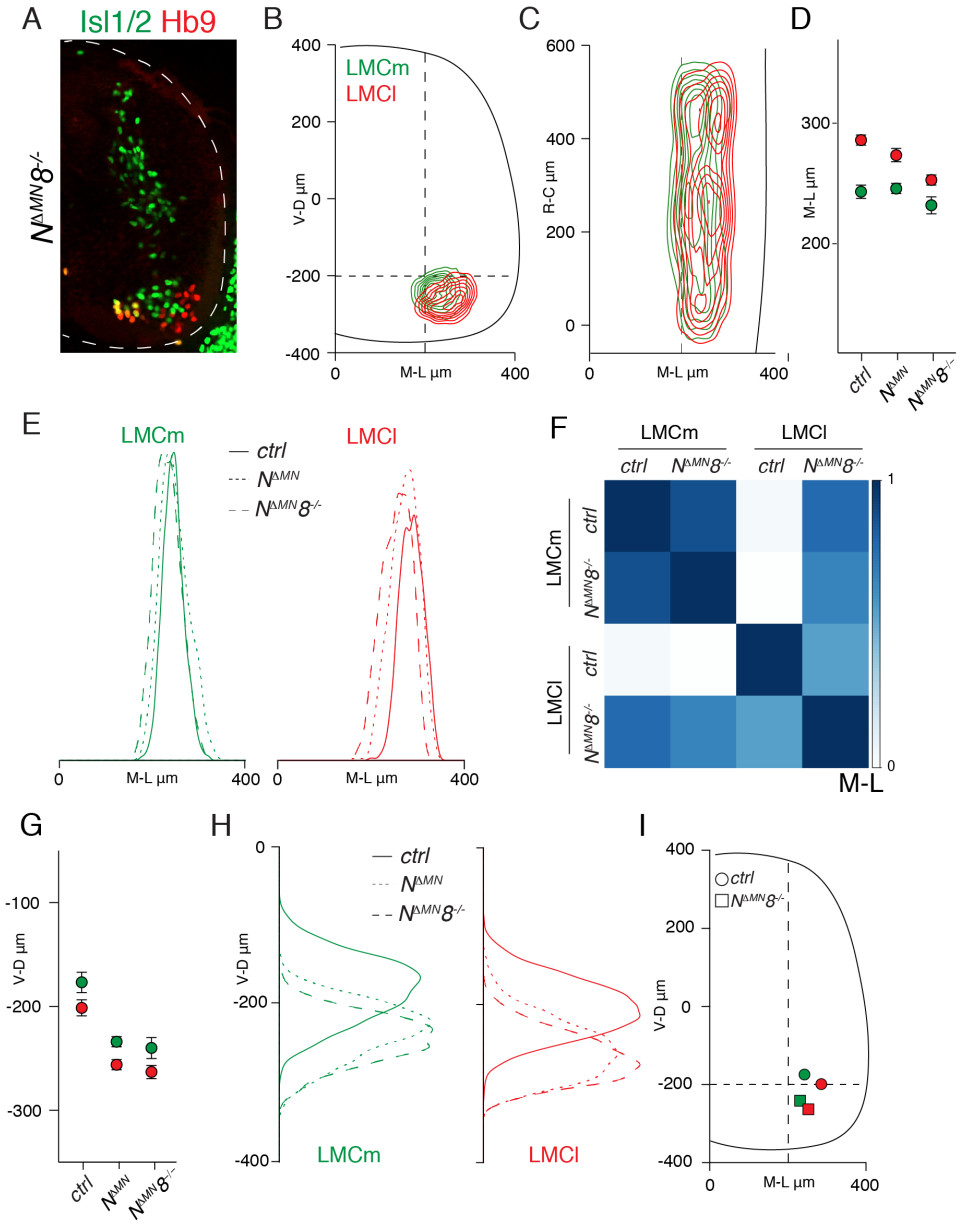

Figure 23: Combined elimination of N-cadherin and cadherin-8 results in divisional organization defects.

(**A**) Organization of Isl1/2^{+} LMCm and Hb9^{+} LMCl neurons at lumbar spinal levels in e13.5 $N^{\Delta MN}8^{-/-}$ embryos. (**B**) Transverse contour density plots of LMCm (green) and LMCl (red) neurons in $N^{\Delta MN}8^{-/-}$ embryos. (**C**) Longitudinal contour density plots of LMCm (green) and LMCl (red) neurons in $N^{\Delta MN}8^{-/-}$ embryos. (**D**) Average medio-lateral position of LMCm (green) and LMCl (red) neurons in control, $N^{\Delta MN}$ and $N^{\Delta MN}8^{-/-}$ embryos (mean ± SD; differences significant for LMCm neurons: control versus $N^{\Delta MN}8^{-/-}$ embryos p=0.038, $N^{\Delta MN}$ versus $N^{\Delta MN}8^{-/-}$ embryos p<0.01; differences significant for LMCl neurons: control versus $N^{\Delta MN}8^{-/-}$ embryos p<0.001, $N^{\Delta MN}$ versus $N^{\Delta MN}8^{-/-}$ embryos p<0.01; one-way ANOVA and post hoc Tukey's HSD test). (**E**) Medio-lateral density plots of LMCm (green) and LMCl (red) neurons in control, $N^{\Delta MN}$ and $N^{\Delta MN}8^{-/-}$ embryos. (**F**) Correlation analysis of medio-lateral LMC neuron positional coordinates in control and $N^{\Delta MN}8^{-/-}$ embryos. The scale bar indicates correlation values. (**G**) Average dorso-ventral position of LMCm (green) and LMCl (red) neurons in control, $N^{\Delta MN}$ and $N^{\Delta MN}8^{-/-}$ embryos (mean ± SD; differences significant for LMCm neurons: control versus $N^{\Delta MN}$ and $N^{\Delta MN}8^{-/-}$ embryos p<0.001; differences significant for LMCl neurons: control versus $N^{\Delta MN}$ and $N^{\Delta MN}8^{-/-}$ embryos p<0.001; one-way ANOVA and post hoc Tukey's HSD test). (**H**) Dorso-ventral density plots of LMCm (green) and LMCl (red) neurons in control, $N^{\Delta MN}$ and $N^{\Delta MN}8^{-/-}$ embryos. (**I**) Average medio-lateral and dorso-ventral positions of LMCm (green) and LMCl (red) neurons in control and $N^{\Delta MN}8^{-/-}$ embryos (mean).

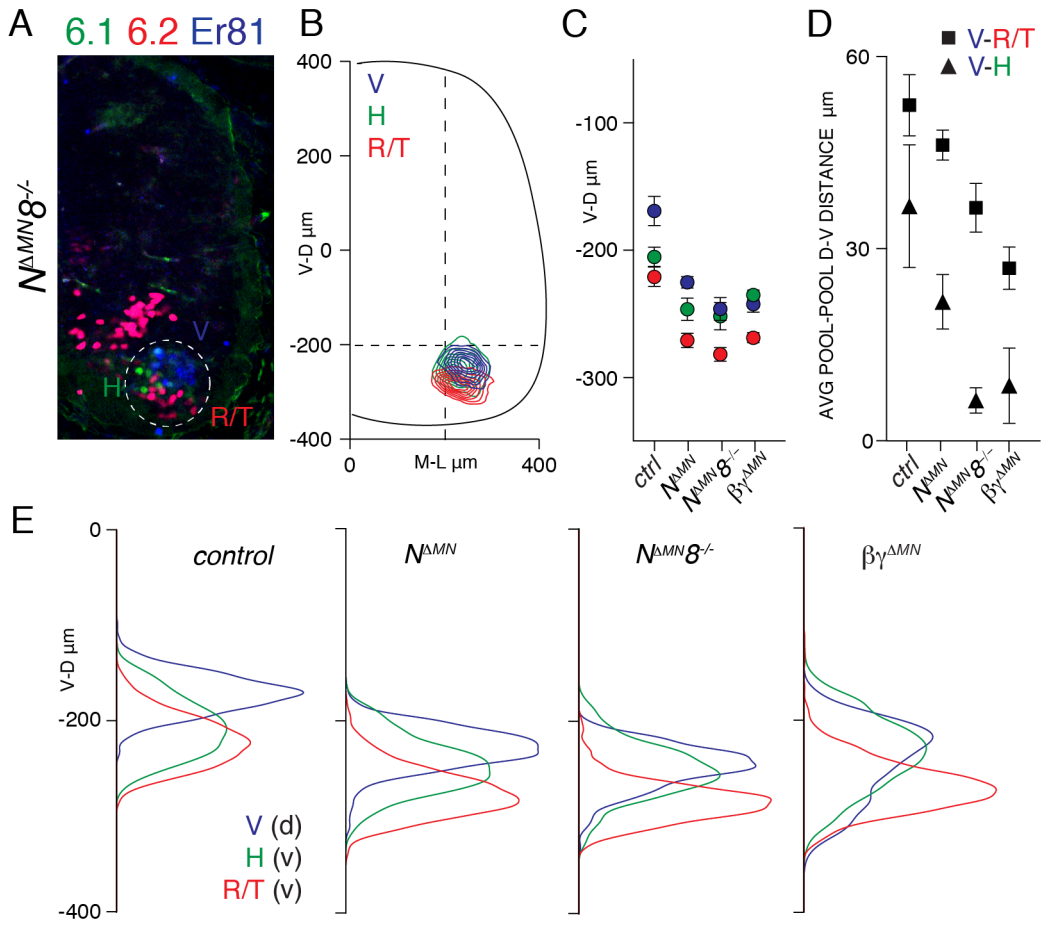

Figure 24: Combined elimination of N-cadherin and cadherin-8 perturbs dorso-ventral pool segregation.

(**A**) Organization of H (Nkx6.1^{+}), R/T (Nkx6.2^{+}), and V (Er81^{+}) motor pools in e13.5 $N^{\Delta MN}8^{-/-}$ embryos. The motor neuron area is delimited by a dashed line. (**B**) Transverse contour density plots of H (green), R/T (red), and V (blue) motor pools in $N^{\Delta MN}8^{-/-}$ embryos. (**C**) Average dorso-ventral position of H (green), R/T (red), and V (blue) neurons in control, $N^{\Delta MN}$, $N^{\Delta MN}8^{-/-}$ and $\beta\gamma^{\Delta MN}$ embryos (mean ± SD; differences significant for H neurons: control versus $N^{\Delta MN}$ and $\beta\gamma^{\Delta MN}$ embryos $p<0.01$, control versus $N^{\Delta MN}8^{-/-}$ embryos $p<0.001$; differences significant for R/T neurons: control versus $N^{\Delta MN}$, $N^{\Delta MN}8^{-/-}$ and $\beta\gamma^{\Delta MN}$ embryos $p<0.001$; differences significant for V neurons: control versus $N^{\Delta MN}$, $N^{\Delta MN}8^{-/-}$ and $\beta\gamma^{\Delta MN}$ embryos $p<0.001$; one-way ANOVA and post hoc Tukey's HSD test). (**D**) Average distance between dorso-ventral positions of V-R/T and V-H pools in control, $N^{\Delta MN}$, $N^{\Delta MN}8^{-/-}$ and $\beta\gamma^{\Delta MN}$ embryos (mean ± SD; differences of V-H and V-R/T neurons not significant between control and $N^{\Delta MN}$ embryos; differences significant for V-H: control versus $N^{\Delta MN}8^{-/-}$ and $\beta\gamma^{\Delta MN}$ embryos $p<0.01$; differences significant for V-R/T: control versus $N^{\Delta MN}8^{-/-}$ embryos $p<0.01$, control versus $\beta\gamma^{\Delta MN}$ embryos $p<0.001$, $N^{\Delta MN}$ versus $N^{\Delta MN}8^{-/-}$ embryos $p<0.05$, $N^{\Delta MN}$ versus $\beta\gamma^{\Delta MN}$ embryos $p<0.001$; one-way ANOVA and post hoc Tukey's HSD test). (**E**) Dorso-ventral density plots of H (green, ventral), R/T (red, ventral), and V (blue, dorsal) neurons in control, $N^{\Delta MN}$, $N^{\Delta MN}8^{-/-}$ and $\beta\gamma^{\Delta MN}$ embryos.

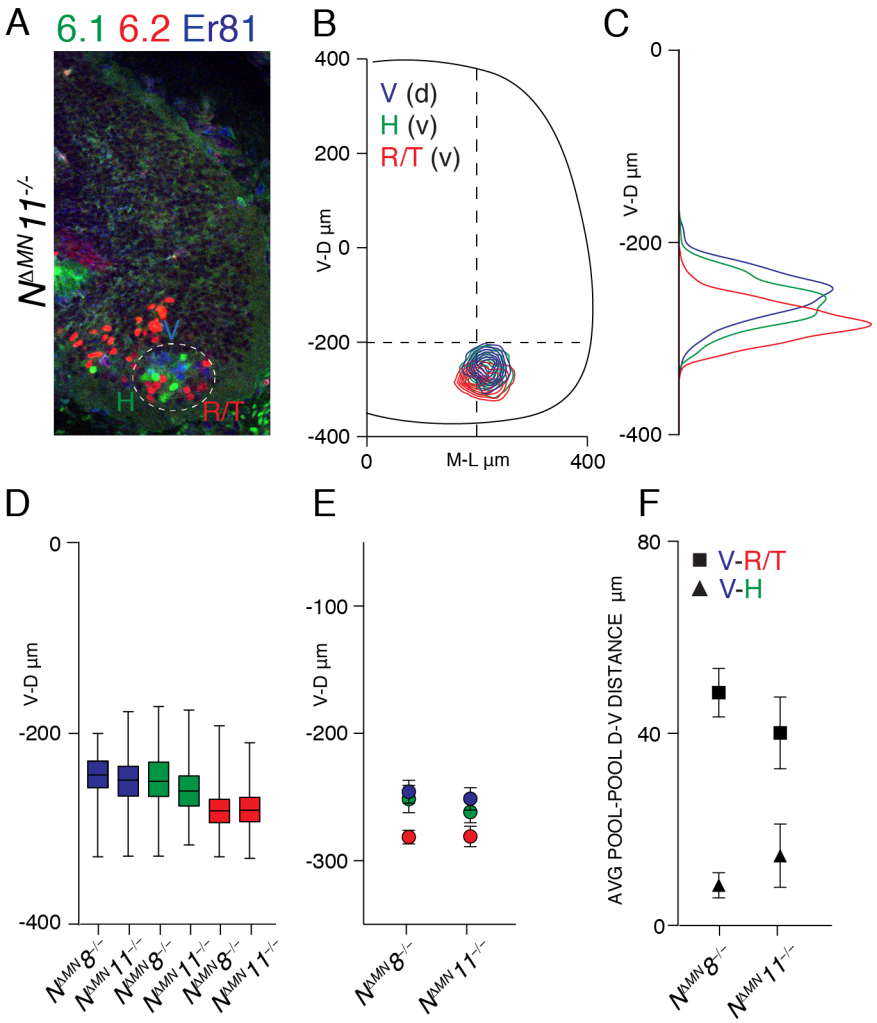

Figure 25: Combined elimination of N-cadherin and cadherin-11 phenocopies defects observed in $N^{\Delta MN}8^{-/-}$ embryos.

(**A**) Organization of H (Nkx6.1^{+}), R/T (Nkx6.2^{+}), and V (Er81^{+}) motor pools at lumbar spinal levels in e13.5 $N^{\Delta MN}11^{-/-}$ embryos. The motor neuron area is delimited by a dashed line. (**B**) Transverse contour density plots of H (green), R/T (red), and V (blue) motor pools in $N^{\Delta MN}11^{-/-}$ embryos. (**C**) Dorso-ventral density plots of H (green, ventral), R/T (red, ventral), and V (blue, dorsal) neurons in $N^{\Delta MN}11^{-/-}$ embryos. (**D**) Box-plots showing dorso-ventral distributions of H (green), R/T (red), and V (blue) neurons in $N^{\Delta MN}8^{-/-}$ and $N^{\Delta MN}11^{-/-}$ embryos (mean ± SD; differences not significant; t-test). (**E**) Average dorso-ventral position of H (green), R/T (red), and V (blue) neurons in $N^{\Delta MN}8^{-/-}$ and $N^{\Delta MN}11^{-/-}$ embryos (mean ± SD; differences not significant; t-test). (**F**) Average distance between dorso-ventral positions of V-R/T and V-H pools in $N^{\Delta MN}8^{-/-}$ and $N^{\Delta MN}11^{-/-}$ embryos (mean ± SD; differences not significant; t-test).

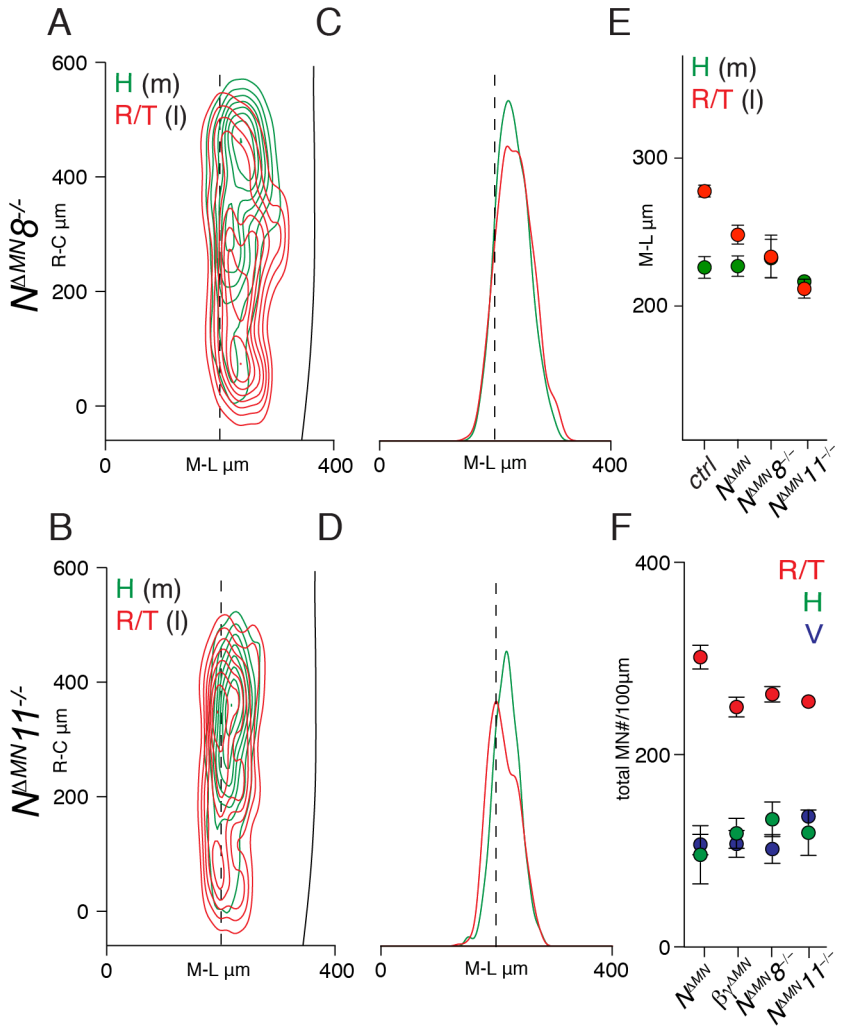

Figure 26: Medio-lateral pool organization is perturbed after concomitant elimination of N-cadherin and a type II cadherin.

(**A** and **B**) Longitudinal contour density plots of H (green) and R/T (red) neurons in $N^{\Delta MN}8^{-/-}$ (**A**) and $N^{\Delta MN}11^{-/-}$ (**B**) embryos. (**C** and **D**) Medio-lateral density plots of H (green) and R/T (red) neurons in $N^{\Delta MN}8^{-/-}$ (**C**) and $N^{\Delta MN}11^{-/-}$ (**D**) embryos. (**E**) Average medio-lateral position of H (green) and R/T (red) neurons in control, $N^{\Delta MN}$, $N^{\Delta MN}8^{-/-}$ and $N^{\Delta MN}11^{-/-}$ embryos (mean ± SD; differences significant for R/T neurons: control versus $N^{\Delta MN}$ embryos $p<0.01$, control versus $N^{\Delta MN}8^{-/-}$ and $N^{\Delta MN}11^{-/-}$ embryos $p<0.001$, $N^{\Delta MN}$ versus $N^{\Delta MN}11^{-/-}$ embryos $p<0.01$, $N^{\Delta MN}8^{-/-}$ versus $N^{\Delta MN}11^{-/-}$ embryos $p<0.05$; one-way ANOVA and post hoc Tukey's HSD test). (**F**) Average total numbers of $Er81^{+}$, $Nkx6.1^{+}$ and $Nkx6.2^{+}$ motor neurons in $N^{\Delta MN}$, $\beta\gamma^{\Delta MN}$, $N^{\Delta MN}8^{-/-}$ and $N^{\Delta MN}11^{-/-}$ embryos in lumbar spinal cord (total motor neuron#/100µm, mean ± SD; differences significant for $Nkx6.2^{+}$ neurons: $N^{\Delta MN}$ versus $\beta\gamma^{\Delta MN}$ and $N^{\Delta MN}11^{-/-}$ embryos $p<0.01$; $N^{\Delta MN}$ versus $N^{\Delta MN}8^{-/-}$ embryos $p<0.05$; one-way ANOVA and post hoc Tukey's HSD test).

5.7 *In vitro* analyses of classical cadherin functions at a cellular level

The described mouse genetic experiments clearly showed that the contributions of type II cadherins become evident only in absence of N-cadherin. However, the molecular and cellular bases of the emerging functions observed after concomitant elimination of N-cadherin and type II cadherins remain unclear. At a structural level, heterophilic binding between type I and type II cadherins is prohibited and, at a cellular level, there is no prior report of such functional interaction controlling adhesive recognition, either *in vitro* or *in vivo* (Patel et al., 2006; Brasch et al., 2012). Thus, the next set of experiments aimed to identify changes in cell adhesion properties upon co-expression of N-cadherin and type II cadherins by investigating adhesive recognition in a heterologous cell system and primary motor neurons. In order to perform the following *in vitro* experiments, first a stable cell line expressing N-cadherin was generated (termed N-cad CHO cells; Figure 27; see Methods section 4.3.3).

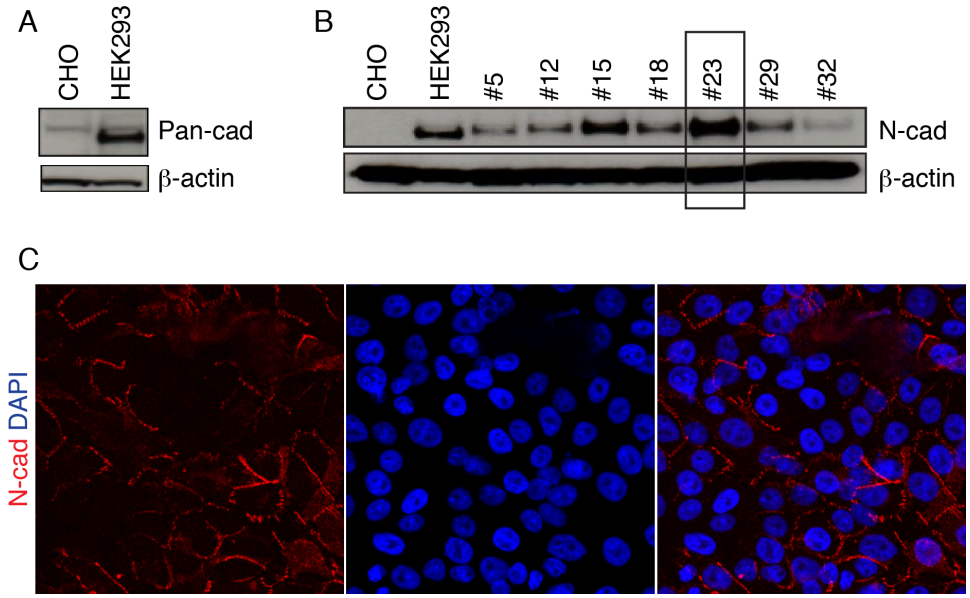

Figure 27: N-cadherin expression in N-cad CHO stable cell line.
(**A**) Immunoblot showing the absence of cadherin expression in CHO cells. β-actin served as a loading control. (**B**) Immunoblot of N-cad CHO lysates showing expression of N-cadherin protein. β-actin served as a loading control. Clone #23 was picked for all subsequent *in vitro* experiments. (**C**) Immunostaining against N-cadherin in N-cad CHO cells (clone #23). DAPI identifies all cell nuclei.

5.7.1 Neurite outgrowth assay

In order to test a new emerging function of type II cadherins in the presence of N-cadherin, neurite outgrowth of motor neurons isolated from e10.5 Hb9:GFP embryos cultured on N-cad CHO or cadherin-11-transfected N-cad CHO cells was monitored (see

Methods section 4.2.1; Figure 28). Previously, it has been shown that N-cadherin substrate enhances neurite outgrowth of primary motor neurons (Demireva et al., 2011; Figure 16), thus a hypothesis was that combined expression of N-cadherin and cadherin-11 by CHO cells could result in a new function, similar to the observed defects *in vivo* in $N^{\Delta MN}11^{-/-}$ embryos, changing motor neuron neurite outgrowth response.

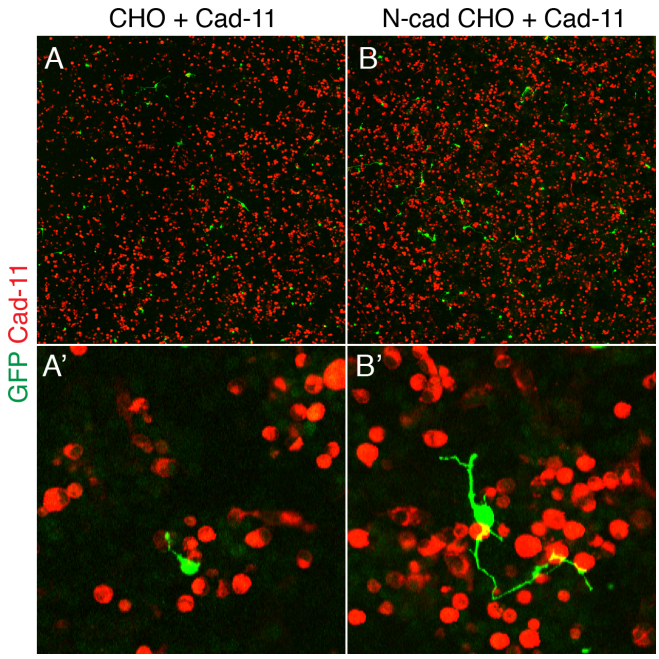

Figure 28: Motor neuron grown on cadherin-11-transfected CHO and N-cad CHO cells.
(**A**) Motor neuron cultured on CHO cells transfected with cadherin-11 (mCherry). (**A'**) Increased magnification of motor neuron cultured on CHO cells transfected with cadherin-11 (mCherry) from A. (**B**) Motor neuron cultured on N-cad CHO cells transfected with cadherin-11 (mCherry). (**B'**) Increased magnification of motor neuron cultured on N-cad CHO cells transfected with cadherin-11 (mCherry) from B.

Number of neurites, neurite length as well as total number of adherent motor neurons cultured on CHO cells transfected with cadherin-11 as a substrate was indistinguishable from naïve CHO cells (Figures 29A and 29B, 29E-269H). Motor neurons grown on N-cad CHO cells showed a 2-fold increase in neurite numbers and length compared to control CHO and cadherin-11-transfected CHO cells, as predicted by previous studies (Figures 29C and 29E-29H; Demrieva et al., 2011). However, no significant increase in neurite length or branching was observed between N-cadherin expressing cells and cadherin-11-transfected N-cad CHO cells (Figures 29C, 29D and 29E-29H). In a different approach, neurite outgrowth of motor neurons grown on purified protein substrate was monitored. However, no enhanced neurite outgrowth and branching

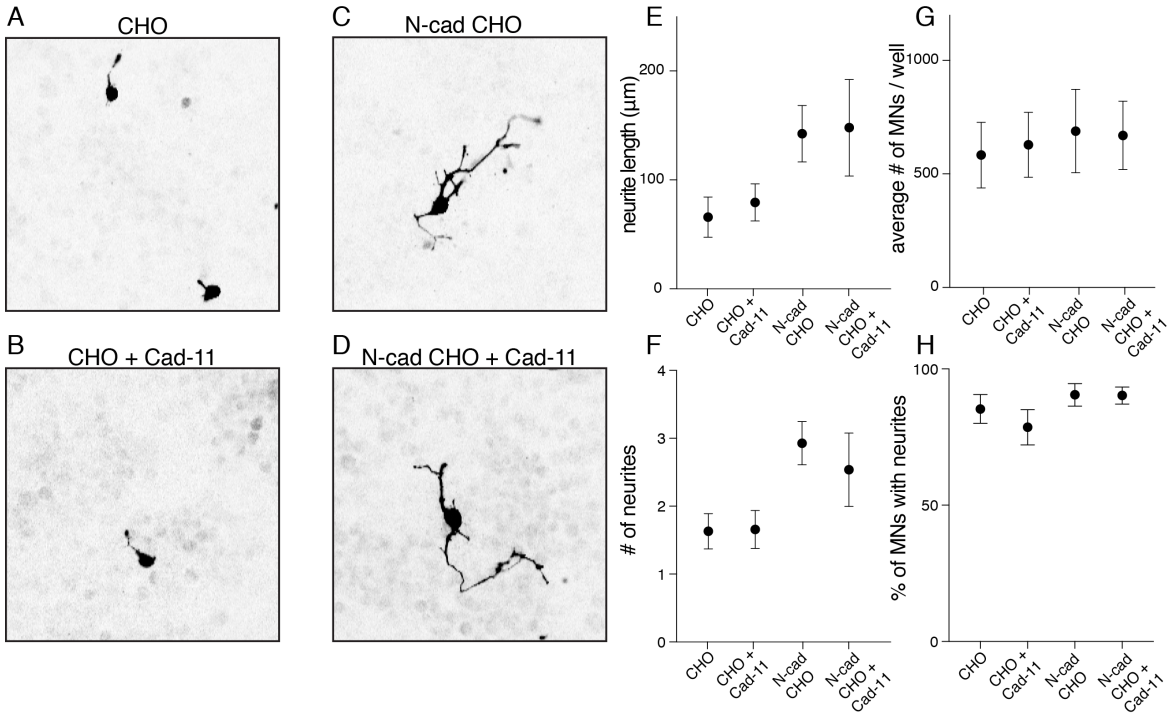

Figure 29: Motor neuron neurite outgrowth on different cadherin expressing CHO cells.
(**A**-**D**) Neurite outgrowth of motor neurons, dissociated from Hb9:GFP e10.5 embryos and seeded on dishes coated with CHO cells (**A**), CHO cells transfected with cadherin-11 (**B**), N-cad CHO cells (**C**) and N-cad CHO cells transfected with cadherin-11 (**D**); motor neurons visualized by GFP immunoreactivity depicted in black. (**E** and **F**) Average motor neuron neurite length (**E**) and number of neurites (**F**) of motor neurons grown on CHO cells, CHO cells transfected with cadherin-11, N-cad CHO cells and N-cad CHO cells transfected with cadherin-11 (mean ± SEM; differences significant for neurite length and average number of neurites: CHO cells and cadherin-11-transfected CHO cells versus N-cad CHO cells and cadherin-11-transfected N-cad CHO cells $p < 0.001$; one-way ANOVA and post hoc Tukey's HSD test). (**G**) Average number of adherent motor neurons per well grown on CHO cells, CHO cells transfected with cadherin-11, N-cad CHO cells and N-cad CHO cells transfected with cadherin-11 (mean ± SD, differences not significant; one-way ANOVA and post hoc Tukey's HSD test). (**H**) Percentage of motor neurons with neurites grown on CHO cells, CHO cells transfected with cadherin-11, N-cad CHO cells and N-cad CHO cells transfected with cadherin-11 (mean ± SD, differences not significant; one-way ANOVA and post hoc Tukey's HSD test). I performed the neurite outgrowth assay but parts of the neurite measurements were done with the help of Sofia Pimpinella.

was measured between N-cadherin-coated or N-cadherin plus cadherin-11-coated dishes, confirming the previous results (Figure 30). Thus, at least in these set of experiments, the presence of N-cadherin does not result in a new emerging function of type II cadherin.

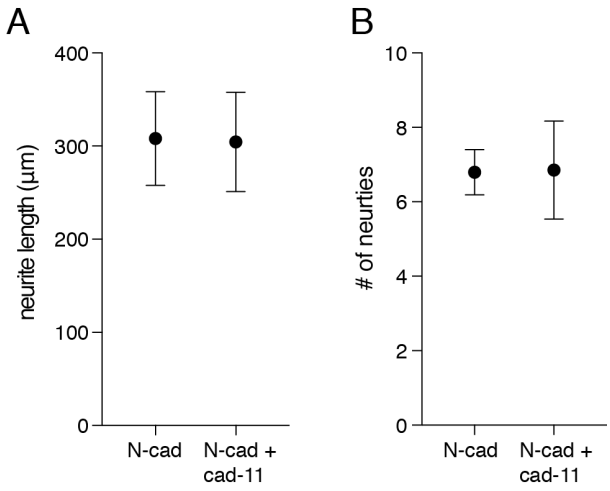

Figure 30: Motor neuron neurite outgrowth on different cadherin protein substrates.
(**A**) Average neurite length of motor neurons, dissociated from Hb9:GFP e10.5 embryos and seeded on dishes coated with N-cadherin or N-cadherin and cadherin-11 purified protein (mean ± SEM, differences not significant; t-test). (**B**) Average number of neurites of motor neurons, dissociated from Hb9:GFP e10.5 embryos and seeded on dishes coated with N-cadherin or N-cadherin and cadherin-11 purified protein (mean ± SD, differences not significant; t-test).

5.7.2 Cell aggregation assay

Next, to determine whether the presence of N-cadherin can change type II cadherins cell adhesive behavior, a cell aggregation assay was performed (Takeichi and Nakagawa, 2001). CHO cells or N-cad CHO cells were transfected with type II cadherins either fused to GFP or mCherry and cell suspensions were mixed (see Methods section 4.3.4 for details). If cadherins bind in *trans*, mixed red and green aggregates form. If the cadherins of the two cell suspensions do not interact heterophilically, separate red and green aggregates form because all cadherins undergo homophilic binding (Basu et al., 2017). The adhesive properties of cells expressing individual cadherins and pair-wise combinations of type I (N-cadherin) and type II cadherins were then tested. Consistent with previous studies, heterophilic cadherin pairs were identified according to specificity groups (Shimoyama et al, 2000; Patel et al., 2006; Basu et al., 2017). Cells expressing type II cadherins belonging to the same specificity group formed mixed aggregates in contrast to cells expressing type II cadherin members of different groups (8/11 versus 6/11; Figures 31A and 31B). Next, the ability of cells expressing type II cadherins to interact with cells expressing N-cadherin (type I) was tested. Aggregates formed by cells expressing type II cadherins segregated from aggregates of cells expressing N-cadherin (Figures 31C and 31D).

Next, aggregation assays were performed with cells expressing type II cadherins on an N-cadherin background using N-cad CHO cells. Mixtures of cells expressing N-cadherin in addition to cadherin-11 and cells expressing only cadherin-11 formed mixed aggregates (Figures 32A). Expression of cadherin-6 in presence of N-cadherin did not inhibit mixed aggregation with N-cadherin aggregates (Figures 32B). Interestingly, the simultaneous expression of N-cadherin did not change type II cadherin adhesive behavior as mixed cadherin-6 and cadherin-11 expressors still formed "separate" aggregates as predicted by specificity groups. However, these aggregates were not completely dispersed but enclosed in a coherent bigger aggregate suggesting a general adhesive role for N-cadherin.

This data needs to be confirmed by repeating the assay with type II cadherins belonging to the same specificity group on an N-cadherin background in order to test whether mixed aggregates within one big coherent aggregate will form. In addition, it will be necessary to quantify the degrees of. However, these findings confirmed and extended studies demonstrating the heterophilic interactions of type II cadherins specificity groups and segregation of cells expressing type II and type I cadherins and showed, surprisingly, that the adhesive binding preferences of type II cadherins do not seem to be affected upon presence of N-cadherin.

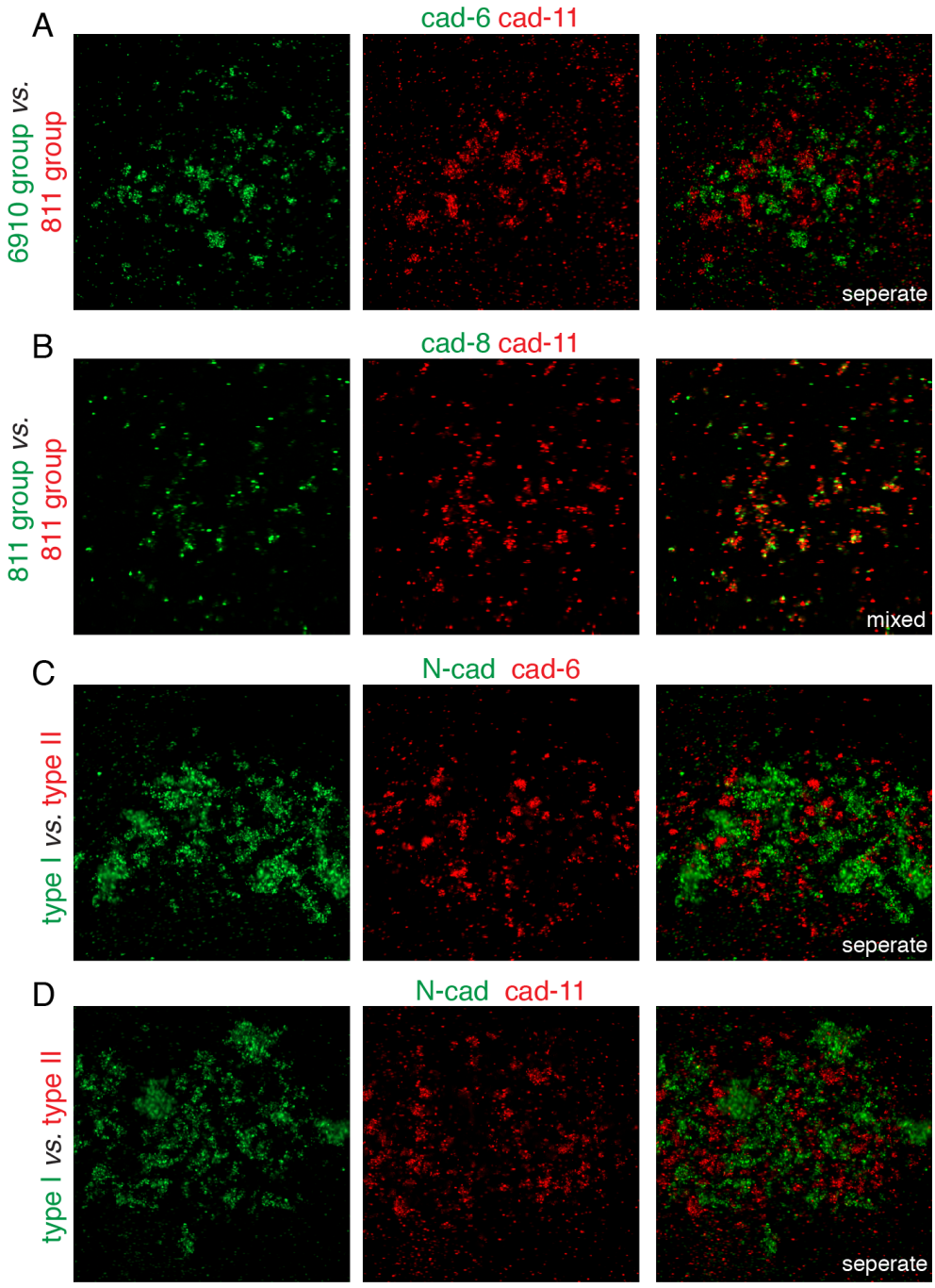

Figure 31: Cell aggregation assay to show heterophilic and homophilic binding between different cadherin pairs.

(**A**) Representative images of CHO cell aggregation assays showing separate red and green aggregates when cadherin-6 cells (green) are mixed with cadherin-11 cells (red) indicating only homophilic trans-cellular interactions of cadherins belonging to different type II cadherins specificity groups. (**B**) Representative images of CHO cell aggregation assays showing mixed red/green aggregates when cadherin-8 cells (green) are mixed with cadherin-11 cells (red) indicating heterophilic trans-cellular interactions of type II cadherins belonging to the same specificity group. (**C**) Representative images of CHO cell aggregation assays showing separate red and green aggregates when N-cadherin (type I) cells (green) are mixed with cadherin-6 (type II) cells (red) indicating only homophilic trans-cellular interactions. (**D**) Representative images of CHO cell aggregation assays showing separate red and green aggregates when N-cadherin (type I) cells (green) are mixed with cadherin-11 (type II) cells (red) indicating only homophilic trans-cellular interactions.

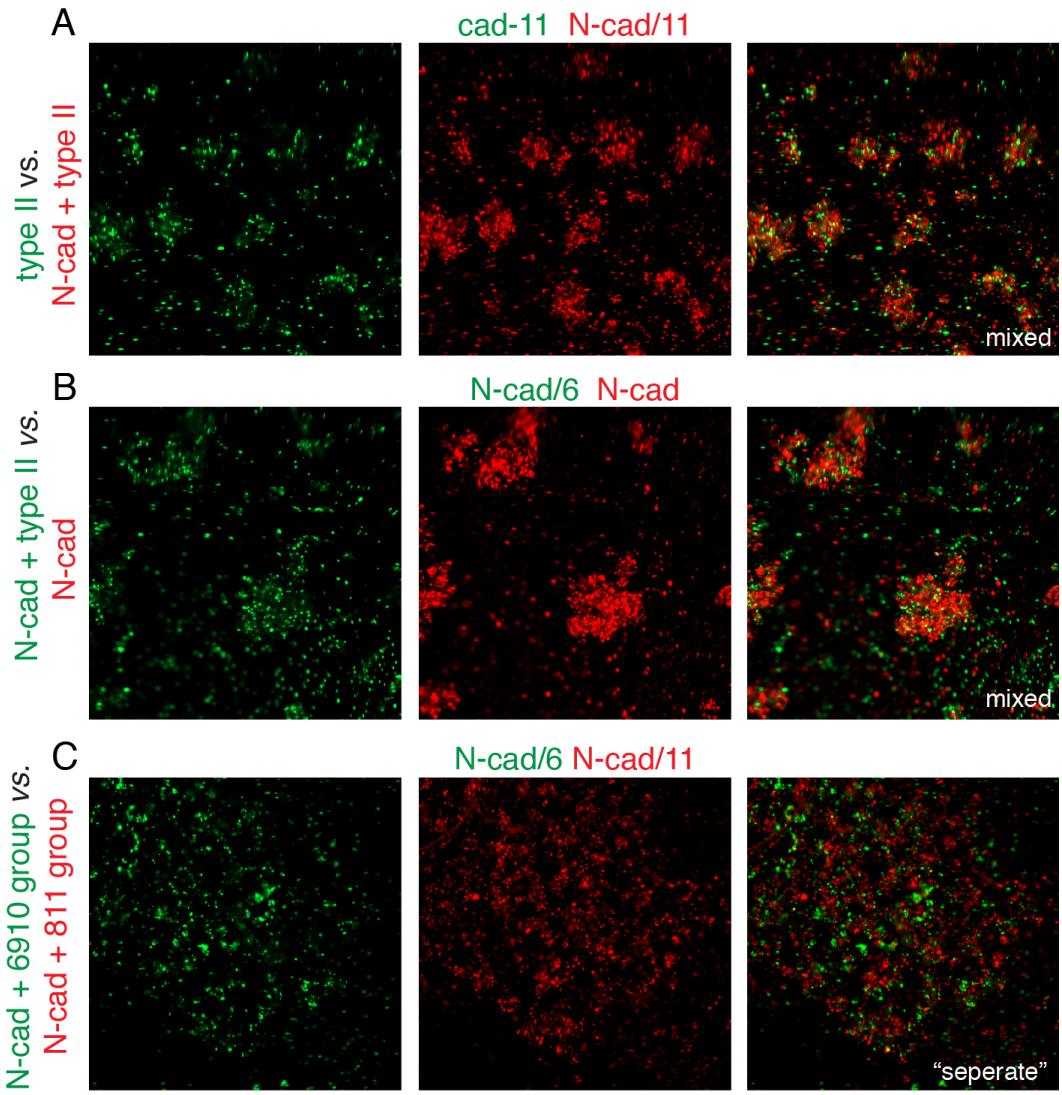

Figure 32: Cell aggregation assay to show heterophilic and homophilic binding between different type II cadherin combinations in presence of N-cadherin.
(**A**) Representative images of CHO cell aggregation assays showing mixed red and green aggregates when cadherin-11 cells (green) are mixed with N-cad/cadherin-11-expressing cells (red). (**B**) Representative images of CHO cell aggregation assays showing mixed red/green aggregates when N-cad/cadherin-6 cells (green) are mixed with N-cadherin cells (red). (**C**) Representative images of CHO cell aggregation assays showing separate red and green aggregates within one big coherent aggregate when N-cad/cadherin-6 cells (green) are mixed with N-cad/cadherin-11 cells (red).

5.7.3 Co-culture assay

To relate our *in vivo* findings of a new emerging function of type II cadherins in the presence of N-cadherin to a cellular system, localization of fluorescently labeled type II cadherins in transfected CHO and N-cad CHO cells was examined. First, type II cadherins, representing members of different specificity groups, were transfected individually into CHO cells that were then co-cultured to allow formation of homotypic cell contacts between cells of the same cell line and heterotypic contacts between cells from different cell lines. Co-culture of these cells produced heterotypic cell contact sites devoid of cadherins, which accumulated only at homotypic sites, confirming binding preferences according to specificity groups (Figure 33A). When cadherin-11 cell lines were co-cultured with cadherin-11-transfected N-cad CHO cell lines, the homophilic cadherin-11 pair co- localized equally to homotypic and heterotypic contacts, reflecting no changes in cadherin localization upon presence of N-cadherin (Figure 33B). Lastly, N-cad CHO cells were transfected with type II cadherins of different specificity groups, resulting in a N-cad/cadherin-6-GFP and N-cad/cadherin-11-mCherry cell line. Type II cadherins localized only to homotypic contact sites, reflecting no changes in cadherin localization upon presence of N-cadherin (Figure 33C). This data needs to be confirmed by repeating the co-culture experiment with type II cadherins belonging to the same specificity group and different type II cadherins combinations with N-cadherin to test whether cadherin localization will change upon co-expression of N-cadherin. In addition, it will be crucial to immunostain for N-cadherin to show concomitant expression with type II cadherins.

However, these preliminary results show that type II cadherin localization is not affected by the presence of N-cadherin, but still mirrors binding preferences according to specificity groups.

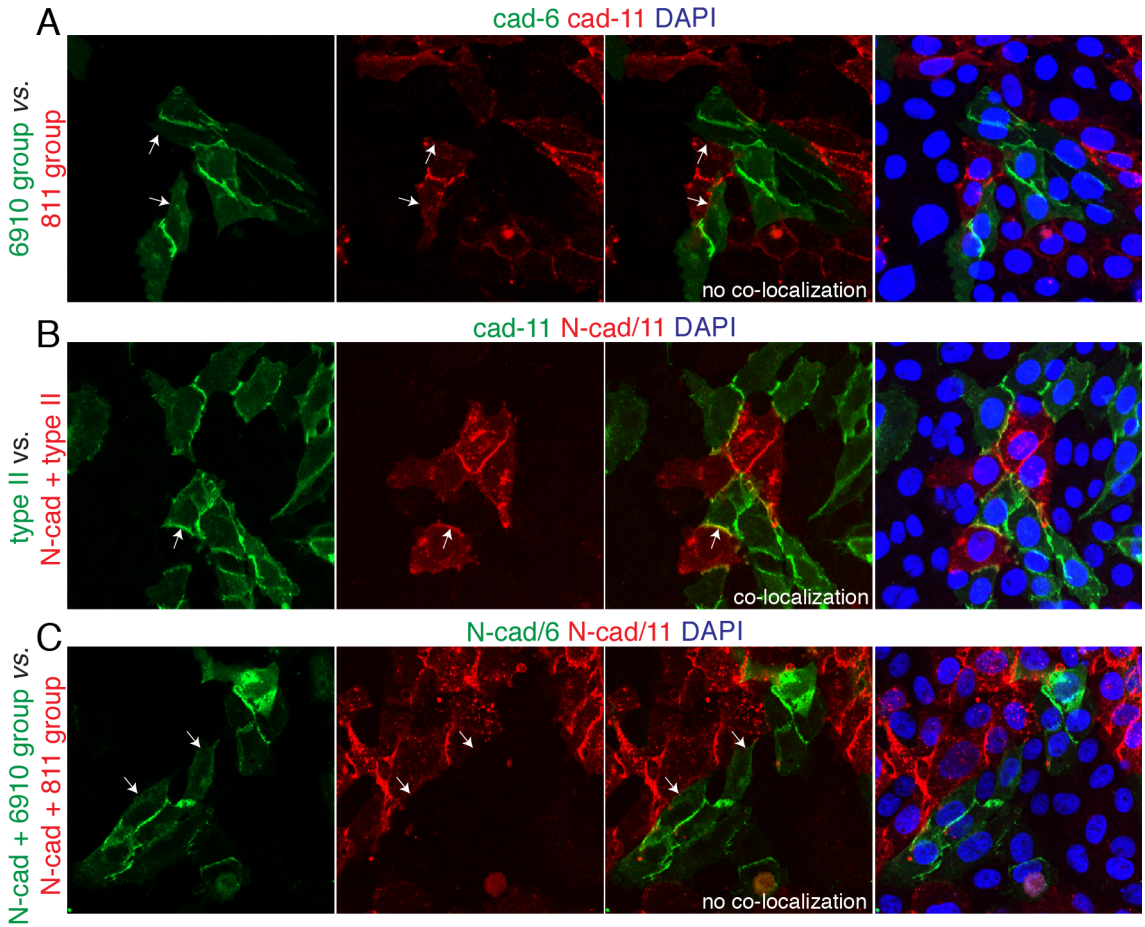

Figure 33: Type II cadherins localization at homotypic and heterotypic contact sites between transfected CHO and N-cad CHO cells in co-culture.
(**A**) Representative co-culture images showing cadherin localization at homotypic red (cadherin-6 / cadherin-6) and green (cadherin-11 / cadherin-11) contact sites and the absence of cadherins localization at heterotypic contact sites between red (cadherin-6) and green (cadherin-11) cells. (**B**) Representative co-culture images showing cadherins localization at homotypic red (N-cad/11 / N-cad/11) and green (cadherin-11 / cadherin-11) contact sites and the presence of cadherins localization at heterotypic contact sites between red (N-cad/11) and green (cadherin-11) cells. (**C**) Representative co-culture images showing cadherins localization at homotypic red (N-cad/11 / N-cad/11) and green (N-cad/6 / N-cad/6) contact sites and the absence of cadherins locatlizion at heterotypic contact sites between red (N-cad/11) and green (N-cad/6) cells. Presence or absence of cadherin localization at heterotypic contact sites is marked by white arrowheads. DAPI identifies all cell nuclei.

6. Discussion

The positioning of newly born neurons is a tightly regulated process that is critical for the assembly of the nervous system. In the spinal cord, nuclear organization of motor neurons into pools is an elaborated morphogenetic feature at the basis of the wiring of spinal sensory motor circuits (Sürmeli et al., 2011; Hinckley et al., 2015; Bikoff et al., 2016). The events controlling motor neuron positioning during development have yet to be clearly defined. Previous studies identified N-cadherin/catenin adhesive signaling as an important regulator of motor neuron organization but did not provide insights into the molecular and cellular events leading to precise positioning (Price et al., 2002; Demireva et al., 2011). The present work reveals that nuclear organization of motor neurons is dependent on inside-out positioning, orchestrated by N-cadherin, catenin and afadin activities, controlling cell body layering on the medio-lateral axis. In addition to this lamination like program, motor neurons undergo a secondary, independent phase of organization, which results in segregation of motor neurons along the dorso-ventral axis of the spinal cord and can proceed even when medio-lateral positioning is perturbed. Interestingly, the data show that this latter process is dependent on combined type I and type I cadherin function.

6.1 Lamination and nuclear organization of spinal motor neurons

Precise control of neurogenesis and migration is used during development as a strategy to position neuronal subtypes into specific coordinates. In the developing cortex, inside-out positioning of neurons tightly links neuronal birth date and migratory pattern, controlling the laminar organization of neurons (Hatten, 1999; Marin et al., 2010). Neurons exiting the cell cycle at early time points populate deep cortical layers, whereas neurons generated at later times settle in superficial layers. In contrast, less is known about the mechanisms controlling nuclear organization. Limb-innervating motor neurons display prominent nuclear organization and are positioned into discrete clusters, termed pools, that are found at precise coordinated in the spinal cord (Dasen and Jessell, 2009). Previous work indicated that motor neurons migrate radially away from the progenitor zone during development (Leber and Sanes, 1995), Indeed, radial migration is supposed to be at the basis of medio-lateral organization of motor neuron divisions.

The present work shows that a lamination-like inside-out migration is the initial step of motor neuron nuclear organization resembling cortex development. N-cadherin/catenins and afadin specifically disrupt divisional segregation by perturbing lateral migration of later-born LMCl neurons, whereas positioning of first-born LMCm neurons is not affected. However, in order to generate distinct nuclei an additional step of migration is required. This independent step segregates neurons along the dorso-ventral axis resulting in motor pool formation and requires combined type I and type II cadherin function.

In conclusion, these results reveal that the events involved in medio-lateral divisional organization closely resemble the ones controlling cortical lamination, suggesting that the same principles are applied in the developing spinal cord.

6.2 N-cadherin mediates lamination-like migration programs

Here, by taking advantage of three-dimensional positional analysis, the data confirms that N-cadherin, via β- and γ-catenin signaling, has a major role in motor neuron organization. It participates in directing the medio-lateral position of LMCl neurons and divisional segregation. Interestingly, in contrast to previous studies, where N-cadherin elimination from motor neurons was described to phenocopy the defects in β- and γ-catenin mutants, the present data reveal that segregation of motor pools along the dorso-ventral axis is mostly spared, indicating the existence of other catenin-interacting effectors controlling these events. These findings are in agreement with previous knowledge on N-expression profiles in motor neurons and its function during the development of the cortex. N-cadherin is expressed by all spinal motor neurons and thus cannot generate the necessary adhesive recognition and distinctions between different motor pools in order to allow their segregation. However, N-cadherin has been shown to be involved in more general aspects like axonal outgrowth and neuronal migration (Hansen et al., 2008, Masai et al., 2003), thus possibly explaining the medio-lateral migratory defects along the medio-lateral axis. Specifically, N-cadherin may promote lateral migration by providing homophilic interactions for motor neurons migrating along radial glial fibers as suggested in the previous section. In support of this view are findings in the mouse cerebral cortex, where elimination of N-cadherin from cortical progenitors results in destroyed architecture of intra-cortical structures, partly due to the disruption of ventricular zone integrity and the radial migration of newly generated neurons (Kadowaki et al., 2007).

In addition, analysis of N-cadherin and β- and γ-catenin mutants revealed an additional role for N-cadherin/catenin signaling in the control of columnar dorso-ventral positioning. Loss of N-cadherin/catenin activities results in a dramatic ventral shift of LMC neurons suggesting severe migratory defects. These findings raise the question whether, similar to migratory patterns of PGC neurons, LMC neurons first migrate ventral-laterally to the outer most boundary of the developing spinal cord and subsequently move dorsally to reach their final settling positions. Results suggest that this latter dorsal movement is impaired after loss of N-cadherin/catenin signaling. It is known that PGC neurons, which innervate sympathetic nervous system targets in the periphery, are located in a dorsal-lateral and dorsal-medial part of the ventral thoracic spinal cord and undergo three different phases of migration (Phelps et al., 1993). First, they migrate radially to the marginal zone, using the same method of migration as LMC neurons. In a second step of migration, PGC neurons tangentially move to a more dorsal position. Finally, a subpopulation migrates medially towards the central canal. Interestingly, within N-cadherin and catenin mutants, PGC neurons fail to reach their dorso-lateral position in the ventral horn and are found in ectopic ventral positions (Demireva et al., 2011). These results lead to the following two hypotheses: ventral migration may be the initial and default mode of migration used by different motor columns and consequent dorsal migration may be a common catenin-dependent mechanism shared by LMC and PGC neurons.

6.3 Identification of afadin as a novel player in motor neuron inside-out migration

In addition to N-cadherin/catenin signaling, afadin was identified as an important player in motor neuron organization. Afadin elimination has a selective role in the control of LMCl medio-lateral settling, confirming that LMCl neuron inside-out positioning is a key step in controlling motor neuron segregation on the medio-lateral axis and proper layering of divisional subtypes. However, similar to the phenotypes observed after N-cadherin elimination, loss of afadin function has no effect on dorso-ventral motor pools segregation, indicating that nectins do not participate in this aspect of motor neuron organization.

Recent studies have shown that precise control of cell adhesive interactions is critical for cortical development, regulating the proliferation of neuronal progenitors, stability of the radial glia scaffold, and migration of post-mitotic neurons (Bielas and

Gleeson, 2004). The classical cadherin and nectin families of adhesion molecules are key components of the machinery that controls the assembly and maintenance of several types of cell junctions, with catenins and afadin interaction regulating the cross-talk between these molecules (Takai et al., 2008; Hirano and Takeichi, 2012). To date, many members of the cadherin/catenin and nectin/afadin signaling systems have been shown to play important roles during cortical development. Elimination of β-catenin in cortical progenitors results in migratory defects in late-born cortical neurons, and, similar to N-cadherin elimination, severe cortical lamination phenotypes are also afadin mutant mice (Machon et al., 2003; Kadowaki et al., 2007; Gil- Sanz et al., 2014; Yamamoto et al., 2015). Moreover, acute disruption of nectin and afadin functions in cortical neurons perturbs radial migration (Jossin and Cooper 2011; Martinez-Garay et al., 2016). Recent evidence indicates that nectin-based adhesion controls radial migration by acting in concert with reelin and N-cadherin (Gil-Sanz et al., 2013). Interestingly, reelin signaling has also been shown to be involved in spinal motor neuron migration, and, in particular, divisional segregation defects have been observed after perturbation of Reelin-Dab1 signaling (Yip et al., 2003; Palmesino et al., 2010). The present findings complement and extend these studies, indicating that interplay by cadherin/catenin and nectin/afadin signaling is a conserved developmental mechanism that controls neuronal positioning not only during the assembly of laminar structures, as exemplified in the cortex, but also of nuclear ones. The precise mechanism behind afadin function in motor neurons and its relationship with cadherin/catenin signaling needs to be further addressed. Surprisingly, this work indicates that afadin is not required for N-cadherin/catenin expression or function in motor neurons, despite several studies showing, that without afadin, cadherin clustering is perturbed leading to defects in the formation of adherens junctions (Ikeda et al., 1999). These findings suggest that afadin might regulate the migration of LMCl neurons by transducing nectin activity. However, nectins are not strongly expressed in the spinal cord during development, indicating the possibility that afadin could control migration in a nectin-independent manner (Miyata et al., 2009). The cell positioning in the neocortex is massively perturbed in afadin mutant mice as a consequence of adherens junction disruptions, leading to a double cortex. Interestingly, genetic deletion of the small GTPase RhoA in the developing cerebral cortex also leads to a double cortex and affects stability of actin in neurons. Furthermore, it has been shown that it is critical for glial guided neuronal migration (Capello et al., 2012). These findings, in addition to known modulating activities of RhoA by afadin, suggest that afadin could act via the RhoA

signaling cascade (Miyata et al., 2009).

Altogether, these data support a key role for afadin, in addition to N-cadherin/catenin adhesive signaling, in lamination of motor neuron divisions, highlighting their role as conserved regulators of inside-out migration in the developing nervous system. It will be interesting in the future to test whether a similar developmental logic and mechanisms are used in the morphogenesis of other spatially ordered structures in the nervous system.

6.4 LMCl neuronal specific migratory defect after elimination of cell-surface proteins

This work indicates that inactivation of either N-cadherin, β- and γ-catenin, or afadin has a specific effect on the medio-lateral positioning of LMCl neurons, which are found in medial locations normally occupied by LMCm neurons whose position is unaffected. These data show for the first time that inside-out radial migration is a key step for layering of motor neuron divisions and that N-cadherin/catenins and afadin functions are prominent regulators of this process. However, what is the cellular basis for the observed LMCl neuronal specific phenotype?

Previous work indicates that motor neurons migrate radially away from the progenitor zone during development, by a process of perikaryal translocation (Dorado et al., 1990; Leber and Sanes, 1995). During their radial migration, motor neurons extend processes that attach to both the ventricular (apical) and pial (basal) surfaces of the spinal cord. Following this bipolar state, they detach and retract their apical processes and undergo nuclear translocation laterally through the intermediate zone of the spinal cord. At the same time, the basal processes pierce the basal lamina and differentiate into axons (Wentworth, 1984). This method of migration is primarily used by the first wave of postmitotic motor neurons; however, later born neurons may migrate along radial glial fibers, which begin, to traverse the grey matter of the spinal cord at e10.5 (Oudega and Marani, 1991). These two migratory methods could explain the observed differences in divisional subtype migratory defects. The data show that N-cadherin/catenins and afadin are specifically involved in the medio-lateral migration of the later born LMCl neurons, suggesting that these neurons are differently affected by the loss of cadherin/catenins and afadin function compared to LMCm neurons. One hypothesis thus is, that the first-born LMCm neurons reach their final settling position via perikaryal translocation, a process independent of cell surface molecules. In contrast, the later-born LMCl neurons may rely

to a greater extend on radial glial fibers-mediated migration or the surface and processes of LMCm neurons, which may be disrupted in the absence of cell surface proteins. Thus, lack of N-cadherin/catenins and afadin dependent interactions impairs the ability of LMCl neurons to migrate past LMCm cells. Another explanation for the LMCl specific migratory defect could result from differences in the efficiency of protein removal from motor neurons. In this study, cell adhesion proteins were eliminated by crossing an *olig2::cre* driver line with conditional N-cadherin/catenin or afadin alleles to restrict recombination to motor neuron progenitors. However, olig2 first starts being expressed by motor neurons around e10.0, indicating that the *olig2::cre* recombinase may be more efficient in removing proteins from later-born LMCl neurons compared to LMCm neurons which are already born around e9.0. Thus, due to differences in the birth date of LMCm and LMCl neurons, LMCm neurons may exhibit incomplete N-cadherin/catenin or afadin protein removal. Consequently, LMCm neuron settling position is not impaired. However, the precise mechanism of cadherin/catenin and afadin function in motor neuron migration still needs to be investigated.

6.5 The mystery of type II cadherins function

The absence of phenotypes for N-cadherin and afadin mutants on dorso-ventral pool segregation imply that other β- and γ-catenin-dependent effectors are in charge of controlling dorso-ventral pool clustering. Type II cadherins exhibit complex combinatorial patterns of expression in several areas of the developing nervous system, including motor neurons in the spinal cord, leading to the hypothesis that this family of molecules might be used to generate an adhesive code responsible for controlling cell-cell recognition during development (Suzuki et al., 1997; Redies, 2000; Krishna-K et al., 2011; Hirano and Takeichi, 2012).

6.5.1 The cadherin adhesive code in the development of the nervous system

Since its discovery**,** the exquisite specificity with which classical cadherins define discrete anatomical features of the nervous system has supported the hypothesis that cadherins set up a cellular adhesive code underlying specific neuronal interactions (Redies and Takeichi, 1996). Type II cadherins, in particular, are broadly expressed in the central nervous system in remarkable combinatorial profiles delineating neuronal circuits and structures like cortical laminae, subdivisions of the basal ganglia and amygdala nuclei

(Suzuki et al., 1997; Hertel et al., 2008; Krishna-K et al., 2011; Hertel et al., 2012). However, defining the functions of different members of the family and the relevance of the adhesive code hypothesis has been challenging as, at a molecular level, cadherins often engage in extensive heterophilic interactions and, at a genetic level, most knock-out mouse models do not show any or only mild obvious phenotype (see Introduction section 1.5.3; Hirano and Takeichi, 2012).

There are several evidences indicating that type II cadherins may work synergistically in defining neuronal adhesive recognition properties (Shimoyama et al., 2000; Demireva et al., 2011; Duan et al., 2014). Comprehensive binding affinity analysis shows that type II cadherins can be divided into three different specificity groups according to their binding preferences, where molecules belonging to the same group can bind to each other in heterophilic manner, but discriminate molecules belonging to different groups (Brasch et al., 2018). Mouse genetic experiments confirmed that redundant functions of subsets of type II cadherins are at the basis of synaptic specificity in the retina and synaptic plasticity in the hippocampus, thus indicating that elimination of multiple members belonging to a specificity group might be necessary to reveal type II cadherins contributions *in vivo* (Basu et al., 2017; Duan et al., 2018). Altogether these data support a model based on an adhesive recognition code where functional redundancy and combinatorial expression of type II cadherins is used to generate developmental programs that are both specific and robust (Jontes, 2018).

6.5.2 Type II cadherin specificity groups and the organization of motor pools

The importance of classical cadherins in controlling the spatial organization of motor pools has been clearly evident since the first studies in chick and mouse embryos (Price et al., 2002; Demireva et al 2011). Unique combinatorial expression profiles of type II cadherins delineate motor pools in the developing chick spinal cord. The adductor (A) pool and the external Femorotibialis (eF) pool can be distinguished by the expression of a single cadherin, cadherin-20. Equalizing the type II cadherin expression profile by either introducing or removing cadherin-20 from either motor pool leads to the intermixing of the two pools (Price et al., 2002). These experiments clearly point to a direct role of type II cadherins function in motor pool segregation. Nevertheless, genetic attempts to address the roles of type II cadherins in mice have failed and elimination of individual type II cadherins did not result in perturbation of motor neuron positioning. Only for N-cadherin, a type I cadherin, a clear function in the segregation of motor neuron divisions has been

previously described (Demireva et al., 2011). These findings could indicate that type II cadherins roles are not conserved between species or that differences between chick and mouse are a result from a much higher complexity of the type II cadherin expression code and that compensation and redundancy are at the basis of the type II cadherin activity in mouse.

However, surprisingly, the data of this thesis imply that the positioning of motor neurons does not follow the same molecular logic, based on a redundant adhesive code, which has been shown to control synaptic properties in the hippocampus and to instruct the assembly of retinal circuits. In particular, in the hippocampus, heterophilic interactions between cadherin-6, -9 and -10 have been shown to control high-magnitude synaptic potentiation between CA3 and CA1 neurons (Basu et al., 2017). Similarly, the ordered patterning of ON-OFF direction selective ganglion cells dendrites into two distinct sublaminae in the retina is based on the redundant function of cadherin-6, -9, and -10, thus requiring elimination of all the members of this specificity group to perturb dendritic organization (Duan et al., 2018). In contrast to these previous findings, in the spinal cord, the same triple cadherin mutant shows no effect on motor neuron generation, differentiation, and positioning. Moreover, also elimination of a different specificity group, consisting of cadherin-8 and -11, did not result in any defects in motor neuron development.

However, notably, due to experimental limitations in this work, positioning of only three different motor pools (H, V and R/T) were analyzed. Thus, defects in positions of different motor pools after elimination of type II cadherin specificity groups cannot be completely excluded. Furthermore, individual cadherin members show differential patterns of expression between forelimb and hindlimb LMC neurons with further variations at rostral and caudal regions; for example, cadherin-9 is only expressed in caudal hindlimb and forelimb motor pools and is not expressed by lumbar H, V and R/T motor pools. Thus, it would be interesting to test in the future whether elimination of the specificity group cadherin-6, -9 and -10 affects more caudally positioned lumbar or forelimb motor pools.

Puzzlingly, the data show that the same molecules seem to have different roles in regard to synaptic specificity and function in contrast to cell body positioning. At a cellular level, cadherins are dynamically expressed in neurons throughout development into adulthood and thus may serve different functions at different times (Hirano and Takeichi, 2012; Astick et al., 2014). In the mouse, classical cadherins start being expressed soon after motor neuron generation but detailed profiles at a pool resolution are only available

around e13.5, a stage where motor pool organization is just completed (Demireva et al., 2011). Thus, it is possible that type II cadherins combinatorial expression may encode recognition properties used for later events in motor neuron development, such as dendritic organization and synaptic specificity. Here, it would be interesting to investigate localization of cadherin proteins in motor neurons to provide information about their expression in somata, dendrites and axons. Furthermore, an important role for classical cadherins in controlling motor neuron dendritic arborization has been previously described, showing that removal of all cadherin function via genetic elimination of β- and γ-catenin results in changes of the stereotypic radial dendritic architecture of adductor motor neurons, with reduced dendritic length and branch numbers (Demireva et al., 2011). Thus, it will be interesting to analyze synapse formation and function in motor neurons lacking type II cadherins specificity groups in the future. Last, it is completely unknown whether compensatory mechanisms exist after the loss of specific cadherins. Motor neurons may sense and regulate the repertoire of present cell surface cadherins and their elimination could trigger changes in the cadherin expression profile. Thus, it would be interesting to precisely monitor the cadherin expression pattern in motor neurons, not only at several developmental time points, but also within cadherin mutant mice.

6.6 Type I and type II cadherins orchestrate pool morphogenesis

One of the most striking findings of the experiments performed in this thesis clearly show that the contributions of type II cadherins become evident only in absence of N-cadherin. First, at a divisional level, a stronger penetrance in the medio-lateral segregation phenotype, as described in N-cadherin mutant embryos, was observed indicating that type II cadherins contribute to the early phase of motor neuron inside-out migration. Second, at a pool level, the analysis reveals a central role for type II cadherins in the segregation of motor pools on the dorso-ventral axis, a phenotype that has been previously observed only after elimination of all classical cadherins function, via deletion of β- and γ-catenin. Interestingly, identical phenotypes are observed by inactivating N-cadherin with either cadherin-8 or -11, which did not show any phenotype when eliminated individually or in conjunction, thus indicating that cross talk between N-cadherin and type II cadherin is indeed a central feature of the mechanisms controlling motor neuron positional organization.

However, the molecular and cellular bases of the emerging functions observed after concomitant elimination of N-cadherin and type II cadherins remain unclear. At a structural level, heterophilic binding between type I and type II cadherins is prohibited due to major differences in their binding domain (see Introduction sections 1.5.1) and, at a cellular level, there is no prior report of such functional interaction controlling adhesive recognition, either *in vitro* or *in vivo* (Patel et al., 2006; Brasch et al., 2012). Thus, based on all previous knowledge on sequence homology, binding affinity and biophysical structure, type I and type II cadherins interactions are not feasible. However, still the present data show a clear genetic interplay of the two proteins. Thus, in the attempt to identify changes in cell adhesion properties and downstream signaling events upon co-expression of N-cadherin and type II cadherins, adhesive recognition in a heterologous cell system and primary motor neurons were investigated, but did not observed any significant effect. In theory, just varying cadherins expression patterns in motor neurons could be sufficient to generate differences in cellular adhesive strengths to drive sorting of different motor neuron subtypes into pools, a mechanism that has been proposed to explain aspects of cell sorting behavior during tissue morphogenesis (Steinberg, 2007). Indeed, in *in vitro* experiments it has been shown that varying levels of cadherins expression between otherwise identical cell populations is sufficient to promote cell segregation (Foty and Steinberg, 2013). It is therefore possible that N-cadherin, may serve to maintain a basal adhesive level among all motor neurons necessary for type II cadherins to modulate relative adhesive strength of different pools thus driving their segregation. However, the lack of dorso-ventral pool segregation defects in single N-cadherin mutants can still not be explained. In addition, as observed for N-cadherin, also cadherin-6 and cadherin-11 are expressed by all motor neurons, thus raising the possibility, that in absence of N-cadherin, cadherin-6 and cadherin-11 may act redundantly. In general, a better understanding of the temporal dynamics of cadherins expression and motor pool morphogenesis, as well as quantitative assessments of surface levels and plasma membrane localization will be necessary to understand the principles behind classical cadherins contributions to cell adhesive behavior.

Altogether, the present results uncover a central role for type II cadherins in the control of pools segregation and positioning. Surprisingly, type II cadherins function does not directly reflect their recognition specificities as predicted by binding affinities at a molecular level, but relies on genetic interaction with N-cadherin, a type I cadherin expressed by all motor neurons. Thus, combinatorial expression of type II cadherins is not

necessarily used to establish an adhesive recognition code, but as it has been proposed for several morphogenetic processes, may just confer differential adhesion properties sufficient to implement a developmental program generating cellular patterns (Steinberg, 2007; Hassan and Hiesinger, 2015; Heler and Fuchs, 2015).

6.7 Migratory arrest at the progenitor zone

In β- and γ-catenin and all mutants lacking N-cadherin, a portion of motor neurons fail to migrate away from the ventricular zone. The ventricular zone is deformed, which may provide a physical impediment to motor neurons to migrate out to their final settling positions. In addition, migratory defects may be non-cell autonomous as also interneurons, which should express normal levels of cadherins/catenins, were arrested, too. However, the altered morphology of the ventricular zone may also be a consequence of the stalled neurons themselves. Normally, β-catenin is highly enriched at the apical surface of the neuroepithelium consistent with previous studies reporting high levels of β-catenin and N-cadherin, which are thought to be localized with adherens junctions in that region (Aaku-Saraste et al., 1996; Kadowaki et al., 2007). All motor neuron subtypes were affected, however, the number of lateral neurons were predominantly influenced and found at higher percentages stalled at the progenitor zone. This could again be explained by differences in birthrate between medial and lateral motor neurons, similar to the specific positioning defect of lateral motor neurons in the ventral horn. As it is not by e10.5 that radial glia traverse the intermediate zone of the spinal cord, it is possible that only the later-born lateral LMC neurons use the available radial glia as a migratory scaffold. Thus, if this process is specifically affected by the loss of β- and γ-catenin and N-cadherin, that would explain why neurons belonging to the lateral division are more affected and consequently fail to migrate out into the ventral horn. In addition, also differences in the efficiency of protein elimination by *olig2::cre* recombinase in first-born medial and later-born lateral motor neurons could explain that primarily lateral neurons are affected.

6.8 Conclusions

In this thesis, by taking advantage of three-dimensional positional analysis, the roles and relative contributions of cell-adhesion molecules in motor neuron organization were uncovered. It was shown that N-cadherin, via β- and γ-catenin signaling, has a dual role in motor neuron organization. First, it controls columnar dorso-ventral position in the ventral horn. Second, it participates in directing the medio-lateral position of LMCl neurons and divisional segregation. Surprisingly, the data reveal that N-cadherin activity is mostly dispensable for motor pool segregation on the dorso-ventral axis. In addition, afadin, the adaptor protein of nectins, was identified as an important player in motor neuron organization. Afadin elimination, similar to removal of N-cadherin, has a selective role in the control of LMCl medio-lateral settling, confirming that LMCl neuron inside-out positioning is a key step in controlling motor neuron segregation on the medio-lateral axis and proper layering of divisional subtypes. In contrast, also loss of afadin function has no effect on dorso-ventral motor pool organization, indicating the existence of other catenin-interacting effectors controlling these events. Indeed, the data show, that type II cadherins are involved in motor pool segregation along the dorso-ventral axis, however, surprisingly, type II cadherins function does not directly reflect their recognition specificities as predicted by binding affinities at a molecular level, but relies on genetic interaction with N-cadherin, a type I cadherin expressed by all motor neurons.

Altogether, these findings may challenge the current understanding of specific adhesive recognition by classical cadherins as it may not be the only force governing cadherin-mediated function.

7. Literature

Aaku-Saraste, E., Hellwig, A., and Huttner, W. B. (1996). Loss of occludin and functional tight junctions, but not ZO-1, during neural tube closure - Remodeling of the neuroepithelium prior to neurogenesis. Developmental Biology, 180(2), 664–679.

Agalliu, D., Takada, S., Agalliu, I., McMahon, A.P., and Jessell, T.M. (2009). Motor Neurons with Axial Muscle Projections Specified by Wnt4/5 Signaling. Neuron 61, 708–720.

Alaynick, William, A., Jessell, T. M., and Pfaff, S. L. (2011). SnapShot: Spinal Cord Development, 146(1), 4–7.

Alexander, T., Nolte, C., and Krumlauf, R. (2009). Hox Genes and Segmentation of the Hindbrain and Axial Skeleton. Annual Review of Cell and Developmental Biology, 25(1), 431–456.

Astick, M., Tubby, K., Mubarak, W.M., Guthrie, S., and Price, S.R. (2014). Central Topography of Cranial Motor Nuclei Controlled by Differential Cadherin Expression. Curr. Biol. 1–7.

Basu, R., Duan, X., Taylor, M.R., Martin, E.A., Muralidhar, S., Wang, Y., Gangi-Wellman, L., Das, S.C., Yamagata, M., West, P.J., et al. (2017). Heterophilic Type II Cadherins Are Required for High-Magnitude Synaptic Potentiation in the Hippocampus. Neuron 96, 160–176.

Beaudoin G.M., Schofield C.M., Nuwal T., Zang K., Ullian E.M., Huang B., and Reichardt L.F. (2012). Afadin, a Ras/Rap effector that controls cadherin function, promotes spine and excitatory synapse density in the hippocampus. J. Neurosci. *32*, 99–110.

Bekirov, I., Nagy, V., Svoronos, A., Huntley, G., and Benson, D. (2008). Cadherin-8 and N-cadherin Differentially Regulate Pre-andPostsynaptic Development of the Hippocampl Mossy Fiber Pathway. Hippocampus, 18(4), 349–363.

Bel-Vialar, S., Itasaki, N., and Krumlauf, R. (2002). Initiating Hox gene expression: in the early chick neural tube differential sensitivity to FGF and RA signaling subdivides the HoxB genes in two distinct groups. Development (Cambridge, England), 129, 5103–5115.

Bello, S.M., Millo, H., Rajebhosale, M., and Price, S.R. (2012). Catenin-dependent cadherin function drives divisional segregation of spinal motor neurons. J. Neurosci. 32,

490–505.

Bielas S.L., and Gleeson J.G. (2004). Cytoskeletal-Associated Proteins in the Migration of Cortical Neurons. J. Neurobiol. *58*, 149–159.

Bikoff, J.B., Gabitto, M.I., Rivard, A.F., Drobac, E., Machado, T.A., Miri, A., Brenner-Morton, S., Famojure, E., Diaz, C., Alvarez, F.J., et al. (2016). Spinal Inhibitory Interneuron Diversity Delineates Variant Motor Microcircuits. Cell 165, 207–219.

Bonanomi, D., and Pfaff, S. L. (2010). Motor Axon Pathfinding. Cold Spring Harbor Perspectives in Biology, 2(3), a001735–a001735.

Brasch, J., Harrison, O.J., Honig, B., and Shapiro, L. (2012). Thinking outside the cell: how cadherins drive adhesion. Trends Cell Biol. 22, 299–310.

Brasch, J., Katsamba, P.S., Harrison, O.J., Ahlsén, G., Troyanovsky, R.B., Indra, I., Kaczynska, A., Kaeser, B., Troyanovsky, S., Honig, B., and Shapiro, L. (2018). Homophilic and Heterophilic Interactions of Type II Cadherins Identify Specificity Groups Underlying Cell-Adhesive Behavior. Cell Rep. 23, 1840–1852.

Brault, V., Moore, R., Kutsch, S., Ishibashi, M., Rowitch, D.H., McMahon, a P., Sommer, L., Boussadia, O., and Kemler, R. (2001). Inactivation of the beta-catenin gene by Wnt1-Cre-mediated deletion results in dramatic brain malformation and failure of craniofacial development. Development 128, 1253–1264.

Brenowitz, G. L., Collins, W. F., and Erulkar, S. D. (1983). Dye and electrical coupling between frog motoneurons. Brain Research, 274(2), 371–375.

Briscoe, J. (2009). Making a grade: Sonic Hedgehog signalling and the control of neural cell fate. EMBO Journal, 28(5), 457–465.

Briscoe, J., and Ericson, J. (2001). Specification of neuronal fates in the ventral neural tube. Current Opinion in Neurobiology, 11(1), 43–49.

Briscoe, J., Pierani, A., Jessell, T. M., and Ericson, J. (2000). A homeodomain protein code specifies progenitor cell identity and neuronal fate in the ventral neural tube. Cell, 101(4), 435–445.

Cappello, S., Böhringer, C. R. J., Bergami, M., Conzelmann, K. K., Ghanem, A., Tomassy, G. S., Götz, M. (2012). A Radial Glia-Specific Role of RhoA in Double Cortex Formation. Neuron, 73(5), 911–924.

Chen, Y. T., Stewart, D. B., and Nelson, W. J. (1999). Coupling assembly of the E-cadherin/β-catenin complex to efficient endoplasmic reticulum exit and basal-lateral membrane targeting of E-cadherin in polarized MDCK cells. Journal of Cell Biology, 144(4), 687–699.

Chang, Q., and Balice-Gordon, R. J. (2000). Gap junctional communication among developing and injured motor neurons. Brain Research Reviews, 32(1), 242–249.

Dasen, J. S., Liu, J.-P., and Jessell, T. M. (2003). Motor neuron columnar fate imposed by sequential phases of Hox-c activity. Nature, 425.

Dasen, J. S., Tice, B. C., Brenner-Morton, S., and Jessell, T. M. (2005). A Hox regulatory network establishes motor neuron pool identity and target-muscle connectivity. Cell, 123(3), 477–491.

Dasen J.S., and Jessell T.M. (2009). Hox networks and the origins of motor neuron diversity. Curr. Topics. Dev Biol. *88*, 169-200.

Dasen, J.S., De Camilli, A., Wang, B., Tucker, P.W., and Jessell, T.M. (2008). Hox Repertoires for Motor Neuron Diversity and Connectivity Gated by a Single Accessory Factor, FoxP1. Cell 134, 304–316.

Davis-Dusenbery, B. N., Williams, L. A., Klim, J. R., and Eggan, K. (2014). How to make spinal motor neurons. Development, 141(3), 491–501.

Delozier, T. C., Kissling, G. E., Coulter, S. J., Dai, D., Foley, J. F., Alyce, J., … Goldstein, J. A. (2009). NIH Public Access. Signal Transduction, 35(4), 682–688.

De Marco Garcia, N.V., and Jessell, T.M. (2008). Early Motor Neuron Pool Identity and Muscle Nerve Trajectory Defined. Neuron 81, 217–231.

Demireva, E.Y., Shapiro, L.S., Jessell, T.M., and Zampieri, N. (2011). Motor neuron position and topographic order imposed by β- And γ-catenin activities. Cell 147, 641–652.

Dessaud, E., Yang, L.L., Hill, K., Cox, B., Ulloa, F., Ribeiro, A., Mynett, A., Novitch, B.G., and Briscoe, J. (2007). Interpretation of the sonic hedgehog morphogen gradient by a temporal adaptation mechanism. Nature 450, 717–720.

Dorado, M. E., Chrnielewski, C. E., Quesada, A., and Prada, F. A. (1990). Two modes of cell migration in the ventral horn of the spinal cord in the chick embryo . A Golgy study, 37–42.

Duan, X., Krishnaswamy, A., De la Huerta, I., and Sanes, J.R. (2014). Type II Cadherins Guide Assembly of a Direction-Selective Retinal Circuit. Cell 158, 793–807.

Duan, X., Krishnaswamy, A., Laboulaye, M.A., Yamagata, M., Toma, K., and Sanes, J.R., (2018). Cadherin Combinations Recruit Dendrites of Distinct Retinal Neurons to a Shared Inerneuronal Scaffold. Neuron 99, 1145–1154.

Eberhart, J., Swartz, M. E., Koblar, S. A., Pasquale, E. B., and Krull, C. E. (2002). EphA4 constitutes a population-specific guidance cue for motor neurons. Developmental

Biology, 247(1), 89–101

Eberhart, J., Swartz, M., Koblar, S. A., Pasquale, E. B., Tanaka, H., and Krull, C. E. (2000). Expression of EphA4, ephrin-A2 and ephrin-A5 during axon outgrowth to the hindlimb indicates potential roles in pathfinding. Developmental Neuroscience, 22(3), 237–250.

Eccles, J., Eccles, R. M., and Lundberg, A. (1957). The convergence of monosynaptic excitatory afferents on to many different species of alpha motor neurons. J. Physiol., (138), 227–252.

Foty, R.A., and Steinberg, M.S. (2013). Differential adhesion in model systems. Rev. Dev. Biol. 2, 631–645.

Foty, R.A., and Steinberg, M.S. (2005). The differential adhesion hypothesis: A direct evaluation. Dev. Biol. 278, 255–263.

Frank, M. E., Bieber, S. L., and Smith, D. V. (1988). The organization of taste sensibilities in hamster chorda tympani nerve fibers. J. Gen. Physiol., 91(6), 861–896.

Gil-Sanz C., Franco S.J., Martinez-Garay I., Espinosa A., Harkins-Perry S., and Müller U. (2013). Cajal-Retzius cells instruct neuronal migration by coincidence signaling between secreted and contact-dependent guidance cues. Neuron *79*, 461–477.

Gil-Sanz C., Landeira B., Ramos C., Costa M.R., and Müller U. (2014). Proliferative defects and formation of a double cortex in mice lacking Mltt4 and Cdh2 in the dorsal telencephalon. J. Neurosci. *34*, 10475–10487.

Ginsberg, D., DeSimone, D., and Geiger, B. (1991). Expression of a novel cadherin (EP-cadherin) in unfertilized eggs and early Xenopus embryos. Development (Cambridge, England), 111(2), 315–25.

Haase, G., Dessaud, E., Garcès, A., De Bovis, B., Birling, M. C., Filippi, P., DeLapeyrière, O. (2002). GDNF acts through PEA3 to regulate cell body positioning and muscle innervation of specific motor neuron pools. Neuron, 35(5), 893–905.

Hansen, S. M., Berezin, V., and Bock, E. (2008). Signaling mechanisms of neurite outgrowth induced by the cell adhesion molecules NCAM and N-Cadherin. Cellular and Molecular Life Sciences, 65(23), 3809–3821.

Harris T.J.C., and Tepass U. (2010). Adherens junctions: from molecules to morphogenesis. Nat. Rev. Mol. Cell Biol. *11*, 502–514.

Harrison, O. J., Vendome, J., Brasch, J., Jin, X., Hong, S., Katsamba, P. S., … Shapiro, L. (2012). Nectin ectodomain structures reveal a canonical adhesive interface. Nat Struct Mol Biol., 19(9), 906–915.

Hassan, B.A., and Hiesinger, P.R. (2015). Beyond Molecular Codes: Simple Rules to Wire Complex Brains. Cell 163, 285–291.

Hatten M.E. (1999). Central Nervous System Neuronal Migration. Annu. Rev. Neurosci *22*, 511–539.

Heller, E., and Fuchs, E. (2015). Tissue patterning and cellular mechanics. J. Cell Biol. 211, 219–231.

Hertel, N., Krishna-K, Nuernberger, M., and Redies, C. (2008). A cadherin-based code for the divisions of the mouse basal ganglia. J. Comp. Neurol. 508, 511–528.

Hertel, N., Redies, C., and Medina, L. (2012). Cadherin expression delineates the divisions of the postnatal and adult mouse amygdala. J. Comp. Neurol. 520, 3982–4012.

Hinckley, C.A., Alaynick, W.A., Gallarda, B.W., Hayashi, M., Hilde, K.L., Driscoll, S.P., Dekker, J.D., Tucker, H.O., Sharpee, T.O., and Pfaff, S.L. (2015). Spinal Locomotor Circuits Develop Using Hierarchical Rules Based on Motorneuron Position and Identity. Neuron 87, 1008–1021.

Hirano, S., and Takeichi, M. (2012). Cadherins in Brain Morphogenesis and Wiring. Physiol. Rev. 92, 597–634.

Hollyday M., and Hamburger V. (1977). An autoradiographic study of the formation of the lateral motor column in the chick embryo. Brain Res. *132*, 197–208.

Hollyday, M., and Jacobson, R. D. (1990). Location of motor pools innervating chick wing. Journal of Comparative Neurology, 302(3), 575–588.

Horikawa, K., Radice, G., Takeichi, M., and Chisaka, O. (1999). Adhesive subdivisions intrinsic to the epithelial somites. Dev. Biol. 215, 182–189.

Huber, A. B., Kania, A., Tran, T. S., Gu, C., De Marco Garcia, N., Lieberam, I., … Kolodkin, A. L. (2005). Distinct roles for secreted semaphorin signaling in spinal motor axon guidance. Neuron, 48(6), 949–964.

Hultborn, H. (2006). Spinal reflexes, mechanisms and concepts: From Eccles to Lundberg and beyond. Progress in Neurobiology, 78(3–5), 215–232

Ikeda W., Nakanishi H., Miyoshi J., Mandai K., Ishizaki H., Tanaka M., Togawa A., Takahashi K., Nishioka H., Yoshida H., et al. (1999). Afadin: A key molecule essential for structural organization of cell- cell junctions of polarized epithelia during embryogenesis. J. Cell Biol. *146*, 1117–1131.

Inoue, A., and Sanes, J. R. (1997). Lamina-specific connectivity in the brain: Regulation by N-cadherin, neurotrophins, and glycoconjugates. Science, 276(5317), 1428–1431.

Inoue, T., Tanaka, T., Takeichi, M., Chisaka, O., Nakamura, S., and Osumi, N. (2001). Role of cadherins in maintaining the compartment boundary between the cortex and striatum during development. Development (Cambridge, England), 128(4), 561–569.

Inuzuka, H., Miyatani, S., and Takeichi, M. (1991). R-cadherin: A novel Ca2+-dependent cell-cell adhesion molecule expressed in the retina. Neuron, 7(1), 69–79.

Jessell, T. M. (2000). Neuronal specification in the spinal cord: inductive signals and transcriptional codes. Nature Reviews. Genetics, 1(1), 20–9.

Jontes, J.D. (2018). The cadherin superfamily in neural circuit assembly. Cold Spring Harb. Perspect. Biol. 10, 1–19.

Jossin Y., and Cooper J.A. (2011). Reelin, Rap1 and N-cadherin orient the migration of multipolar neurons in the developing neocortex. Nat. Neurosci. *14*, 697-703.

Kadowaki M., Nakamura S., Machon O., Krauss S., Radice G.L., and Takeichi M. (2007). N-cadherin mediates cortical organization in the mouse brain. Dev. Biol. *304*, 22–33.

Kania, A., and Jessell, T. M. (2003). Topographic motor projections in the limb imposed by LIM homeodomain protein regulation of ephrin-A:EphA interactions. Neuron, 38(4), 581–596.

Katsamba, P., Carroll, K., Ahlsen, G., Bahna, F., Vendome, J., Posy, S., … Honig, B. H. (2009). Linking molecular affinity and cellular specificity in cadherin-mediated adhesion. Proceedings of the National Academy of Sciences, 106(28), 11594–11599.

Kawauchi D., Taniguchi H., Watanabe H., Saito T., and Murakami T. (2006). Direct visualization of nucleogenesis by precerebellar neurons: involvement of ventricle-directed, radial fibre-associated migration. Development *133*, 1113–1123.

Kemler, R. (1993). From cadherins to catenins: cytoplasmic protein interactions and regulation of cell adhesion. Trends Genet. 9. 317–321.

Kobielak, A., and Fuchs, E. (2004). α-catenin: At the junction of intercellular adhesion and actin dynamics. Nature Reviews Molecular Cell Biology, 5(8), 614–625.

Kostetskii, I., Li, J., Xiong, Y., Zhou, R., Ferrari, V.A., Patel, V. V., Molkentin, J.D., and Radice, G.L. (2005). Induced deletion of the N-cadherin gene in the heart leads to dissolution of the intercalated disc structure. Circ. Res. 96, 346–354.

Krishna-K, K., Hertel, N., and Redies, C. (2011). Cadherin expression in the somatosensory cortex: Evidence for a combinatorial molecular code at the single-cell level. Neuroscience 175, 37–48.

Ladle, D. R., Pecho-Vrieseling, E., and Arber, S. (2007). Assembly of motor

circuits in the spinal cord: driven to function by genetic and experience-dependent mechanisms. Neuron, 56(2), 270–283.

Lallemend, F., and Ernfors, P. (2012). Molecular interactions underlying the specification of sensory neurons. Trends in Neurosciences, 35(6), 373–381.

Lance-Jones, C., Omelchenko, N., Bailis, A., Lynch, S., and Sharma, K. (2001). Hoxd10 induction and regionalization in the developing lumbosacral spinal cord. Development Cambridge England, 128(12), 2255–2268.

Landmesser, L. (1978). The development of motor projection patterns in the chick hind limb. The Journal of Physiology, 284(1), 391–414.

Landmesser L.T. (2001). The acquisition of motoneuron subtype identity and motor circuit formation. Int. J. Dev. Neurosci. *19*, 175–182.

Leber S.M., and Sanes J.R. (1995). Migratory paths of neurons and glia in the embryonic chick spinal cord. J. Neurosci. *15*, 1236–1248.

Lemons, D., and McGinnis, W. (2006). Genomic Evolution of Hox Gene Clusters. Science, 313(5795), 1918–1922.

Leone D.P., Srinivasa K., Chen B., Alcamo E., and McConnell S.K. (2008). The determination of projection neuron identity in the developing cerebral cortex. Curr. Opin. Neurobiol. *18*, 28–35.

Lin J.H., Saito T., Anderson D.J., Lance-Jones C., Jessell T.M., and Arber S. (1998). Functionally related motor neuron pool and muscle sensory afferent subtypes defined by coordinate ETS gene expression. Cell *95*, 393–407.

Lin, J., Wang, C., and Redies, C. (2012). Expression of delta-protocadherins in the spinal cord of the chicken embryo. Journal of Comparative Neurology, 520(7), 1509–1531.

Liu, J.-P., Laufer, E., and Jessell, T. M. (2001). Assigning the Positional Identity of Spinal Motor Neurons. Neuron, 32(6), 997–1012.

Livet, J., Sigrist, M., Stroebel, S., De Paola, V., Price, S. R., Henderson, C. E., … Arber, S. (2002). ETS gene Pea3 controls the central position and terminal arborization of specific motor neuron pools. Neuron, 35(5), 877–892.

Luria, V., Krawchuk, D., Jessell, T. M., Laufer, E., and Kania, A. (2008). Specification of Motor Axon Trajectory by Ephrin-B:EphB Signaling: Symmetrical Control of Axonal Patterning in the Developing Limb. Neuron, 60(6), 1039–1053.

Machon O., van den Bout C.J., Backman M., Kemler R., and Krauss S. (2003). Role of β-catenin in the developing cortical and hippocampal neuroepithelium.

Neuroscience *122*, 129–143.

Manabe, T., Togashi, H., Uchida, N., Suzuki, S. C., Hayakawa, Y., Yamamoto, M., Chisaka, O. (2000). Loss of cadherin-11 adhesion receptor enhances plastic changes in hippocampal synapses and modifies behavioral responses. Molecular and Cellular Neurosciences, 15(6), 534–546.

Mandai, K., Nakanishi, H., Satoh, A., Obaishi, H., Wada, M., Nishioka, H., Itoh, M., Mizoguchi, A., Aoki, T., Fujimoto, T., et al. (1997). Afadin: A novel actin filament-binding protein with one PDZ domain localized at cadherin-based cell-to-cell adherens junction. J. Cell Biol. *139*, 517–528.

Marín O., Valiente M., Ge X., and Tsai L.H. (2010). Guiding neuronal cell migrations. Cold Spring Harb. Perspect. Biol. *2*, 1–21.

Martinez-Garay I., Gil-Sanz C., Franco S.J., Espinosa A., Molnár Z., and Mueller U. (2016). Cadherin2/4-signaling via PTP1B and catenins is critical for nucleokinesis during radial neuronal migration in the neocortex. Development *143,* 2121-2134.

Masai, I., Lele, Z., Yamaguchi, M., Komori, A., Nakata, A., Nishiwaki, Y., … Okamoto, H. (2003). N-cadherin mediates retinal lamination, maintenance of forebrain compartments and patterning of retinal neurites. Development, 130(11), 2479–2494.

Matsunami, H., Miyatani, S., Inoue, T., Copeland, N. G., Gilbert, D. J., Jenkins, N. A., and Takeichi, M. (1993). Cell binding specificity of mouse R-cadherin and chromosomal mapping of the gene. The Journal of Cell Biology, 409, 401–409.

McHanwell S., and Biscoe T.J. (1981). The sizes of motoneurons supplying hindlimb muscles in the mouse. Proc. R. Soc. London *213*, 201–216.

McMahon, J. A., Takada, S., Zimmerman, L. B., Fan, C. M., Harland, R. M., andMcMahon, A. P. (1998). Noggin-mediated antagonism of BMP signaling is required for growth and patterning of the neural tube and somite. Genes and Development, 12(10), 1438–1452.

Mizutani, K., and Takai, Y. (2016). Nectin spot: a novel type of nectin-mediated cell adhesion apparatus. Biochemical Journal, 473(18), 2691–2715.

Miyata, M., Ogita, H., Komura, H., Nakata, S., Okamoto, R., Ozaki, M., Majima, T., Matsuzawa, N., Kawano, S., Minami, A., et al. (2009). Localization of nectin-free afadin at the leading edge and its involvement in directional cell movement induced by platelet-derived growth factor. J. Cell Sci. *122*, 4319–4329.

Miyata, M., Maruo, T., Kaito, A., Wang, S., Yamamoto, H., Fujiwara, T., Mizoguchi, A., Mandai, K., and Takai, Y. (2017). Roles of afadin in the formation of the

cellular architecture of the mouse hippocampus and dentate gyrus. Mol. Cell. Neurosci. 79, 34–44.

Montague, K., Lowe, A. S., Uzquiano, A., Knüfer, A., Astick, M., Price, S. R., and Guthrie, S. (2017). The assembly of developing motor neurons depends on an interplay between spontaneous activity, type II cadherins and gap junctions. Development, 144(5), 830–836.

Nelson, W.J. (2008). Regulation of cell–cell adhesion by the cadherin–catenin complex. Biochem. Soc. Trans. 36, 149–155.

Niessen, C. M. (2007). Tight junctions/adherens junctions: Basic structure and function. Journal of Investigative Dermatology, 127(11), 2525–2532.

Nishimura, E. K., Yoshida, H., Kunisada, T., and Nishikawa, S. I. (1999). Regulation of E- and P-cadherin expression correlated with melanocyte migration and diversification. Developmental Biology, 215(2), 155–166.

Nollet, F., Kools, P., and Van Roy, F. (2000). Phylogenetic analysis of the cadherin superfamily allows identification of six major subfamilies besides several solitary members. Journal of Molecular Biology, 299(3), 551–572.

Nornes, H. O., and Carry, M. (1978). Neurogenesis in spinal cord of mouse: an autoradiographic analysis. Brain Research, 159(1), 1–16.

Nornes, H. O., and Das, G. D. (1974). Temporal pattern of neurogenesis in spinal cord of rat. I. An autoradiographic study - time and sites of origin and migration and settling patterns of neuroblasts. Brain Research, 73(1), 121–138.

O'Gorman, S., Fox, D. T., and Wahl, G. M. (1991). Recombinase-mediated gene activation and site-specific integration in mammalian cells. Science, 251(4999), 1351–1355.

Oishi K., Nakagawa N., Tachikawa K., Sasaki S., Aramaki, M., Hirano S., Yamamoto N., Yoshimura Y., and Nakajima K. (2016). Identity of neocortical layer 4 neurons is specified through correct positioning into the cortex. Elife *5*, 1–26.

Okabe N, Shimizu K, Ozaki-Kuroda K, Nakanishi H, Morimoto K, Takeuchi M, Katsumaru H, Murakami F, Takai Y (2004) Contacts between the commissural axons and the floor plate cells are mediated by nectins. Dev. Biol. *273*, 244–256.

Osterhout, J. A., Josten, N., Yamada, J., Pan, F., Wu, S. wen, Nguyen, P. L., … Huberman, A. D. (2011). Cadherin-6 mediates axon-target matching in a non-image-forming visual circuit. Neuron, 71(4), 632–639.

Oudega, M., and Marani, E. (1991). Expression of vimentin and glial fibrillary

acidic protein in the developing rat spinal cord: an immunocytochemical study of the spinal cord glial system. Journal of Anatomy, 179, 97–114.

Ozawa, M., Baribault, H., and Kemler, R. (1989). The cytoplasmic domain of the cell adhesion molecule uvomorulin associates with three independent proteins structurally related in different species. The The European Molecular Biology Organization Journal, 8(6), 1711–1717.

Palmesino, E., Rousso, D.L., Kao, T-J.J., Klar, A., Laufer, E., Uemura, O., Okamoto, H., Novitch, B.G., and Kania, A. (2010). Foxp1 and Lhx1 Coordinate Motor Neuron Migration with Axon Trajectory Choice by Gating Reelin Signalling. PLoS Biol. 8, e1000446.

Patel, S.D., Ciatto, C., Chen, C.P., Bahna, F., Rajebhosale, M., Arkus, N., Schieren, I., Jessell, T.M., Honig, B., Price, S.R., et al. (2006). Type II cadherin ectodomain structures: implications for classical cadherin specificity. Cell 124, 1255–1268.

Personius, K. E., Chang, Q., Mentis, G. Z., O'Donovan, M. J., and Balice-Gordon, R. J. (2007). Reduced gap junctional coupling leads to uncorrelated motor neuron firing and precocious neuromuscular synapse elimination. Proceedings of the National Academy of Sciences, 104(28), 11808–11813.

Phelps, P. E., Barber, R. P., and Vaughn, J. E. (1993). Embryonic development of rat sympathetic preganglionic neurons: Possible migratory substrates. Journal of Comparative Neurology, 330(1), 1–14.

Pokutta, S., Drees, F., Takai, Y., James Nelson, W., & Weis, W. I. (2002). Biochemical and structural definition of the 1-afadin- and actin-binding sites of α-catenin. Journal of Biological Chemistry, 277(21), 18868–18874.

Pokutta, S., and Weis, W. I. (2007). Structure and Mechanism of Cadherins and Catenins in Cell-Cell Contacts. Annual Review of Cell and Developmental Biology, 23(1), 237–261.

Price, S.R., De Marco Garcia, N.V., Ranscht, B., Jessell, T.M. (2002). Regulation of motor neuron pool sorting by differential expression of type II cadherins. Cell 109, 205–216.

Radice, G. L., Rayburn, H., Matsunami, H., Knudsen, K. A., Takeichi, M., and Hynes, R. O. (1997). Developmental defects in mouse embryos lacking N-cadherin. Developmental Biology, 181(1), 64–78.

Rakic P. (1974). Neurons in Rhesus monkey visual cortex: systematic relation

betwen time of origin and eventual disposition, Science *183*, 425-427.

Ramon y Cajal S. (1894). La fine structure des centres nerveux. Proc. R. Soc. London 55, 444–468.

Redies, C., and Takeichi, M. (1996). Cadherins in the developing central nervous system: An adhesive code for segmental and functional subdivisions. Dev. Biol. 180, 413–423.

Romanes, G., J. (1951). Motor cell columns of the lumbo-sacral spinal. Journal of Comparative, 94(2), 313–363.

Romanes G.J. (1964). The motor pools of the spinal cord. Prog. Brain Res. 11, 93–119.

Rousso, D. L., Gaber, Z. B., Wellik, D., Morrisey, E. E., and Novitch, B. G. (2008). Coordinated Actions of the Forkhead Protein Foxp1 and Hox Proteins in the Columnar Organization of Spinal Motor Neurons. Neuron, 59(2), 226–240.

Ruiz, P., Brinkmann, V., Ledermann, B., Behrend, M., Grund, C., Thalhammer, C., Vogel, F., Birchmeier, C., Günthert, U., Franke, W.W., et al. (1996). Targeted mutation of plakoglobin in mice reveals essential functions of desmosomes in the embryonic heart. J. Cell Biol. 135, 215–225.

Shapiro L., and Weis I. W. (2012). Structure and Biochemistry of Cadherins and Catenins. Journal of Chinese Pharmaceutical Sciences, 21(5), 477–482.

Shi W., Xianyu A., Han Z., Tang X., Li Z., Zhong H., Mao T., Huang K., and Shi, S.-H. (2017). Ontogenetic establishment of order-specific nuclear organization in the mammalian thalamus. Nat. Neurosci. *20*, 516–528.

Shimoyama, Y., Tsujimoto, G., Kitajima, M., and Natori, M. (2000). Identification of three human type-II classic cadherins and frequent heterophilic interactions between different subclasses of type-II classic cadherins. Biochem. J. 349, 159–167.

Shirasaki, R., and Pfaff, S. L. (2002). Transcriptional Codes and the Control of Neuronal Identity. Annual Review of Neuroscience, 25(1), 251–281.

Sockanathan, S., and Jessell, T.M. (1998). Motor Neuron–Derived Retinoid Signaling Specifies the Subtype Identity of Spinal Motor Neurons. Cell 94, 503–514.

Steinberg, M.S. (2007). Differential adhesion in morphogenesis: a modern view. Curr. Opin. Genet. Dev. 17, 281–286.

Stepien A.E., Tripodi M., and Arber S. (2010). Monosynaptic rabies virus reveals premotor network organization and synaptic specificity of cholinergic partition cells. Neuron *68*, 456–472.

Stifani, N. (2014). Motor neurons and the generation of spinal motor neuron diversity. Frontiers in Cellular Neuroscience, 8(October), 293.

Sürmeli, G., Akay, T., Ippolito, G.C., Tucker, P.W., and Jessell, T.M. (2011). Patterns of spinal sensory-motor connectivity prescribed by a dorsoventral positional template. Cell 147, 653–665.

Suzuki, S.C., Furue, H., Koga, K., Jiang, N., Nohmi, M., Shimazaki, Y., Katoh-Fukui, Y., Yokoyama, M., Yoshimura, M., and Takeichi, M. (2007). Cadherin-8 is required for the first relay synapses to receive functional inputs from primary sensory afferents for cold sensation. J. Neurosci. 27, 3466–3476.

Suzuki, S.C., Inoue, T., Kimura, Y., Tanaka, T., and Takeichi, M. (1997). Neuronal circuits are subdivided by differential expression of type-II classic cadherins in postnatal mouse brains. Mol. Cell. Neurosci. 9, 433–447.

Takai Y., Ikeda W., Ogita H., and Rikitake Y. (2008). The immunoglobulin-like cell adhesion molecule nectin and its associated protein afadin. Annu. Rev. Cell Dev. Biol. *24*, 309–342.

Takai, Y., Miyoshi, J., Ikeda, W., and Ogita, H. (2008). Nectins and nectin-like molecules: Roles in contact inhibition of cell movement and proliferation. Nature Reviews Molecular Cell Biology, 9(8), 603–615.

Takai Y., and Nakanishi H. (2003). Nectin and afadin: novel organizers of intercellular junctions. J. Cell Sci. *116*, 17–27.

Takeichi, M. (1995). Morphogenetic roles of classic cadherins. Current Opinion in Cell Biology, 7(5), 619–627.

Takeichi, M. (2007). The cadherin superfamily in neuronal connections and interactions. Nature Reviews. Neuroscience, 8(1), 11–20.

Tanabe, Y., William, C., and Jessell, T. M. (1998). Specification of motor neuron identity by the MNR2 homeodomain protein. Cell, 95(1), 67–80.

Thoreson, M. A., Anastasiadis, P. Z., J., D., Ireton, R., Wheelock, M., Johnson, K., Reynolds, A. (2000). Selective Uncoupling of p120 from E-cadherine disruots strong adhesion. Journal of Cell Biology, 148(1), 189–201.

Togashi, H., Kominami, K., Waseda, M., Komura, H., Miyoshi, J., Takeichi, M., and Takai, Y. (2011). Nectins Establish a Checkerboard-Like. Science, 333(26), 1144–1147.

Toseny, K. W., and Landmesser, L. (1985). Specificity of early motorneuron growth cone outgrowth in the chick embryo. The Journal of N, 5(9), 2336–2344.

Tsuchida, T., Ensini, M., Morton, S. B., Baldassare, M., Edlund, T., Jessell, T. M., andPfaff, S. L. (1994). Topographic organization of embryonic motor neurons defined by expression of LIM homeobox genes. Cell, 79(6), 957–970.

Vanderhorst, V.G., and Holstege, G. (1997). Organization of lumbosacral motoneuronal cell groups innervating hindlimb, pelvic floor, and axial muscles in the cat. J. Comp. Neurol. 382, 46–76.

Vrieseling, E., and Arber, S. (2006). Target-Induced Transcriptional Control of Dendritic Patterning and Connectivity in Motor Neurons by the ETS Gene Pea3. Cell, 127(7), 1439–1452.

Watanabe H., and Murakami F. (2009). Real time analysis of pontine neurons during initial stages of nucleogenesis. Neurosci. Res. *64*, 20–29.

Wentworth, L. E. (1984). The development of the cervical spinal cord of the mouse embryo. I. A Golgi analysis of ventral root neuron differentiation. Journal of Comparative Neurology, 222(1), 81–95.

Wichterle, H., Lieberam, I., Porter, J. A., & Jessell, T. M. (2002). Directed differentiation of embryonic stem cells into motor neurons. Cell, 110(3), 385–397.

Yamagata, M., Herman, J. P., Sanes, J. R., Morrison, J., Ji, Z.-X., Esteban, E., and Lynch, G. (1995). Lamina-specific expression of adhesion molecules in developing chick optic tectum. The Journal of Neuroscience : The Official Journal of the Society for Neuroscience, 15(6), 4556–71.

Yamamoto, H., Maruo, T., Majima, T., Ishizaki, H., Tanaka-Okamoto, M., Miyoshi, J., Mandai, K., and Takai, Y. (2013). Genetic deletion of afadin causes hydrocephalus by destruction of adherens junctions in radial glial and ependymal cells in the midbrain. PLoS One *8*, 1–10.

Yamamoto H., Mandai K., Konno D., Maruo T., Matsuzaki F., and Takai, Y. (2015). Impairment of radial glial scaffold-dependent neuronal migration and formation of double cortex by genetic ablation of afadin. Brain Res. *1620*, 139–152.

Yip Y.P., Capriotti C., and Yip J.W. (2003). Migratory pathway of sympathetic preganglionic neurons in normal and reeler mutant mice. J. Comp. Neurol. *460*, 94–105.

Zhang, B., Xiong, W. C., and Mei, L. (2009). Get Ready to Wnt: Prepatterning in Neuromuscular Junction Formation. Developmental Cell, 16(3), 325–327.

8. Appendix

8.1 Curriculum vitae

For reasons of data protection, the curriculum vitae is not included in the online version.

8.2 List of Publications

8.2.1 Articles

Dewitz, C., Duan, X., Zampieri, N. (**2019**). N-cadherin and type II cadherins coordinate motor neuron organization into pools. (*submitted at Cell Reports, currently in revision*)

Dewitz, C., Pimpinella, S., Hackel, P., Akalin, A., Jessell, T.M., and Zampieri, N. (**2018**). Nuclear Organization in the Spinal Cord Depends on Motor Neuron Lamination Orchestrated by Catenin and Afadin Function. Cell Rep. 22, 1681–1694.

Dewitz, C., McEachern, E., Shin, S., Akong, K., Nagel, D.G., Broide, D.H., Akuthota, P., Crotty Alexander, L.E. (**2017**). Hypoxia-inducible Factor-1α Inhibition Modulates Airway Hyperresponsiveness and Nitric Oxide Levels in a BALB/c Mouse Model of Asthma. Clin Immunol. 176:94-99

McEachern, E.K., Hwang, J.H., Sladewski, K.M., Nicatia, S., **Dewitz, C.**, Matthew, D.P., Nizet, V., Crotty Alexander, L.E. (**2015**). Analysis of the Effects of Cigarette Smoke on Staphylococcal Virulence Phenotypes. Infect Immun. 83(6):2443-52

Roloff, F., Scheiblich, H., **Dewitz, C.**, Dempewolf, S., Stern, M., Bicker, G. (**2015**). Enhanced Neurite Outgrowth of Human Model (NT2) Neurons by Small-Molecule Inhibitors of Rho/ROCK Signaling. PLoS One 25;10(2):e0118536.

8.2.2 Posters

Dewitz, C., Hackel, P., Zampieri, N. (**2018**) Dissecting Classical Cadherins Roles in Motor Neuron Positioning. Forum of Neuroscience (FENS) conference, Berlin, Germany

Dewitz, C., Hackel, P., Zampieri, N. (**2017**) Dissecting Classical Cadherins Roles in Motor Neuron Positioning. Society for Neuroscience (SfN) conference, Washington D.C, U.S.A.

Dewitz, C., Skarlatou, S., Zampieri, N. (**2016**). Molecular Mechanisms Controlling Motor Neuron Organization in the Mouse Spinal Cord. NeuroMarseille 3rd INT neuroscience conference, Marseille, France

Dewitz, C., Nicatia, S., McEachern, E.K., Rojas, I., Johnson, R., Nizet, V., Crotty Alexander, L.E. (**2014**). Hypoxia Inducible Factor (HIF)-2α In Myeloid Cells Promotes Allergic Inflammatory Airways Disease Pathogenesis In Mice. American Thoracic Society International Conference (ATS), San Diego, U.S.A.

8.2.3 Presentations

Neuroscience Seminar, Max-Delbruck-Center for Molecular Medicine in the Helmholtz Association, Berlin, Germany, September **2018**

NeuroCure Lunchtime Seminar, Charité, Universitätsmedizin Berlin, December, **2016**